# Tribological effect of the mixtures of ZDDP and various organic friction modifiers and their friction-reducing mechanisms

SHEN WEIQI

2023

KYOTO UNIVERSITY

DOCTORAL THESIS

# Tribological effect of the mixtures of ZDDP and various organic friction modifiers and their friction-reducing mechanisms

*Author:*
SHEN WEIQI

*Advisor:*
Professor Tomoko Hirayama

*Committee member:*
Professor Tomoko Hirayama
Professor Atsushi Matsubara
Professor Masaharu Komori

Department of Mechanical Engineering and Science
Functional Mechanical Elements Laboratory
Graduate School of Engineering

February 2023

# *Abstract*

This thesis focuses on a series of phenomena, such as adsorption and the reaction of additives, tribofilm formation, and tribological effects with the lubrication of the mixture of Zinc Dialkyl Dithiophosphate (ZDDP), an anti-wear additive, and an organic friction modifier (OFM) for the optimization of engine oil additives to reduce $CO_2$ emissions from automobiles. In particular, since ZDDP is a reactive additive and OFM is an adsorption additive, it is still unclear how the mixture forms the tribofilm and affects the tribological properties.

First, the relationship between the state of adsorption film formation by the additive and the coefficient of friction is investigated using Neutron Reflectometry and Atomic Force Microscopy. The results show that when an OFM is used alone, friction reduction is achieved by the formation of its adsorption film, but in a mixture with ZDDP, in addition to the additive adsorption film, the presence of metallic soap formed by the reaction between the additive and the interface significantly affects the friction properties. Next, this thesis focuses on the formation of tribofilms by the mixture of additives, which is observed and evaluated using Atomic Force Microscopy. Tribofilms were formed by sliding across the interface using colloidal probes, and their friction coefficients were obtained. In particular, the effect of surface pressure was also investigated by acquiring friction coefficients at different contact surface pressures. The results show that although the mixture of additives suppressed the formation of high-friction tribofilms and made it possible to maintain low friction at high temperatures, the OFM can cause the excessive formation of metallic soap. The metallic soap induced wear on the sliding surface and limited the friction reduction effect. Based on these results, a model for friction reduction with an additive mixture was proposed.

Then, to elucidate the mechanism of friction reduction and wear resistance improvement when additives are used together in practical systems, the morphology of tribofilms was observed, and their friction properties were evaluated on macro-scale experiments. N-Oleyol Sarcosine (NOS) was used as the practical OFM, and the results show that the mixture of ZDDP and NOS improved the friction properties by suppressing the formation of high-friction ZDDP-derived tribofilms. Although the ZDDP-derived tribofilm formation reaction becomes active at high temperatures, the high temperatures also promote the adsorption of NOS, which suppresses the formation of ZDDP tribofilms. Moreover, the oil film retention effect of NOS suppresses wear and reduces friction with better durability. At last, a model of tribofilm formation by the additive mixture was proposed, and the contribution of each additive to friction reduction at various temperature conditions was clarified.

## Content

Il n'y a qu'un héroïsme au monde: c'est de voir le monde tel qu'il est et de l'aimer.

Romain Rolland

# Chapter 1. Introduction

## 1.1 Background

Mitigating global warming and building a sustainable society have become one of the most critical issues of the 21st century. According to publicly available data from the World Bank, carbon dioxide ($CO_2$) emissions have increased from 20.6 billion tons to 34.3 billion tons in the 30 years from 1990 to 2019 [1], which poses a severe challenge to environmental protection. In Japan, according to the Ministry of Land, Infrastructure, Transport and Tourism, the transportation sector (185 million tons) accounts for 17.7% of Japan's $CO_2$ emissions (1,044 million tons) in fiscal year (FY) 2020. Of this, automobiles account for 87.6% of the transportation sector (15.5% of Japan's total), with passenger cars accounting for 48.4% (8.6% of Japan's total) and freight vehicles accounting for 39.2% (6.9% of Japan's total) [2]. Japan's $CO_2$ emissions from the transportation sector have decreased yearly since 2013, with a 19.2% reduction in FY 2020 compared to FY 2013 due to the coronavirus disease (COVID-19) outbreak in 2019. However, automobiles remain one of the most significant contributors to $CO_2$ emissions. Globally, the transportation sector is also one of the primary sources of $CO_2$ emissions. According to the World Bank, the transportation sector accounted for as much as 20.4% of global $CO_2$ emissions from fuel combustion in 2014 [3], making it essential to cut $CO_2$ emissions from the transportation sector. In this context, hybrid and new energy vehicles are gaining total momentum.

In automatic vehicles, 33% of the fuel energy is used to overcome friction, with 17% of that energy being consumed in the engine and transmission [4]. Two main approaches are being taken to reduce friction losses in engines and transmissions: to use low-viscosity engine oils, and to add boundary friction modifier additives. The use of low-viscosity engine oils minimizes hydrodynamic shear, churning, and pumping losses [5]. Society of Automotive Engineers (SAE) revised the 0W-16 viscosity of engine oils in 2013 and added 0W-8 and 0W-12 viscosities in 2015 [6–7]. Multi-grade 0W-8 oils entered the market in 2019; however, the popularity of 0W-8 is limited by engine design and performance credibility [8]. While low-viscosity oils can greatly reduce hydrodynamic friction losses, they can also lead to oil film breakdown. It would increase the risk of direct contact, friction and wear on engine components operating under boundary-mix lubrication (i.e., valve train and piston-cylinder) or at high temperatures. Therefore, the development of engine oils requires a comprehensive understanding of additive technology. Research has focused on three additives: viscosity index improvers (VII), anti-wear additives (AW), and friction modifiers (FM). VII reduces changes in lubricant viscosity due to temperature changes. The addition of VII maximizes the viscosity decrease of the lubricant at high temperatures, ensuring a sufficient oil film between the friction surfaces to provide adequate protection [9].

On the other hand, AW and FM contribute to the tribological behavior of engine components operating under boundary-mix lubrication. One of the most widely used AW, zinc dialkyl dithiophosphate (ZDDP), forms a tribofilm on the metal surface to prevent wear [10], while FM molecules adsorb to or react with the metal surface to form a low shearing resistance lubricating film that slides easily against the other side [5]. Although there has been much discussion on ZDDP and FMs in the past decades, the effect on friction reduction and wear resistance when they are used together is unclear [10]. Therefore, recent research interest has been to investigate the tribological mechanisms of ZDDP-FM mixtures.

## 1.2 ZDDP

ZDDP is one of the most widely used oil additives because of its excellent anti-wear properties. Figure 1–1 shows the molecular structure of ZDDP.

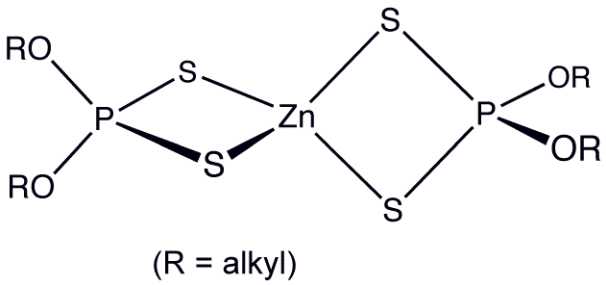


Figure 1–1. The molecular structure of ZDDP, quoted from File: Zn(dtp)2.png on Wikipedia.

Spikes published a review paper on ZDDP in 2004, detailing the history of ZDDP and summarizing the research done on ZDDP over the last sixty years [10]. In this paper, the author cites Spikes' review paper to review the history of ZDDP and provides an overview of relevant research conducted after 2004.

The use of ZDDP as an oil additive date back to the 1930s. However, it was not until the 1940s that the anti-wear properties of ZDDP became known [10]. Since then, ZDDP has been studied intensively, with the main aim of understanding the anti-wear mechanism of ZDDP. The research has concluded that ZDDP can form a tribofilm on the contact surface by rubbing, which effectively prevents direct contact at the friction interface and exhibits anti-wear properties [11–15].

Spikes divided the studies of ZDDP into two categories, those investigating the reaction of ZDDP itself and those investigating the tribofilm-forming properties of ZDDP. The study of ZDDP films predates the study of the ZDDP itself. As early as the 1950s, Loeser, Wiquist, and Twiss carried out a study using the radiotracer technique to trace the Sulfur (S) and Phosphate (P) elements contained in ZDDP extreme pressure films [11], [16]. Although no specific compounds

were identified, both studies traced S and P in the extreme pressure (EP) film and investigated the ratio of the two elements. The results showed that, although the SP ratio in the additive was 1:2, the SP ratio in the EP film was as high as 8:1 [16].

In addition to the study of the film composition, Bennett conducted a morphological study of the tribofilm [17]. This study proposed a mechanism regarding the film formation of ZDDP, whereby high temperatures in the frictional contact area led to the thermal decomposition of ZDDP and the formation of a thin film chemically bonded to the metal surface [17]. The results also confirmed that this tribofilm increases the surface roughness of the contact area [17].

It was not until the 1960s that research focused on the ZDDP itself, the first type of research described earlier. Many studies investigated the thermal decomposition of ZDDP and proposed different mechanisms [18–21]. However, in the 1970s, Jones and Coy used Nuclear Magnetic Resonance (NMR) techniques to clarify the thermal decomposition products of ZDDP [22]. By testing $^{1}H$ and $^{31}P$-NMR, Coy and Jones confirmed S/O exchange in ZDDP, in which the alkyl groups bound to O are exchanged to S at high temperatures, which causes a series of degradation reactions [23]. The specific mechanisms are not repeated in this paper, but it is of interest, however, there is no direct evidence, that S/O exchange and thermal decomposition of ZDDP may be related to thermal film formation and tribofilm formation by ZDDP [10], [24]. Thermal films, solid-like films of ZDDP up to 20 nm thick, are formed on the surface of steel balls at temperatures above 150°C [25]. Even without rubbing, these thermal films can still be formed, and their thickness increases with increasing temperature [26], where the thickest can be up to 400 nm at 200°C [27]. Two reaction mechanisms for thermal film formation are outlined in Spikes' review: first, iron and other metal oxides act as Lewis acids and should therefore catalyze the ZDDP thermal degradation reaction. Secondly, zinc in ZDDP undergoes substitution reactions with other metal ions to form dithiophosphates [10].

In the 1970s, with the development of interfacial analysis techniques, the investigation of the tribofilm composition became possible. Bird and Galvin compared the tribofilm and the thermal film compositions of ZDDP using XPS, and the results showed that they were similar in composition [28]. However, later studies showed that, unlike tribofilms, thermal films contain almost no iron ions but only zinc ions derived from ZDDP [29].

In the 1980s, Martin carried out an analysis of tribofilm composition based on analytical techniques such as Auger Electron Spectroscopy (AES), X-ray Photoelectron Spectroscopy (XPS), and X-ray Absorption Fine Structure (XAFS) [30–33]. These studies using XAFS showed that ZDDP could digest iron oxide by wrapping it during tribofilm formation, thereby removing coarse iron oxide abrasive debris and thereby reducing friction while protecting the sliding interface [31],

[33]. The analysis of the tribofilm composition continued beyond 2000. In his subsequent study, Martin measured the cation distribution by combining X-ray Absorption Near Edge Structure (XANES), AES, Secondary Ion Mass Spectrometry (SIMS), and XPS. The results suggested higher Zinc near the tribofilm surface and higher metal content near the metal surface [34].

Another trend of the ZDDP study around 2000 was in situ tribofilm observation based on the spacer layer imaging method (SLIM). Exactly SLIM studies started in the 1990s, but only rolling friction surfaces could be observed, so most studies were conducted on ZDDP thermal films [10]. After 2000, as non-contact SLIM was introduced, Spikes and his team conducted many studies on ZDDP tribofilms using Space Layer Imaging–Mini Traction Machine (SLIM-MTM). These studies revealed a good relationship between friction time and tribofilm thickness, and the results showed that the film thickness of ZDDP tribofilms does not increase indefinitely but remains constant after reaching saturation [12–14]. [35–36].

After 2000, more research began to identify the mechanisms of ZDDP film formation and the factors affecting film formation. One of the most influential studies was published in the journal Science by Carpick et al. [37]. This study used lateral force microscopy (LFM) in Atomic Force Microscope (AFM) to test the rate of tribofilm growth at different pressures and temperatures. The results showed that although ZDDP tribofilms and thermal films have similar compositions, tribofilms are not simply transformed by rubbing from thermal films. Figure 1–2 shows the tribofilm model proposed in this study, with iron sulfide and zinc sulfide near the friction surface, glassy metal phosphate on top, and zinc polyphosphates, organic sulfide, and undecomposed ZDDP on the surface of the tribofilm. The study also discussed the growth rate dependence on the contact pressure, as shown in Figure 1–3, in which the growth rate of tribofilm is strongly influenced by the contact pressure, and Carpick has proposed a stress-activated film formation response model based on the results as follow:

$$\Gamma_{growth\,rate} = \Gamma_0 exp\left(-\frac{\Delta G_{act}}{k_B T}\right),$$

where $\Delta G_{act}$ is the free activation energy, $kB$ is the Boltzmann constant, and $T$ is the absolute temperature. When pressure is applied,

$$\Delta G_{act} = \Delta U_{act} - \sigma \Delta V_{act},$$

where $\Delta U_{act}$ is the internal activation energy (energy barrier in the absence of stress), σ is the average value of the stress components affecting the activation barrier (assumed to be the compressive contact pressure) and $\Delta V_{act}$ is the activation volume.

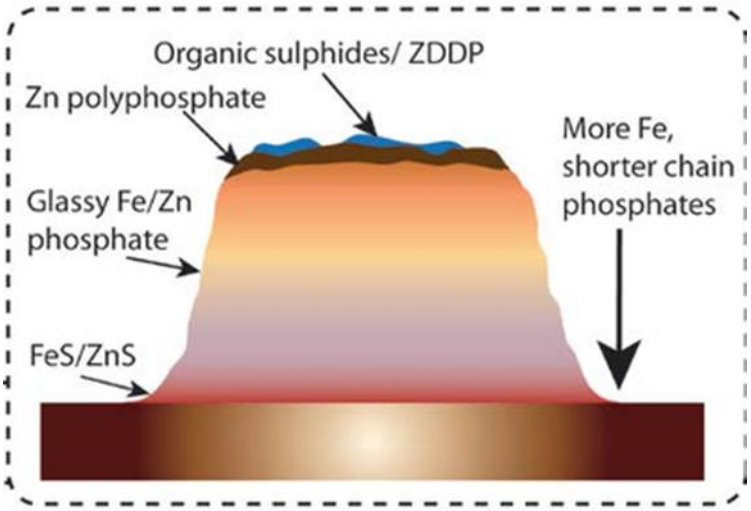

Figure 1–2. The structure of ZDDP tribofilm, cited from [37] and modified.

In 2016 Zhang and Spikes validated a shear stress model for ZDDP tribofilm formation [38]. This model is similar to the stress activation model and is based on the Eyring model. The shear stress model can be formulated as follows:

$$\text{Probability} = \text{Aexp}(-\frac{E_0 - \tau\Delta v}{k_B T}).$$

The shear stress model and the stress activation model are very similar in form. The shear stress model shows that solid contact is not necessary for ZDDP tribofilm formation and that ZDDP tribofilm can be formed on the sliding surface by applying sufficient shear stress. The model proposed by Zhang and Spikes is a good explanation for why ZDDP can form a tribofilm even at room temperature, why its surface is rough and padded, and why the ZDDP tribofilm does not grow endlessly. In addition, recent studies have shown that compressive and shear stresses contribute to the formation and growth of ZDDP tribofilms. However, their results suggest that compressive stress inhibits tribofilm growth under constant shear stress and temperature. [39].

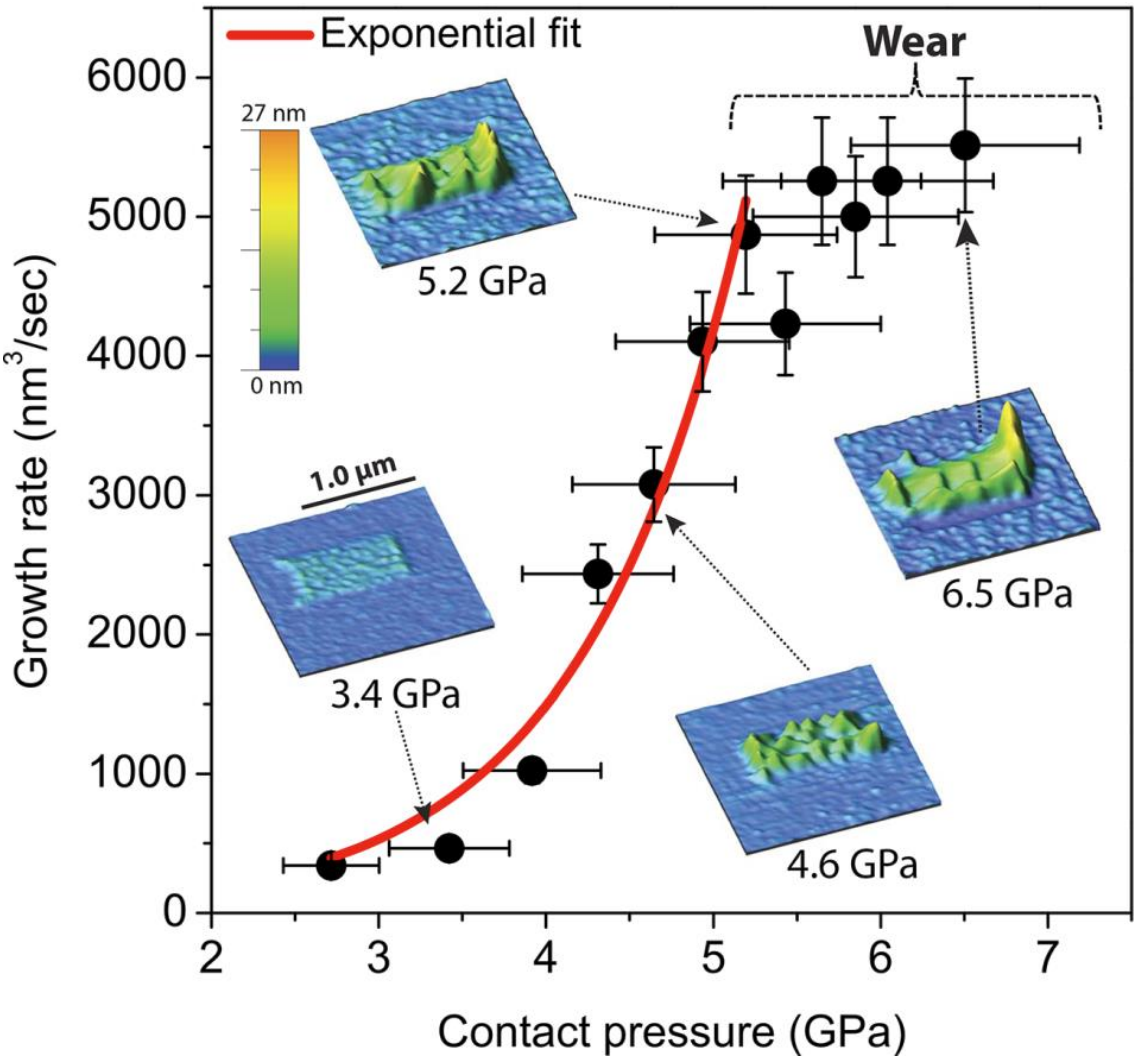


Figure 1–3. Tribofilm volumetric growth rate dependence on contact pressure cited from [37].

ZDDP has good anti-wear ability on the one hand, but on the other hand, it leads to a rise in friction under boundary and mixed lubrication [12], [24], [40]. In practical applications in the last century, a large amount of ZDDP was often combined with engine oil in order to improve the protection of sliding components [10]. However, in recent years, with the development of machining and engine material technology and the deepening environmental protection awareness, reducing friction rather than preventing wear has gradually become the focus of research attention.

There are two main hypotheses about the causes of high friction caused by ZDDP tribofilm: the first, high friction is caused because of the rough surface of ZDDP tribofilm [41]; the other, lubricant slips on the glassy ZDDP reaction film surface, preventing the entrainment of lubricant, which in turn causes high friction [10]. Although neither hypothesis has been fully verified, many studies have been conducted on reducing the high friction caused by the ZDDP tribofilm. One of the best-known is the synergistic effect of molybdenum dithiocarbamate (MoDTC) and ZDDP. MoDTC can be decomposed by rubbing to form $MoS_2$, which has a low coefficient of friction

due to its meager shearing resistance [42–46]. The research on MoDTC will be explained in the next sector, but it is evident that reducing friction while retaining the anti-wear properties of ZDDP has become the need of the hour and the research trend.

In the 2010s, as the latest low-viscosity specifications were curated, there was a surge in demand for additive designs that offered better interfacial protection under boundary lubrication while reducing friction. This was one of the motivations for this research. On the other hand, research on ZDDP has proceeded to a new stage. The research on ZDDP tribofilm has been limited by SLIM, and most of the research on ZDDP tribofilm was under sliding-rolling friction [10]. In pure sliding reciprocating friction tests, although previous studies have confirmed the performance of ZDDP on anti-friction and anti-seizure, there is a great lack of research on how ZDDP films are formed under sliding conditions. Shimizu and Spikes published two articles in 2016 that illustrated the properties of ZDDP films under different rolling-sliding rates [47–48]. The rate of ZDDP tribofilm formation was approximately the same at different rolling rates. However, wear of the contact area was observed in pure sliding. As shown in Figure 1–4, ZDDP forms an S-rich film on the contact area; however, this film becomes enriched in Zn and P with proceeded sliding. These findings suggest that in sliding conditions, ZDDP first exerts its extreme pressure properties and therefore has more S in the film composition; as the experiment proceeds, P demonstrates its wear resistance in the gentler friction condition [48]. These two studies also indicate that ZDDP forms tribofilms with different compositions in different contact conditions. The discussion on ZDDP tribofilms formed in boundary lubrication conditions is still insufficient.

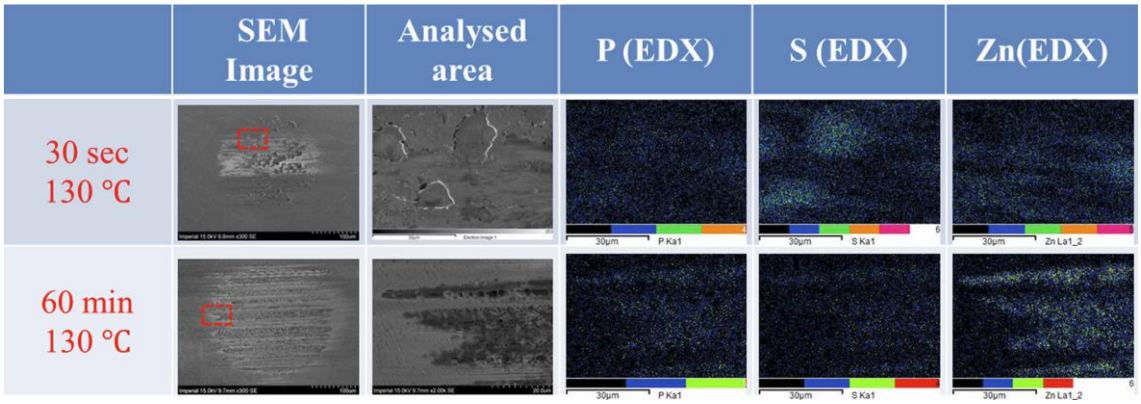


Figure 1–4. Intensity results of elements using SEM–EDX after 30 seconds and 60 minutes at 130°C, cited from [47] and modified.

## 1.3 Friction Modifier (FM)

In the review paper by Spikes, FM was divided into four main categories, which are generally accepted, namely organic friction modifiers (OFM), soluble Mo-containing compounds,

functional polymers, and nanoparticles [5]. Of these, functional polymers and nanoparticles have only recently been shown to have friction-reducing effects but are not yet used widely in industry. In contrast, OFM has a long history, dating back to the 1920s [49–50].

The discovery of OFM began when lubricants defied the Reynolds equation, which states that viscosity is the only governing factor of friction [5]. In practical scenarios, lubricants containing vegetable or animal fats gave lower friction than mineral oils. Adding vegetable fats to mineral oils was also found to reduce the coefficient of friction in later studies, which at the time attributed it to the wetting effect of the oiliness agent [51]. More friction reduction mechanisms were proposed in subsequent studies, such as Hardy's monolayer theory [52], Bowden and Tabor's development of the monolayer theory [53], and Allen's multilayer theory [54], but these theories did not adequately explain the friction reduction principle of OFM. Although it is generally accepted that OFM reduces friction by forming an adsorbed film at the friction interface, and the monolayer theory can be adequately verified by the Langmuir–Blodgett (LB) film method [55], there is no evidence in practical scenarios that OFM spontaneously forms a monolayer film at the sliding interface.

Another class of frequently discussed FMs is Mo-containing compounds represented by MoDTC and molybdenum dialkyl dithiophosphate (MoDDP). In contrast to OFM, the mechanism of MoDTC lubrication is well-defined. As mentioned above, it is widely believed that MoDTC forms $MoS_2$ by rubbing, which can effectively reduce friction because of its meager shear resistance [42-46]. In addition, because ZDDP promotes the formation of $MoS_2$, MoDTC is often used with ZDDP, and its synergistic effect has become the focus of many studies [56–59]. In this sector, the authors will introduce Mo-containing compounds and several representative OFMs, respectively, and their effects on ZDDP.

### 1.3.1 Mo-containing compounds

Previous studies have reported that both MoDTC and MoDDP exhibit high friction coefficients at the beginning of friction tests, followed by a sudden drop in coefficient of friction as shown in Figure 1–5 at specific cycles [60–61]. The sudden drop in the coefficient of friction is related to the formation of $MoS_2$, and the concentration and purity of MoDTC may affect its tribological performance [61]. In the 1980s, Yamamoto established a link between the drop in the coefficient of friction and $MoS_2$ formation through the XPS technique [60], [42]. Subsequent studies have observed the presence of $MoS_2$ nanosheets at the frictional interface by TEM, and AFM has confirmed its low lateral force [62–65]. However, Mo oxides such as $MoO_2$ and $MoO_3$ are also produced along with $MoS_2$ formation, and $MoS_2$ may also oxidize to $MoO_3$ [66].

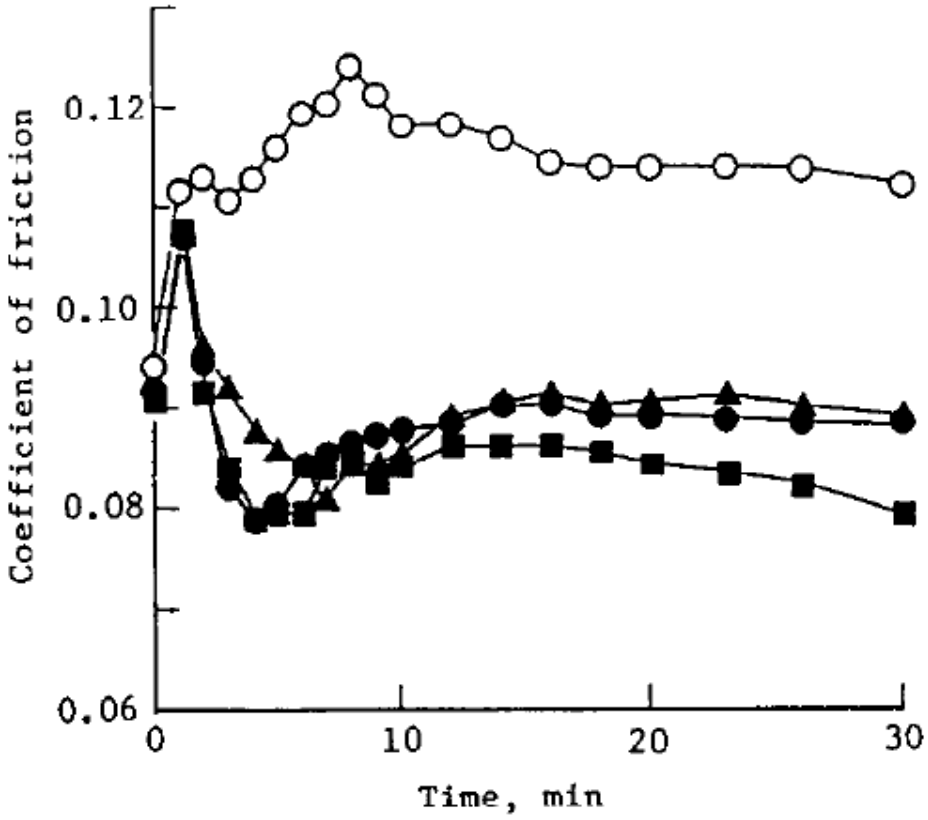


Figure 1–5. The sudden drop in coefficient of friction with MoDTC-containing oils (legends in black), cited from [60].

Most studies suggested that a mixture of MoDTC and ZDDP shows synergistic effects in friction reduction and wear resistance [67–71], and the process is shown in Figure 1-6. However, as reported by Morina et al., the ZDDP/MoDTC ratio affects the tribological performance considerably, and the result suggested that the mixture may restrict the anti-wear property from ZDDP or the friction-reducing property from MoDTC [72]. Although the mechanism has not been fully proved, it is generally believed that ZDDP can provide sulfur atoms that promote $MoS_2$ formation while reducing the formation of high-friction sulfides [56-59].

On the other hand, the tribofilm of ZDDP can encapsulate the high-friction molybdenum oxide [69]. However, the tribological performance of MoDTC as a reactive additive is limited by temperature and friction conditions [73]. First, when MoDTC is used alone, it is difficult to observe a reduction in the coefficient of friction below 60 °C. Secondly, when MoDTC and ZDDP are used together, the temperature affects the ratio of MoDTC- to ZDDP-derived components in the tribofilm, and when the percentage of ZDDP-derived components is higher, the friction-reducing effect is limited [73]. In addition, since the $MoS_2$ formation reaction is considered autocatalytic [61], it takes time to form, leading to an increase in the coefficient of friction and wear during the early stages. In light of the recent trend to reduce lubricant viscosity and the

introduction of hybrid cars, additional additives are needed to provide oil film retention and protect the friction interface without additional tribological chemistry reactions to be effective. OFM is one kind of additive that has these effects.

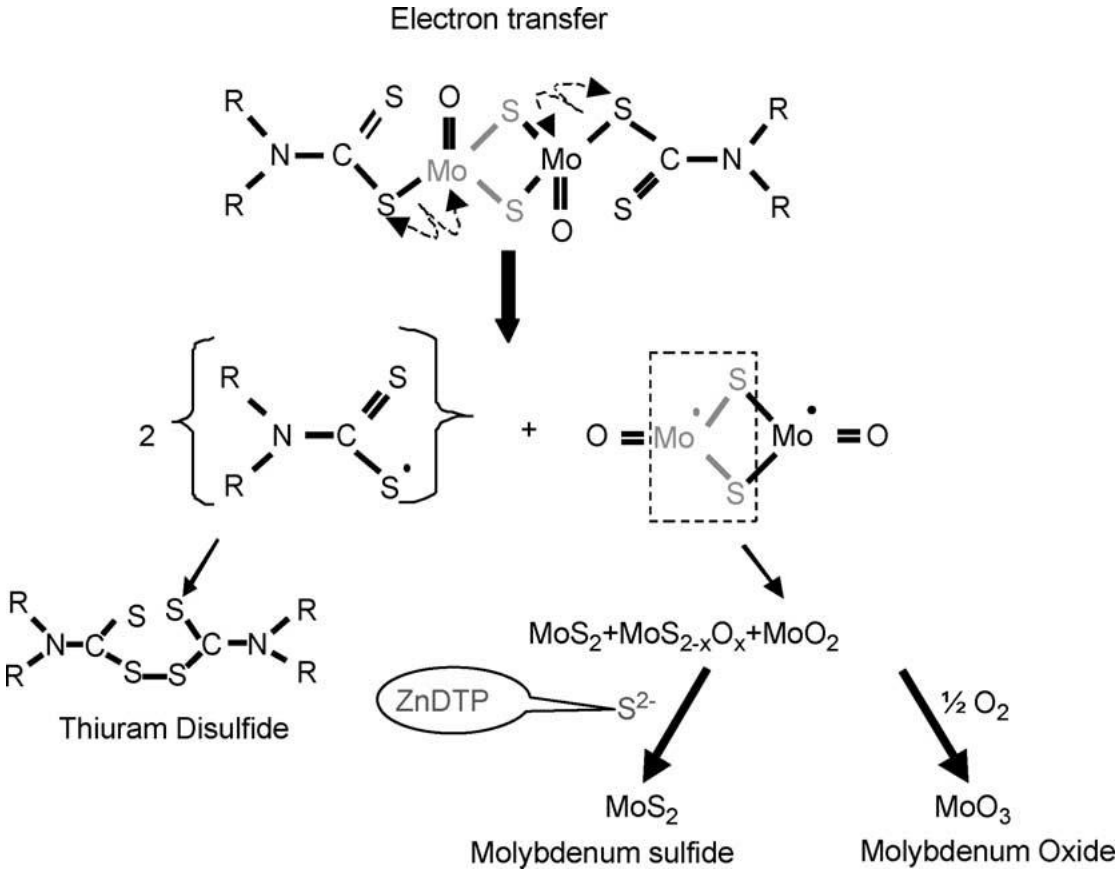


Figure 1-6. The chemical process of the $MoS_2$ formation from MoDTC and the ZDDP-MoDTC synergy, cited from [58].

### 1.3.2 Organic friction modifier

The research on OFM is much less than that on ZDDP. For the convenience of explanation, the authors divide the commonly used OFMs into two categories. The first category is OFM, with a single functional group, such as fatty acids containing carboxyl groups, amines, and amides containing amino groups. The second type is substances with multiple functional groups, such as glycerol monooleate (GMO) and N-oleoyl sarcosine (NOS). Of course, molecules such as alcohols and esters are also OFMs, but they are not discussed in this paper.

The fatty acids are the first OFMs. Representative fatty acids, such as oleic acid, stearic acid, palmitic acid, are corrosive and can react with bearing metals, causing severe corrosion [74–75]. Therefore, in practical scenarios, OFM is more amines, amides, or substances with multiple functional groups. However, this does not prevent fatty acids from being studied as model OFM.

Unlike ZDDP, the monolayer adsorption film of fatty acids is very thin, making it difficult to observe them directly. The history of research on fatty acids will be presented in Chapter 2, and in this chapter, the authors directly summarize the current understanding of fatty acids. First, as with most OFM, the polar carboxyl groups in fatty acids spontaneously adsorb to the metal surface, forming an adsorption film. The concept of the monolayer was proposed by Hardy and Bowden with intimate solid surface contact, as shown in Figure 1–7. This monolayer reduces friction because the alkyl groups on the surface of the adsorbed film slide more easily [5]. Many experiments have examined the monolayer film and its friction-reducing effect. However, for the same fatty acid metal soap and itself, the coefficient of friction may be different despite the fact that the sliding surfaces are tightly packed with alkyl tails [76–77].

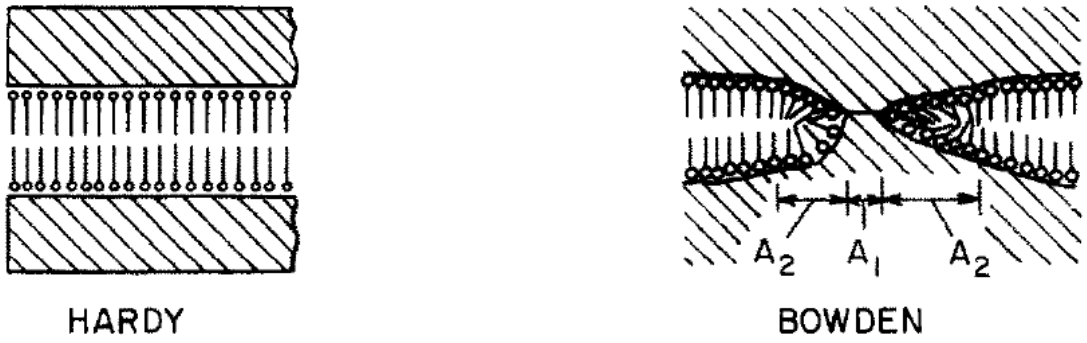


Figure 1–7. The concept of monolayers by Hardy and Bowden, cited from [54].

In this regard, it has been suggested that fatty acids may reduce friction by forming metal soaps in addition to forming monolayers. Soap-based films formed by fatty acids can also be seen in some real engineering contacts. However, their effect on the friction coefficient, their formation conditions, have not been thoroughly investigated. An important reason for this is the lack of suitable observation means. Despite the increasing development of Surface Forces Apparatus (SFA), AFM, and other techniques, simultaneous in-tribo determination of film thickness and analysis of film composition has not yet been achieved.

Another issue regarding fatty acid research is that, in most cases, lubricants contain anti-wear agents [10]. However, the interaction of fatty acids and antiwear additives is not clear. Amines have similar friction-reducing properties to fatty acids, except for functional groups' differences. Most studies have concluded that fatty acids and amines are more effective at reducing friction on iron surfaces than other OFMs, which suggests a stronger or closer adsorption film by these molecular [78]. Another characteristic of amines is that when combined with ZDDP, amines can convert the neutral ZDDP to the basic salt of ZDDP [79]. In ZDDP-amine mixtures, most amines can act synergistically with ZDDP to form tribofilms with lower friction coefficients while maintaining their antiwear properties [80–84]. Moreover, a recent study suggested that amine can

prevent the micro pitting wear caused by ZDDP [83]. However, most studies have reported that amines have the effect of removing the pre-formed ZDDP tribofilm, which may cause the destruction of the ZDDP tribofilm and thus wear and destruction [35], [85].

GMO is more commonly used in actual motor oil applications than fatty acids or fatty amines [5]. GMO consists of an unsaturated oleic acid tail linked to an ester group and two alcohol groups, as shown in Figure 1–8. It is believed that GMO can break down during rubbing to release oleic acid and reduce friction by forming an adsorbent film or metal soap [86–87]. A study has shown that GMO shows a friction coefficient close to that of oleic acid in the metal-polymer interface [88], corroborating the mechanism that GMO produces oleic acid by decomposition. However, it has also been shown that GMO can be effective in reducing friction at high temperatures, which is the exact opposite of oleic acid, which produces higher friction at high temperatures [89–90].

Another reason for the interest in GMO is their effectiveness in reducing the friction of tetrahedral amorphous carbon diamond-like carbon (ta:C DLC). It is believed that the glycerol in GMO reacts with the ta:C surface to form OH groups, and the low energy of these groups, combined with the high hardness of ta:C, results in very low friction [91]. In addition to studies on GMO themselves, many studies have explored the synergistic effects of GMO and ZDDP. In 2003 Talyor and Spikes investigated the frictional behavior of GMO-ZDDP mixtures under mixed lubrication [40]. The results showed that the GMO-ZDDP mixture exhibited a low coefficient of friction under mixed lubrication; however, the coefficient of friction suddenly increased and exceeded that of the ZDDP lubrication as the friction test proceeded. In addition, the tribofilm formed by lubrication with the GMO-ZDDP mixture is thinner and has a smoother surface compared to the ZDDP tribofilm [40]. Recent studies have focused more on the frictional properties of GMO-ZDDP mixtures under boundary lubrication. Tasdemir, Okubo, et al. have investigated the friction and wear of GMO+ZDDP lubricated surfaces of different materials; however, none of these studies were able to determine the existence of synergy between the two additives [92–95].

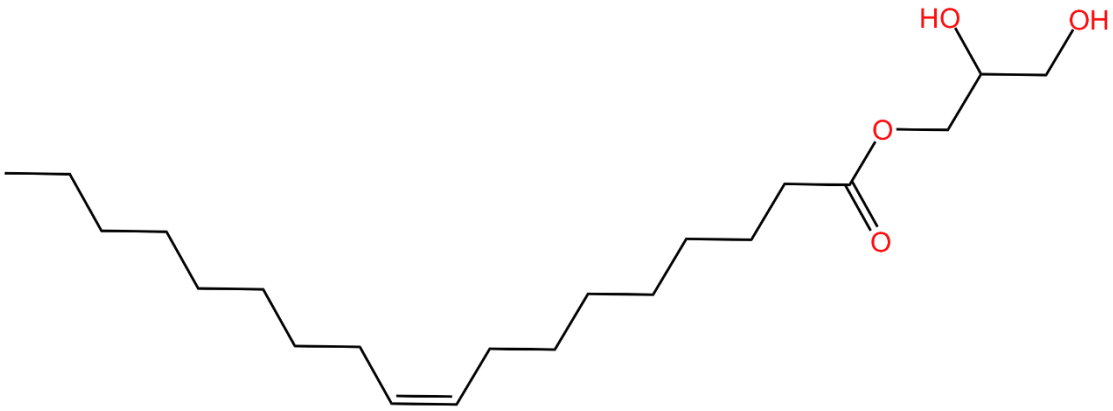


Figure 1–8. Molecular structure of GMO.

Another OFM of interest to the authors is the N-oleoyl sarcosine (NOS). NOS has a long history as a lubricant additive, which was used as a rust inhibitor [96–97] until a recent study reported its potential as a friction-reducing additive [98]. By construction, as shown in Figure 1–9, the sarcosine head can form a chelate-like configuration with the metal, which is very much in line with the design ideas for OFM, as chelation enhances the adsorption of molecules [5]. On the other hand, the oleic tail can isolate the friction surface, increasing the solubility, providing sufficient protection to the surface, and reducing friction. However, NOS is not well studied and discussed at present.

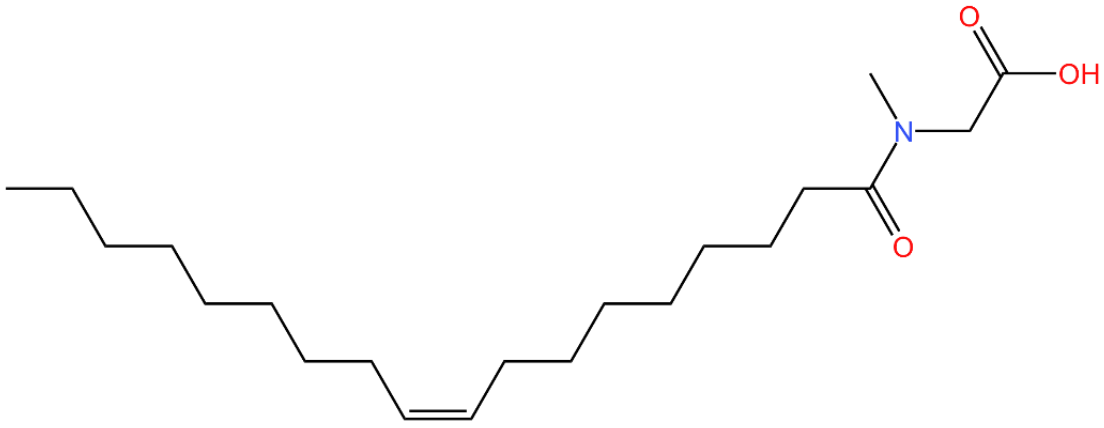


Figure 1–9. Molecular structure of NOS.

## 1.4 Research Direction and Research Objectives

The anti-wear additive ZDDP and several friction modifiers were introduced in the previous sections, respectively, and many studies have revealed their properties and mechanisms. Yet, many issues have to be addressed. The authors summarize several issues of interest as follows.

1. High friction of ZDDP

While earlier studies have suggested that ZDDPs cause high friction only in mixed lubrication, more recent studies have found that ZDDPs may also cause high friction in boundary lubrication depending on their alkyl configuration. As the lubricant viscosity decreases, the frictional components in the engine are more likely to migrate to the boundary-mixed lubricated condition. It is urgent to solve the problem of high friction in ZDDPs from the perspective of fuel economy and engine longevity.

2. Anti-wear mechanism of ZDDP under boundary lubrication condition

In sliding-rolling experiments, the SP ratio in the ZDDP film was up to 8:1. However, in pure sliding experiments, the S component of the film decreased as friction proceeded, while the P component increased. It is noted that ZDDP exerts its anti-wear effect more in pure sliding than in extreme pressure in sliding and rolling. However, the discussion of the anti-wear mechanism of ZDDP under boundary lubrication is minimal so far.

3. Adsorption and friction performance of friction modifiers

Although many studies have investigated the friction-reducing effect of monolayers through techniques such as LB films, the situation at the solid-liquid interface and *in-lubrication* is quite different. In solutions containing additives, do additive molecules form similar adsorption films? If possible, how do their adsorption films behave with respect to friction? The answers to these questions are not yet known.

4. The effect of friction on the action of additives

ZDDP can form tribological films by friction, and many studies have verified and proposed the mechanism. However, for OFM, the effect of friction on its tribological effect has not been adequately discussed.

5. Synergistic effect of friction modifier and anti-wear agent

Along with the reduction in oil viscosity, recent research has focused on reducing friction as much as possible while maintaining anti-wear. In this context, in addition to the MoDTC-ZDDP mixture, OFM needs to be added to increase the protection of the friction surface, reduce the boundary film rub and improve the oil film retention. However, the current discussions on the synergistic effect of OFM and ZDDP focus on GMO. At the same time, there is not enough experimental evidence to prove the synergistic effect of GMO with ZDDP. In addition, the synergy between NOS, a molecule that can form a chelate-like structure, and ZDDP has not been fully discussed.

With these questions in mind, the authors designed this study. In this study, the authors divided

the process for additives to exhibit tribological properties into three stages. First, the additives in solution form an adsorbed film on a sliding surface. Second, rubbing leads to the formation of some tribofilm from the adsorbed film. Third, the tribofilm shows its frictional properties. In this paper, the authors have selected oleic, stearic, and palmitic acids as model OFMs and NOS as practical OFM to discuss each of these three stages. In Chapter 2, this study investigates the relationship between adsorbed film formation and friction of additives in combination with Neutron reflectometry (NR) and AFM. In Chapter 3, AFM was employed to rub the iron surface, and friction experiments were conducted on the rubbed area at different contact pressures. In Chapters 4 and 5, the authors verified the results of Chapters 2 and 3 with macroscopic experiments, evaluated the synergistic effect of NOS and ZDDP in terms of both friction reduction and wear resistance, and proposed the synergistic mechanism. In Chapter 6, a summary is made.

# Chapter 2. Relationship between the interfacial adsorption of additive molecules and the reduction of friction coefficient

## 2.1. Introduction

Surface adsorption is the first step for an additive to exhibit some tribological effect. Surface adsorption can be divided into physical adsorption and chemisorption. Physical adsorption is dominated by van der Waals forces and is susceptible to factors such as temperature because its interaction energy is very weak. In contrast to physical adsorption, chemisorption involves the formation of new chemical bonds between the additive and the adsorbate material [99]. This chapter will focus on the chemisorption of fatty acids on metal surfaces.

As shown in Figure 1–6, Hardy and Bircumshaw proposed a conception of boundary lubrication by monolayer adsorption in 1925 [52]. Bowden and Tabor developed this conception and proposed a new model to complement the situation where asperity contact occurs on sliding surfaces [53]. This model shows that the monolayer supports the normal load within the asperity in the contact area. Later, Allen proposed a multilayer model in which fatty acids such as stearic acid align themselves parallel to the adsorbed surface through mutual interactions [54]. However, the sliding surface damage observed in boundary lubricants suggested that the reduction in friction is not only due to sliding between single or multiple layers [100]. Furthermore, although LB film studies revealed that a single monolayer could reduce friction, continuous lubricant replenishment is indispensable [55].

Bowden, Gregory, and Tabor thus proposed a boundary lubrication mechanism by metallic soaps [100]. They concluded that fatty acids are more effective at higher temperatures or heavier loads, that they react actively with metals to form metal soaps, and that soap films are responsible for reducing boundary friction. However, although the above models and mechanisms, with a large amount of experimental data, suggested that polar molecules do play a role in boundary friction reduction, the boundary lubrication film theory was still controversial because there was no suitable method to measure the adsorption film quantitatively.

In 1997, Fischer, Hu, and Hsu studied the adsorption of stearic acid on copper by X-ray adsorption spectroscopy [101]. They proposed that stearic acid adsorbs on copper by interacting with copper oxide. They also proposed that friction chemically converts stearic acid monolayers to cupric stearate. Their study deepened the understanding of boundary lubrication films. However, it is essential to mention that this study was not performed in situ, i.e., the stearic acid was not dissolved in a solvent. Efforts were made to "directly" observe the adsorbed layers formed

by OFM additives starting in the late 1990s [5]. The most representative techniques are SFA, QCM, ellipsometry, and AFM.

Tabor and Winterton first designed the SFA to measure the force between two surfaces interacting [102]. It uses the principle of the spring and measures the spring's displacement precisely with an optical interferometer that can achieve a high resolution of 0.1 nm for a distance and 10 nN for a force. SFA studies were mainly carried out on the surface of mica or cobalt to ensure optical interference. Previous SFA studies have observed monolayer formation of saturated OFM on their surfaces. More recently, SFA has enabled the measurement of shear forces through piezoelectric sliders, which might be used to measure friction between adsorbed films [103].

Unlike SFA, QCM applies an entirely different principle altogether. QCM quantifies the mass of substances adsorbed on the sensor surface at the nanogram level. Fry reported on the adsorption of various amines and acids, and the results showed that saturated linear chains give thicker adsorption films [104]. He also applied the same additives to Ellipsometry, and the results correlated with those of QCM. While these techniques have been successful for in situ measurements of boundary films, liquid cell AFM is impressive through its "direct observation" of boundary films. Campen used liquid cell AFM to observe a mica surface immersed in a fatty acid solution [105]. As shown in Figure 2–1, the injection of the stearic acid solution resulted in the formation of irregular islands. The islands were about 1.6 nm thick and had a lower lateral force than the inter-island regions. In contrast, the injection of oleic acid solution led to globular films of varying sizes and thicknesses, possibly due to its cis-bond structure that limits the formation of close-packed monolayers.

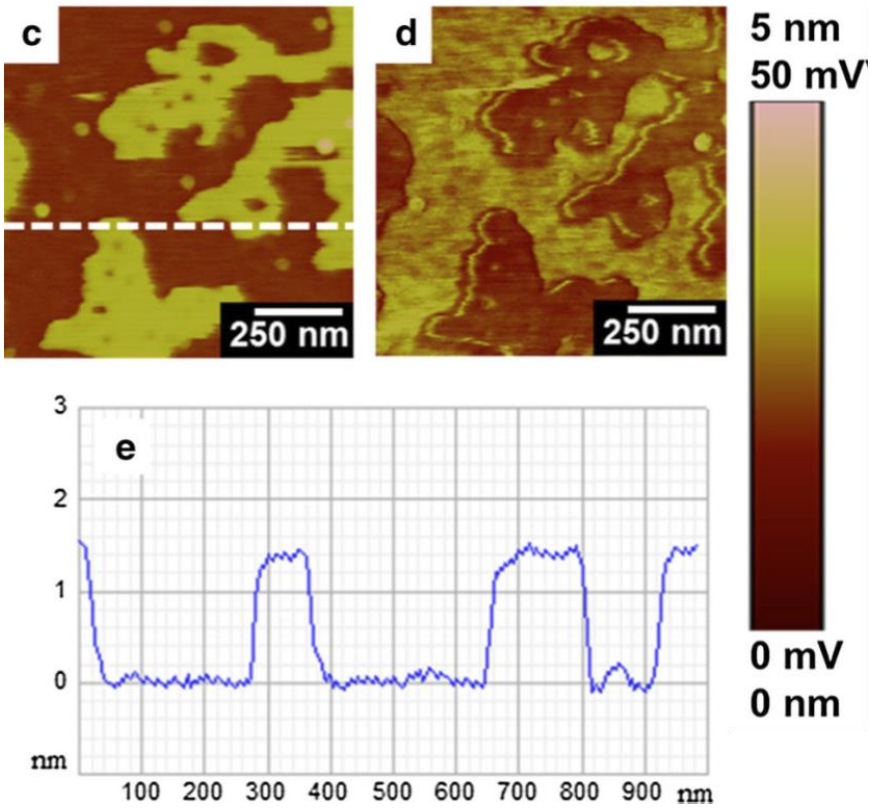


Figure 2–1. Contact mode AFM height (c) and simultaneously obtained lateral force (d) images of 0.001M stearic acid solution in hexadecane on mica surface, cited from [105] and modified.

Looking back at the studies on boundary lubrication film, from the simple monolayer theory to the realization of a "direct observation" of the fatty acid adsorption layer, we have gained a deeper understanding of OFM adsorption. However, these studies were conducted on a single OFM, whereas, as explained in Chapter 1, figuring out the interactions between additives is the need of the hour. In additive mixtures, different additive adsorption forms may occur. For example, as shown in Figure 2–2, a) only one additive in the mixture is adsorbed, or b) two additives are adsorbed in a specific ratio, or c) reactions occur between additives leading to the creation and adsorption of new substances, or d) the formation of a complex between additives leading to a decrease in adsorption.

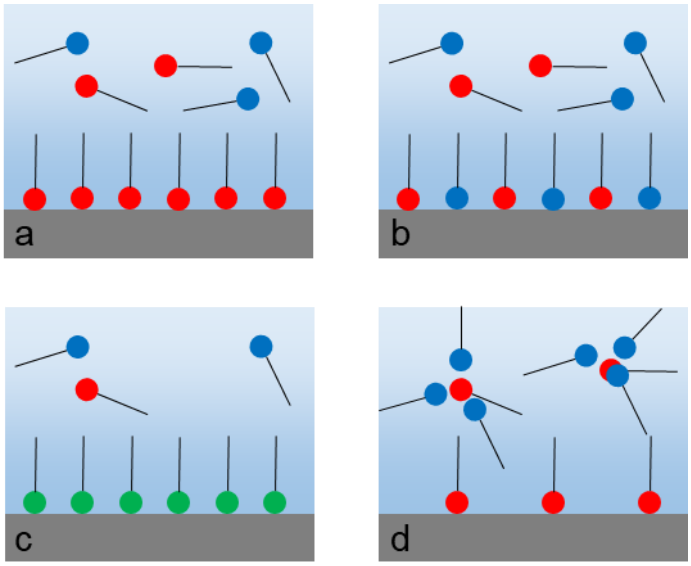


Figure 2–2. Different additive adsorption forms in an additive mixture.

NR was used in this study to measure additive adsorption. NR is a technique that measures the depth structure near the surface of a material. NR provides information on the thickness, density, composition, and roughness of layers near the surface with nanometer accuracy. NR has also been used to determine the thickness and density of the additive layer adsorbed at the liquid-solid interface. T. Hirayama measured the acetic acid adsorption on the metal surface, which suggests that they form a homogenous layer as thin as 2 nm on the metal surface [106]. N. Yamashita has used NR to determine the adsorbed layer thickness of a highly-swollen Polymer FM. The results suggested that the layer thickness was three times larger at 100°C than at 23°C [107].

In the case of neutron scattering, the interaction intensity is determined by a quantity called the scattering length density (SLD). Each atom, cluster, or molecule possesses its unique scattering length, from which the SLD of a particular material can be calculated. The difference in the SLD is used to calculate the scattering amplitude. In this study is the thickness and density of the adsorption layer. More than many previously mentioned methods, NR can be used to observe the adsorption properties of a single additive in the mixture by deuterating it to greatly increase its SLD, distinguishing it from other components in the solution. In the current manuscript, NR is used to determine the thickness and density of the adsorbed OFM layer on metal surfaces with OFM solution alone or the mixture of OFM and ZDDP solution.

On the other hand, this study used AFM to measure the friction force to elucidate the relationship between adsorption film and friction. AFM is a scanning microscope that can examine surface topography by scanning the surface of a substrate with a tip attached to the free end of a small flat plate called a cantilever and detecting its warpage and vibration. In the contact mode LFM, the vertical load on the tip is detected as deflection (signal in the vertical direction on the detector),

and the horizontal friction is detected as torsion (signal in the horizontal direction on the detector). The friction force can then be calculated from its observed amount.

This chapter focuses on the surface adsorption of additives and their frictional behavior, and the aim is to clarify the relationship between them. First, friction tests were performed with the lubrication with OFM solutions and OFM-ZDDP solutions, after which we performed in-situ observations on OFM adsorption using NR.

## 2.2 Experimental

### 2.2.1 Testing oils

In this study, Poly-α-olefin (PAO4, $C_{10}H_{21}(C_{10}H_{20})_nH$, ENEOS Corporation) was used as the base oil (BO). PAO is a fully synthetic carbon-hydrogenated polymer with a composition similar to mineral oils but with a higher viscosity index and lower flow point for use in a wide temperature range. They are actively used in various industrial lubricants, including advanced engine oils. Fatty acids were used as model OFMs. Three kinds of fatty acids were compared in this study, saturated fatty acids, stearic acid (STA)and palmitic acid (PLA), and unsaturated fatty acid oleic acid (OLA). In addition to the model OFM, a practical OFM additive was tested in this study, which is the NOS introduced in Chapter 1. They were added to BO or BO containing ZDDP (Secondary type, R=$C_4H_9$), respectively. The above additives' molecular structures are shown in Figures 2–3 (STA, PLA, and OLA) and Figure 1–8 (NOS). The specific addition concentrations are shown in Table 1.

Deuterated fatty acids were used to achieve a good contrast of SLD in the NR measurements. The concentration of deuterated fatty acids was the same as that used in the friction measurement. The deuterated material of NOS is unavailable, so only the adsorption of model OFM was tested in this study, and the adsorption properties of NOS were inferred from it.

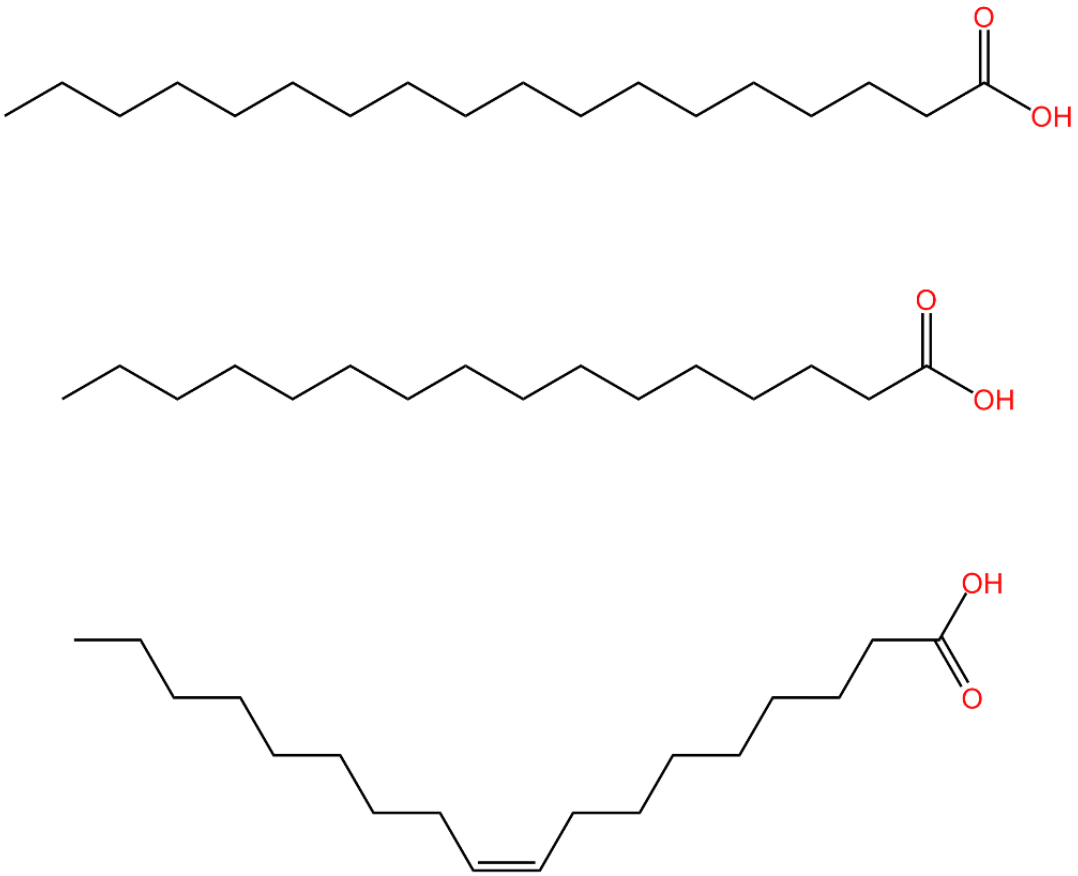


Figure 2–3. Molecular structures of STA, PLA and OLA.

Table 2–1. Lubricating oil mixtures

| **Base oil + additive(s)** | **Content** | **Measurement** |
|---|---|---|
| BO | PAO4 | Friction |
| BO+ZDDP | ZDDP (P 700 ppm) in PAO4 | |
| BO+OLA | OLA (0.1 wt%) in PAO4 | |
| BO+OLA+ZDDP | ZDDP (P 700 ppm) and OLA (0.1 wt%) in PAO4 | |
| BO+STA | STA (0.1 wt%) in PAO4 | |
| BO+STA+ZDDP | ZDDP (P 700 ppm) and STA (0.1 wt%) in PAO4 | |
| BO+PLA | PLA (0.1 wt%) in PAO4 | |
| BO+PLA+ZDDP | ZDDP (P 700 ppm) and PLA (0.1 wt%) in PAO4 | |
| BO+NOS | NOS (0.1 wt%) in PAO4 | |
| BO+NOS+ZDDP | ZDDP (P 700 ppm) and NOS (0.1 wt%) in PAO4 | |
| BO+d-OLA | d-OLA (0.1 wt%) in PAO4 | Neutron reflectivity |
| BO+d-OLA+ZDDP | ZDDP (P 700 ppm) and d-OLA (0.1 wt%) in PAO4 | |
| BO+d-STA | d-STA (0.1 wt%) in PAO4 | |
| BO+d-STA+ZDDP | ZDDP (P 700 ppm) and d-STA (0.1 wt%) in PAO4 | |
| BO+d-PLA | d-PLA (0.1 wt%) in PAO4 | |
| BO+d-PLA+ZDDP | ZDDP (P 700 ppm) and d-PLA (0.1 wt%) in PAO4 | |

### 2.2.2 Friction force measurement

#### 2.2.2.1 AFM Principles and Apparatus

As mentioned above, an AFM is a scanning microscope that can examine surface topography and other features by attaching a probe to the free end of a tiny cantilever and scanning the substrate surface while detecting its warping and vibration. The basic configuration of an AFM is shown in Figure 2–4.

The laser light is reflected from the back of the cantilever, redirected by the mirror, and then enters the photodetector. The AFM can be operated in two main modes: contact mode and dynamic mode. In contact mode, the surface is scanned with feedback control in the height direction so that the warp of the cantilever is constant, i.e., the force acting between the cantilever and the substrate is constant. A four-segment photodetector is often used in an AFM. In contact mode LFM, vertical loads and horizontal frictional forces are applied to the tip, which is detected as deflection in the upper and lower detectors and as torsion in the left and right detectors, respectively. In other words, the surface morphology and the frictional force can be measured simultaneously. In addition, scanning with the LFM makes it possible to perform sliding with a constant force. This study conducted surface profile observations and friction force measurements using LFM. The AFM used in this study is SPM-9700 (Shimazu).

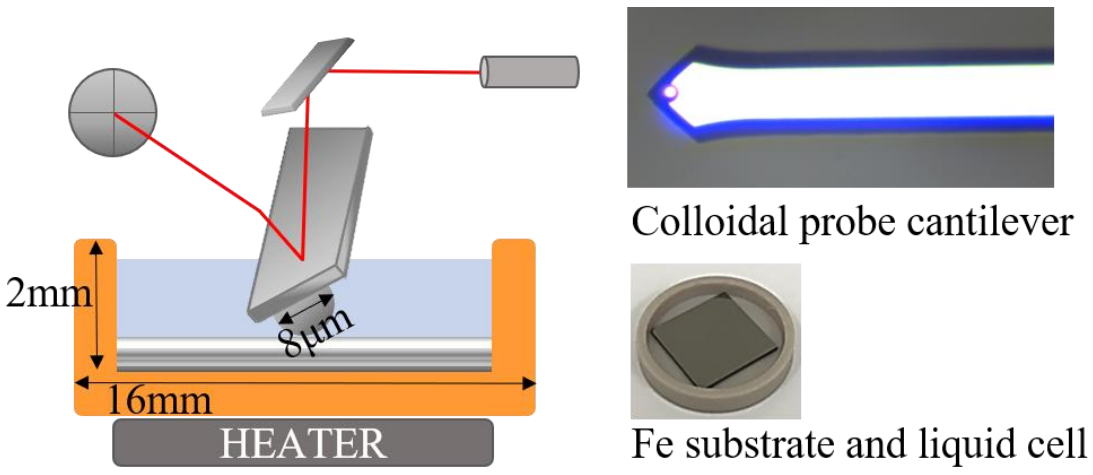


Figure 2–4. Left: Schematic illustration of AFM, right: cantilever and substrate

The AFM can apply a variety of probe cantilevers, the common being the point probe. Its needle tip is sharp with a tip size of several tens of nanometers, allowing clear surface morphology to be obtained. However, because repeated scanning causes tip wear, the contact area between the tip and the substrate surface cannot be determined, making the friction experiment much less reproducible.

On the other hand, the colloidal probe is a cantilever to which a spherical colloidal particle with a diameter of a few microns is attached rather than a sharp needle tip. Therefore, the contact area can be determined, thus solving the problem of the point probe. For these reasons, the colloidal probes were used in this study. The colloidal probes were hand-made by attaching an 8-μm $SiO_2$ spherical particle to each tip-less cantilever (TL-FM, NANOSENSORS). Preliminary experiments were conducted to confirm the effectiveness of the self-made colloidal probes.

#### 2.2.2.2 Materials and procedure

The friction tests were performed on Fe layers sputtered on silicon wafers (<001>) with a DC sputter machine. The total layer thickness was about 150 nm. The original surface roughness of the wafers was about 0.05 nm Ra, as measured with the AFM colloidal probes. After the Fe sputtering, the surface roughness was about 0.5 to 0.6 nm Ra.

Friction measurements were conducted at 25°C and 100°C under various contact pressures. The lubricating oils were dropped onto each substrate and kept at the test temperature for 10 minutes before measurement. Friction force was measured with the substrate immersed in oil.

The force curve between the probe and the substrate was first measured with an AFM colloidal probe. The force curve is a graph that plots the forces between the probe and the substrate as the probe is moved up and down toward the substrate surface. When the cantilever is approached from a distance from the substrate, the initial downward deflection is caused by the gravitational force, followed by an upward deflection when the cantilever contacts the substrate, and a further approach is made. When the cantilever is moved straight upwards to the substrate surface, the adhesion force between the tip and the substrate causes a downward deflection. The cantilever returns to the horizontal position when the upward force due to deflection exceeds the adhesion force. Afterward, the Hertzian contact pressure was calculated from the force curves.

The friction stroke was 5 μm, measured every 25 MPa from 175 MPa to 300 MPa at 25°C and every 25 MPa from 200 MPa to 300 MPa at 100°C. The sliding speed during the friction measurements was 10 μm/s. The measurement was performed six times and averaged at each contact pressure. All tests were repeated at least three times to confirm reproducibility.

### 2.2.3 Surface adsorption of additive molecules

#### 2.2.3.1 NR Principles and Experimental Facilities

Neutrons are particles that make up the nucleus, have about the same mass as protons, and are neutral particles with no electric charge. Since they have no charge, they do not interact with the material being observed and can pass through the material for nondestructive observation. Typical

neutron experiments include scattering, spectroscopy, reflection, and transmission, but in this study, we focus on analyzing scattering and reflection to image the structure of interfaces.

NR is similar to X-ray reflection and ellipsometry, which use the principle of light interference. Neutrons have a refractive index that varies with the medium. The refractive index depends on the interaction between neutrons and the medium. The parameter that indicates the strength of the interaction between a material and a neutron is called the SLD. The composition and density of the material determines SLD. On the other hand, if a neutron is made to be incident at a very shallow angle to the substrate surface, it will be reflected at the same angle as the angle of incidence, which is called specular reflection. The probability of specular reflection is called reflectance. However, as shown in Figure 2–5, the presence of a thin film on the substrate causes interference between reflections from the air-side interface and reflections from the substrate-side interface. The interference condition is expressed by the following Equation 2-1.

$$2dn\ sin\theta = m\lambda, \text{ (2-1)}$$

where d is the film thickness, n is the refractive index, θ is the angle of incidence, and λ is the wavelength. The interference condition depends on the wavelength. Therefore, showing the reflectance as an angular dependence is not a good practice.

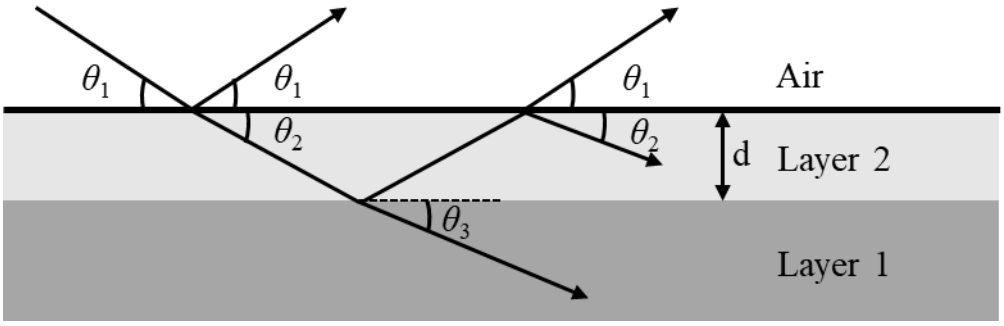


Figure 2–5. Beam reflectance on Air-Solid interface.

By using the scattering vector **Q**, the wavelength dependence of reflectance can be normalized, and the interference condition can be rewritten as in Equation 2-2.

$$Q_z = 2\pi m/d, \text{ (2-2)}$$

Then, the reflectance shows a dependence on $Q_z$. If the film being observed has a different SLD than the underlying material, this will cause amplitude and period variations in the interference. These variations can be analyzed to assess the composition, the thickness, and density of the film.

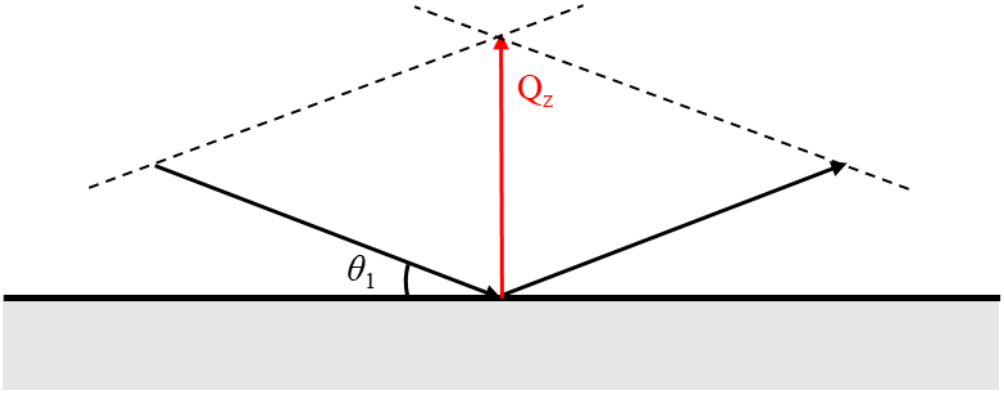


Figure 2–6. Normalization with scatter vector to eliminate wavelength dependence.

In this study, NR measurements were performed at the Materials and Life Sciences Experiment Facility at the J-PARC facility using the SOFIA horizontal neutron reflector, an angularly distributed neutron reflector [108]. SOFIA uses a downward-tilted beam to inject neutrons into a sample that cannot be tilted, such as a gas-liquid interface. The design diagram of the device is shown in Figure 2–7. The wavelength of the neutron line is 0.2-0.88 nm. The incidence angles θ were set to 0.3°, 0.6°, and 1.2°. A reflection profile was obtained by connecting the results of each incidence angle.

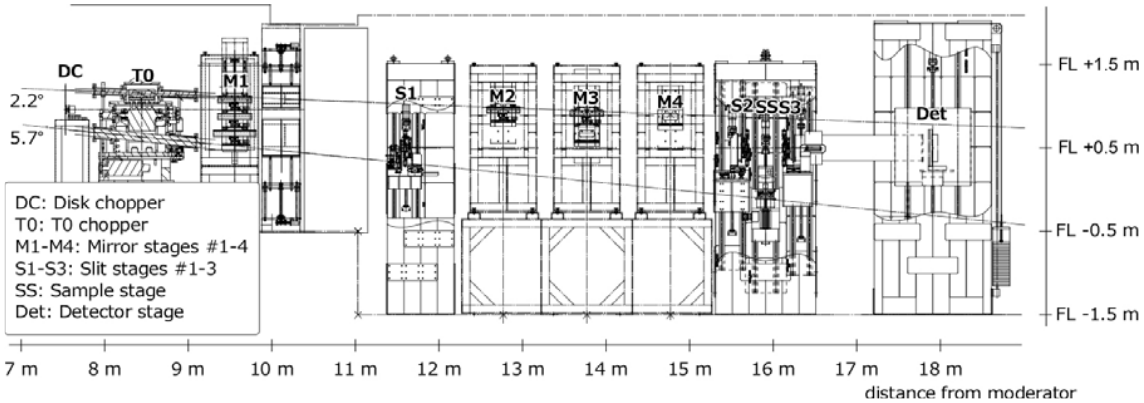


Figure 2–7. The design diagram of SOFIA, quoted from [108].

### 2.2.3.2 Materials and procedures

A schematic of the NR measurement setup and the theoretical SLD values for each layer are shown in Figure 2–8. A silicon block (50 × 50 × t10 mm) sputtered with copper on the surface was chosen as the substrate material for this study. The thickness of the copper film was about 30 nm and was prepared by an ion beam sputtering system (KUR-IBS) [109]. The reason for using a Cu layer instead of a Fe layer is because d-fatty acids show similar adsorption properties on Cu and Fe surfaces, and because Cu is a non-magnetic metal, it is easier to obtain structural analysis results on Cu surfaces than on Fe surfaces. However, Fe has better corrosion resistance due to its lower chemical activity than Cu. The irradiation footprint of neutrons is 40 × 40 mm.

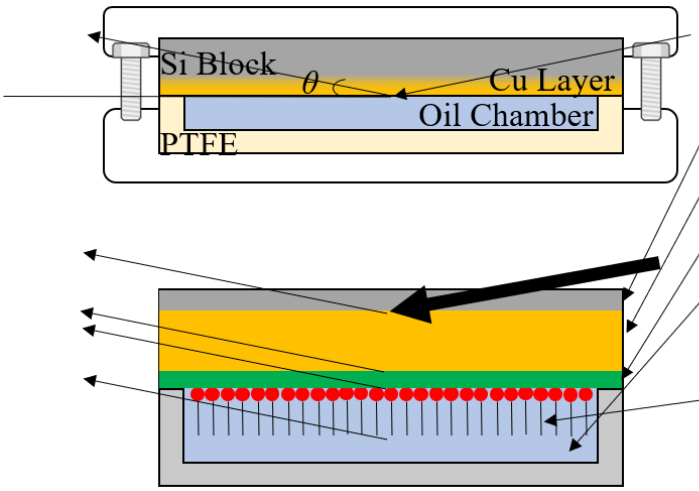


| SLD[Å$^{-2}$×10$^{-6}$] | | |
|---|---|---|
| $SiO_2$ | | 3.47 |
| Cu | | 6.54 |
| $Cu_2O$ | | 5.40 |
| Base oil | | -0.37 |
| d-additive | OLA | 6.81 |
| | STA | 6.98 |
| | PLA | 6.92 |

Figure 2–8. Schematic of NR measurement setup and theoretical SLD values of layers

The measurement and analysis process is shown in figure 2-9. In the measurements, reflectance curves were first obtained from BO only to determine the structure of the Cu layer. Then BO was replaced by lubricating oils with additives (on separate substrates) to obtain the reflectance profile of the adsorbed layer of d-fatty acid. Measurements were performed at 25°C, 50°C, 75°C, and 100°C, starting at 25°C. The test started at each temperature after 10 minutes of temperature stabilization. Each test took approximately 10 minutes. The results were analyzed using the MOTOFIT reflectance analysis package running in the IGOR Pro environment [110]. The reflectance curve of BO was first analyzed to determine the substrate thickness, which is the sum of the thicknesses of the $SiO_2$, Cu, and $Cu_2O$ layers. Once the substrate thickness was determined, the adsorbed layer thickness was analyzed. The adsorption density was calculated by dividing the SLD value obtained from the analysis by the theoretical value.

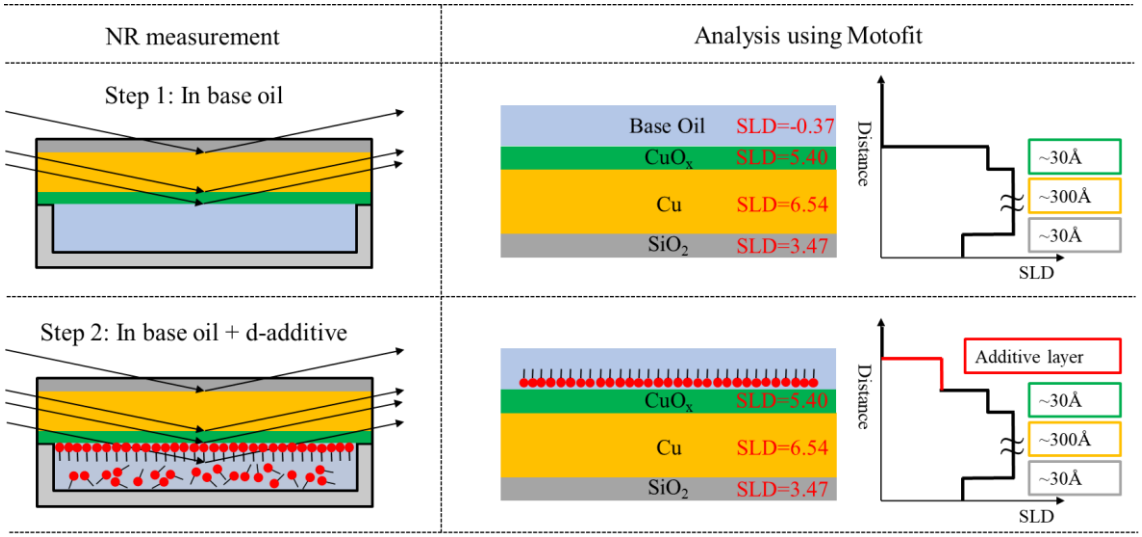


Figure 2-9. Process of NR measurement and analysis using Motofit.

## 2.3 Results

### 2.3.1 Friction coefficient results

The friction coefficients with the lubrication of the above lubricating oils at 25°C are shown in Figure 2–10. The horizontal axis shows the contact pressure calculated according to Hertzian theory. The vertical axis shows the friction coefficient. Note that the vertical axis is disconnected. Adding OFM to BO effectively reduced the friction coefficient. Among them, a significant pressure dependence was seen with the lubrication of BO+OLA, BO+STA, and BO+PLA, i.e., the friction coefficient increased with increasing contact pressure. Although the friction coefficients varied at different surface pressures, generally, they were approximately the same for the three lubricating oils, especially at pressure conditions from 200 to 300 MPa. In contrast, no pressure dependence was seen with PAO+NOS lubrication. The friction coefficient remained consistently around 0.32 at different contact pressures.

When ZDDP and OFM were mixed with BO, the friction characteristics changed noticeably compared to BO+OFM. Among them, the unsaturated OFM and ZDDP mixture showed a synergistic effect, i.e., the friction coefficient became smaller with the mixture. In contrast, the saturated OFM and ZDDP mixture showed antagonistic effects, exhibiting a higher friction coefficient, even higher than that of BO+ZDDP at some contact pressure conditions. In addition, the friction coefficient was no longer dependent on contact pressure with BO+STA+ZDDP and BO+PLA+ZDDP. This suggests that OFM no longer plays a role in reducing friction in the additive mixture oils.

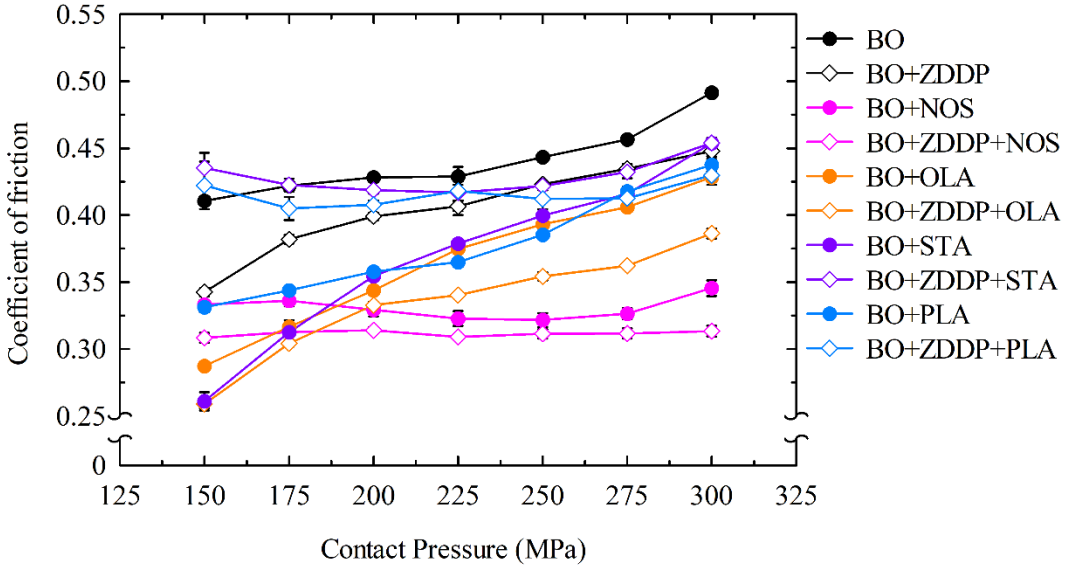


Figure 2–10. Friction coefficients for base oil and oil mixtures at 25°C.

Figure 2–11 shows that the friction coefficient decreased at 100°C for all lubricating oils, including BO. The main reason is thought to be the reduction in viscous resistance due to the viscosity decrease that accompanies the temperature increase. At 100°C, the friction coefficient with the lubrication of BO+STA and BO+PLA was approximate. Moreover, although their mixture with ZDDP was antagonistic at 25°C, it became synergistic at 100°C. Among them, the friction coefficient was lower with BO+STA+ZDDP.

On the other hand, the friction coefficient with BO+OLA at 100 °C was close to that of BO. BO+OLA did not show any friction-reducing properties. Nevertheless, the BO+OLA+ZDDP showed a synergistic effect; that is, the friction coefficient was lower than BO+OLA and BO+ZDDP, although it was higher than the other lubricating oils with additives. The friction characteristics of NOS at 100°C are similar to those at 25°C. Although the friction coefficient is not the lowest, it maintains almost the same friction coefficient at different contact pressures. Furthermore, the BO+NOS+ZDDP consistently exhibits a synergistic effect.

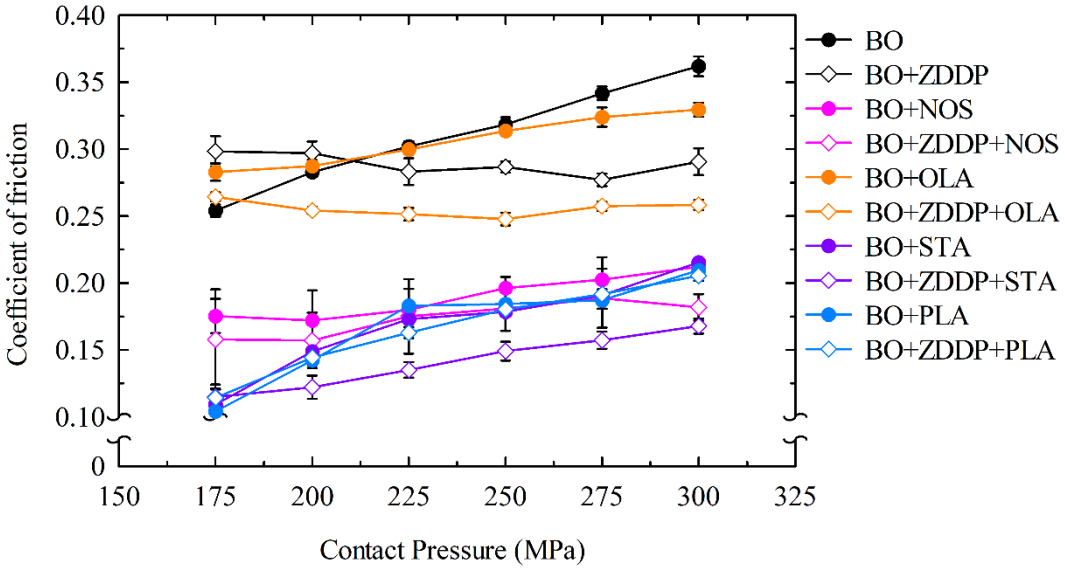


Figure 2–11. Friction coefficients for base oil and oil mixtures at 100°C.

These results above suggest that the friction reduction ability of OFM in BO depends on the temperature, while the additive interaction more influences the friction reduction ability of the OFM-ZDDP mixture. In addition, it is essential to note that when synergistic effects of additive mixtures are observed, such as BO+ZDDP+NOS, BO+OLA+ZDDP at 25°C, or BO+STA+ZDDP at 100°C, the tendency between the friction coefficient and contact pressure of the OFM-ZDDP mixture was similar to that of OFM alone. This suggests that OFMs greatly reduce friction even in these additive combinations.

### 2.3.2 Interface analysis

NR measurements were performed to explain the differences in friction coefficients of different lubricating oils. As mentioned earlier, deuterated fatty acids were used in this study to enhance their mutual sway with neutrons to obtain their adsorption state on the metal surface. The reflectance waveforms and analyzed curves are shown in Figures 2–12 to 2–18. For each graph, the BO was first analyzed. Since the SLD of BO is only -0.37, it cannot be observed in NR as a layer. The analyze results then represent the layer thicknesses of $SiO_2$, Cu, and $Cu_2O$, as shown in Figure 2-9, which were fixed in the subsequent analyses. When a lubricating oil containing additives is tested, the peaks and valleys of the reflectivity waveform shift to the left when an adsorbed layer (new layer) is observed, according to the Bragg formula. Conversely, a shift to the right indicates a decrease in the total layer thickness, including the substrate material $SiO_2$, Cu, and $Cu_2O$. Since the layer thickness of the substrate is fixed and cannot be reduced in the analysis, when the analyzed results deviate from the experimental data, it indicates the occurrence of corrosion.

As shown in Figure 2–12, when BO+d-OLA was introduced, the peak and valley shifted to the left at 25°C compared to the waveform of BO, which indicates that d-OLA formed an adsorption layer on the substrate surface. No detectable changes were observed when the sample was heated to 50°C or 75°C. However, the peak valley shifted to the right when the sample was heated to 100°C. The analyzed curve also deviated from the original waveform, which indicates that the adsorbed layer of d-OLA desorbed from the substrate surface and was accompanied by a slight decrease in the thickness of the substrate material.

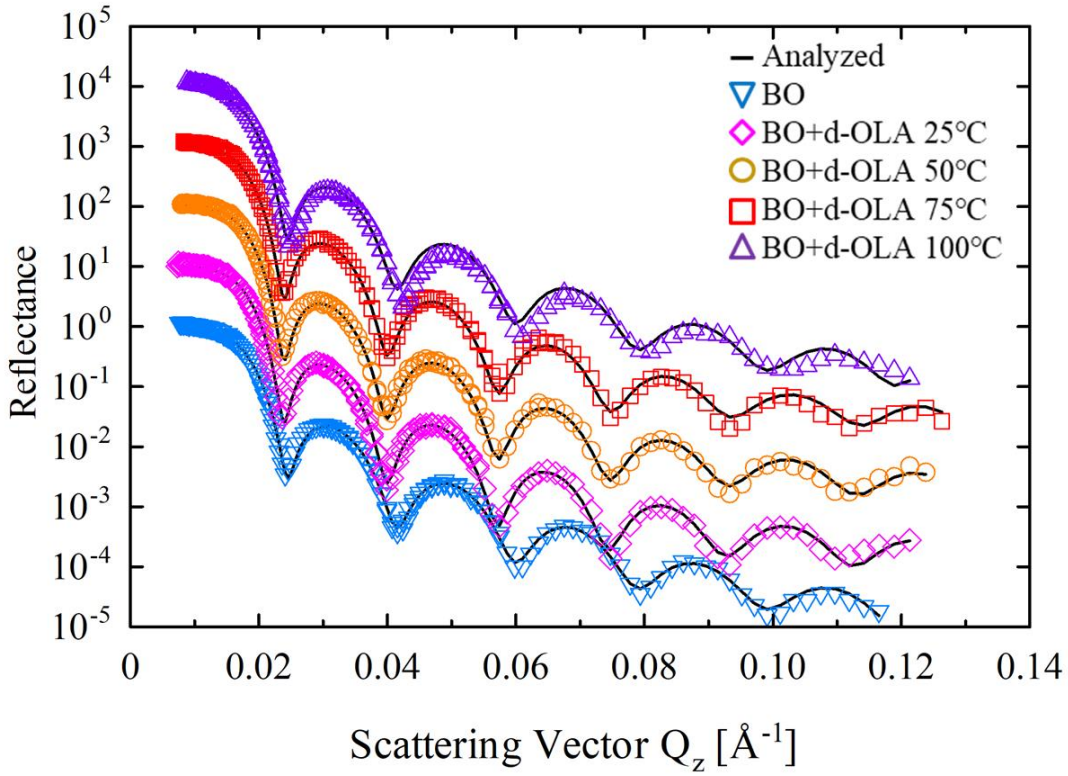


Figure 2–12. NR waveform of BO+d-OLA

Figure 2–13 shows the results of BO+d-OLA+ZDDP. The adsorption behavior was different from that of BO+d-OLA. At 25°C, the waveform of BO+d-OLA+ZDDP shifted slightly to the left compared to BO. However, when the sample was heated to 50°C, the waveform shifted noticeably to the right and deviated greatly from the initially analyzed waveform. Moreover, its amplitude intensity is also attenuated. The rightward shift of the waveform implies a decrease in substrate thickness, and the intensity attenuation indicates a decrease in reflectivity, which may be due to corrosion or surface dissolution. The results at 75°C and 100°C could not be measured due to the reduced reflectivity.

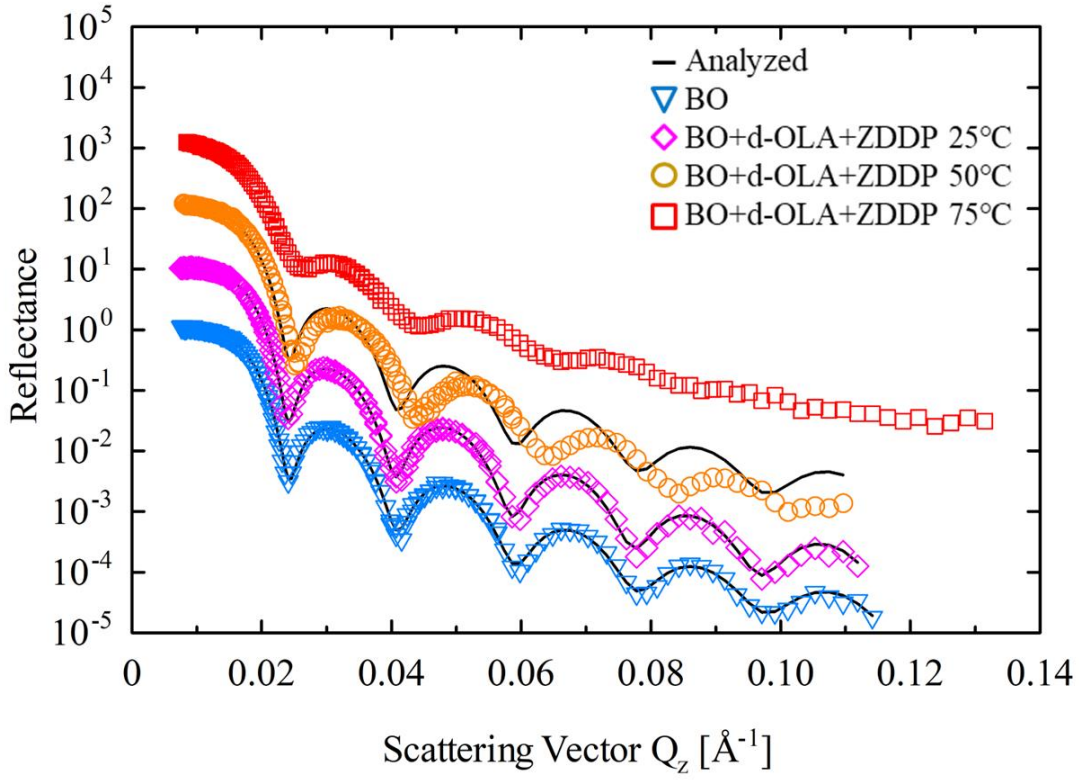


Figure 2–13. NR waveform of BO+d-OLA+ZDDP

Figure 2–14 shows the waveforms of d-STA at different temperatures. Unlike d-OLA, the peaks and valleys of the waveforms of BO+d-STA kept shifting to the left as temperature increased. Even at 100°C, the waveform was still shifting to the left compared to the waveform at 50°C, suggesting that the adsorption density of d-STA increased with higher temperature.

In contrast, significant waveform changes with temperature were not observed for BO+d-STA+ZDDP. As shown in Figure 2–15, the waveform peaks and valleys at 25°C and 50°C did not change significantly compared to BO, which indicates that the d-STA did not form an adsorption layer. However, at 100°C, the analyzed waveform slightly deviated from the original waveform, which indicates a reduction in the substrate thickness.

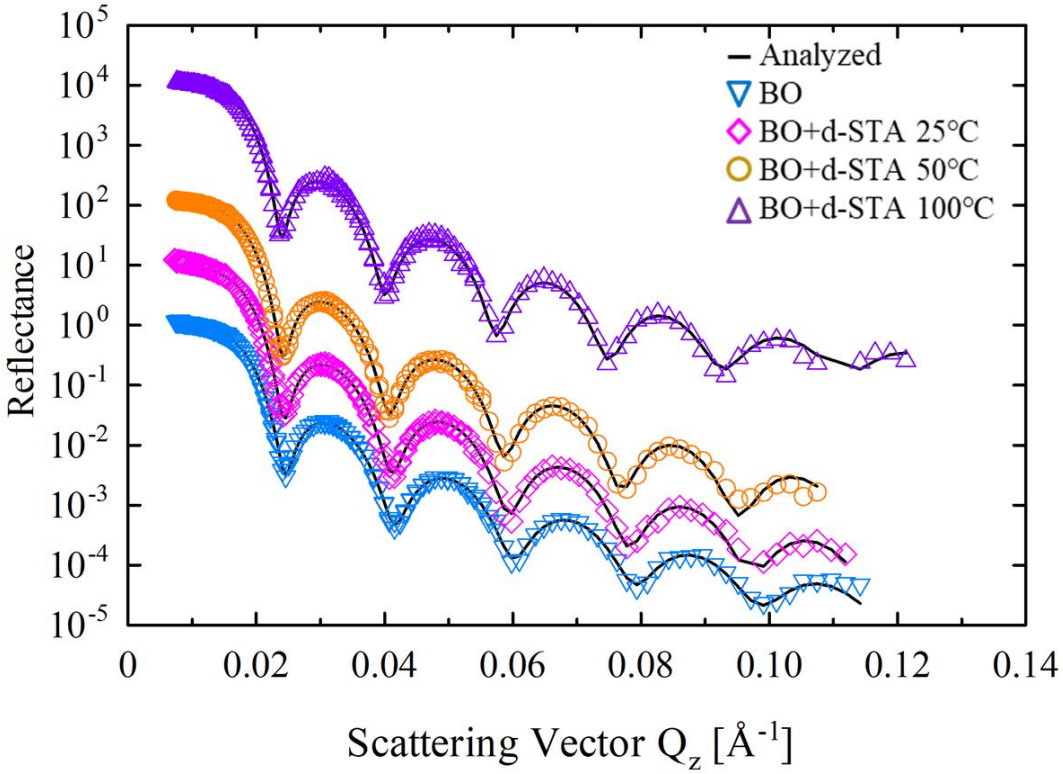


Figure 2–14. NR waveform of BO+d-STA

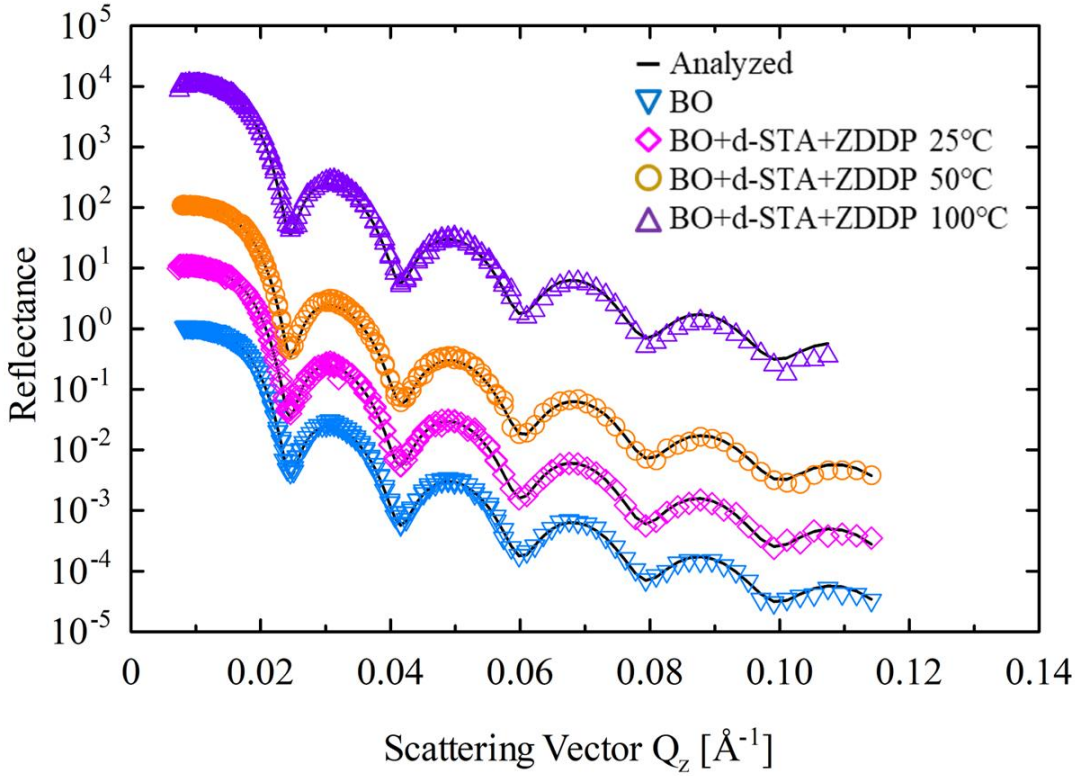


Figure 2–15. NR waveform of BO+d-STA+ZDDP

Although PLA and STA are both saturated fatty acids, their NR results differ. As shown in Figure 2–16, there was a significant leftward shift of the waveform at 25°C compared to BO. However, heating to a higher temperature did not change the waveform which indicates that, similar to d-OLA, the adsorption of d-PLA is less affected by temperature.

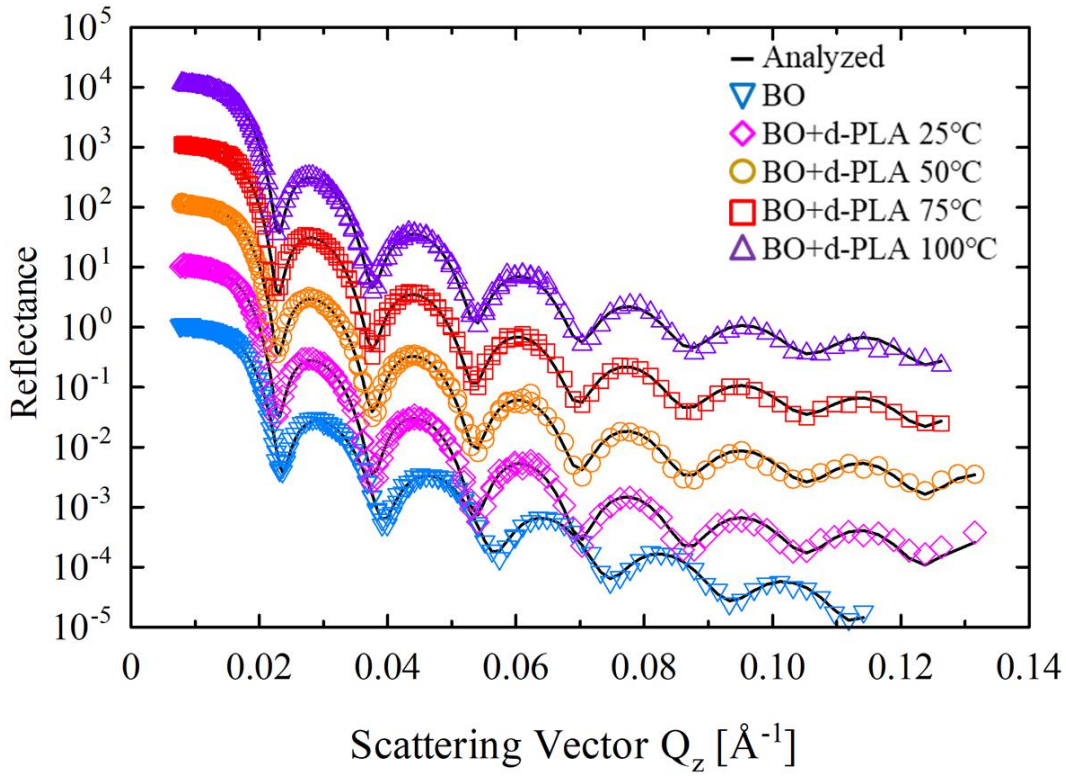


Figure 2–16. NR waveform of BO+d-PLA

However, the addition of ZDDP caused a change in the adsorption characteristics of d-PLA. As shown in Figure 2–17, for BO+d-PLA+ZDDP, the waveform at 25°C shifted to the left noticeably compared to BO, which was similar to the waveform shift for BO+d-PLA shown in Figure 2–16. However, when heated to 50°C, the waveform started to shift to the right. This suggests that d-PLA started to dissociate from the substrate surface. At 75°C, the waveform almost lost its recurring character, which suggests the substrate was dissolved and no more reflection occurred.

The reflectance of BO+ZDDP was measured as a negative control. The results are shown in Figure 2–18. As the ZDDP was not deuterated, the SLD was almost zero. Therefore, no adsorption layer could be observed using the SOFIA neutron reflectometer. The decrease in the layer thickness of the substrate was also not observed because the waveform remained stable at different temperatures. The analyzed results agreed with the raw waveform exactly.

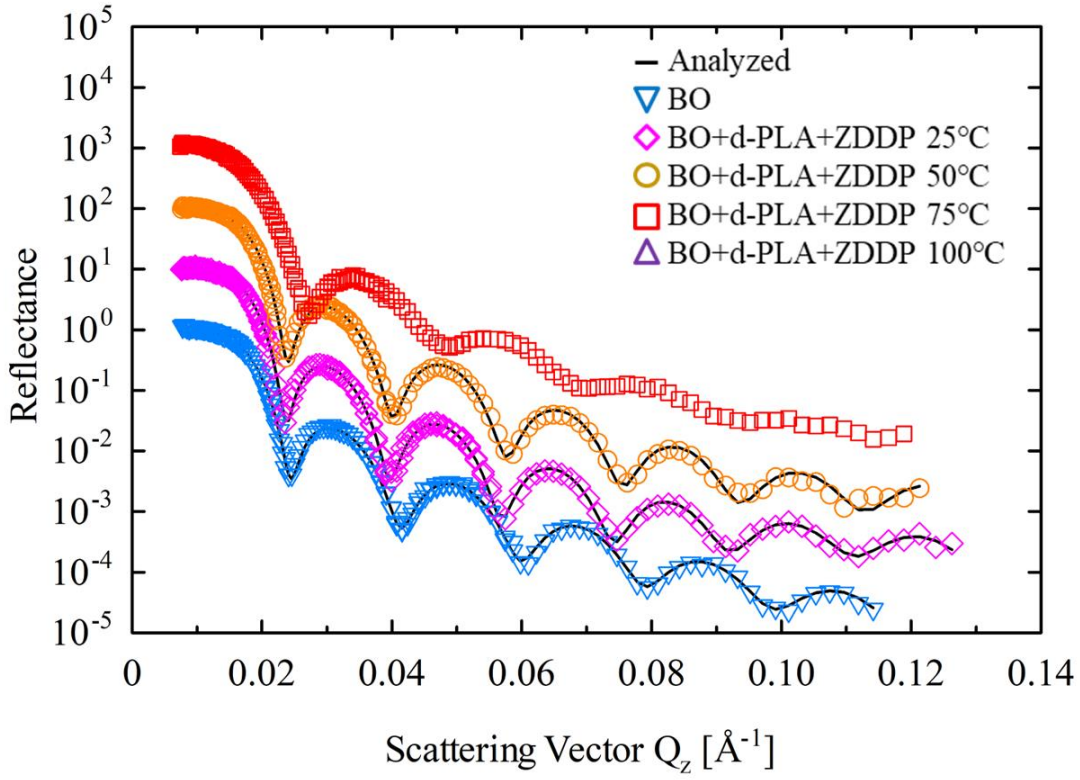


Figure 2–17. NR waveform of BO+d-PLA+ZDDP

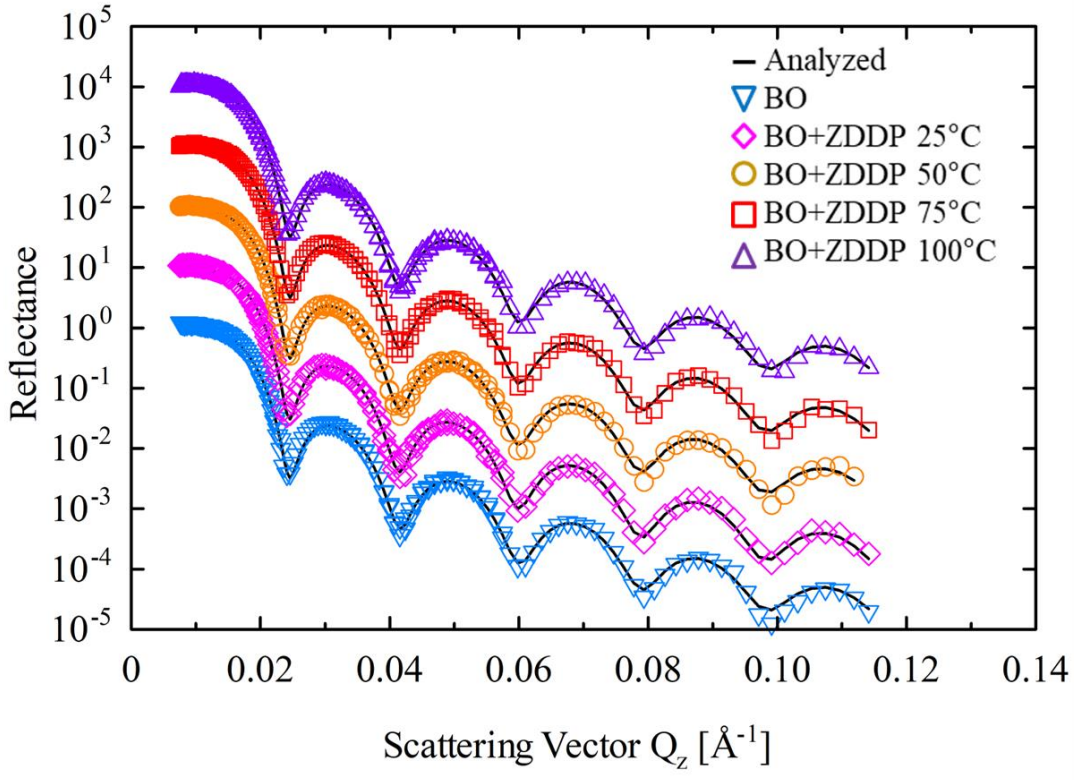


Figure 2–18. NR waveform of BO+ZDDP

The numerical analysis results obtained using the Motofit reflectivity analysis package are shown in Table 2–1. For BO+d-OLA, the adsorption density of the d-OLA layer was 57% at 25°C, and its adsorption density increased with heating until it increased to 73% at 75°C. Then, at 100°C, the adsorbed layer desorbed from the substrate, and the thickness of the substrate layer decreased slightly. For BO+d-OLA+ZDDP, the addition of ZDDP resulted in a very low adsorption density of the d-OLA layer (9% at 25°C). Moreover, with the increase in temperature, the dissolution of the metal surface occurred. For BO+d-STA, the adsorption density of the d-STA layer was only 19% at 25°C, which was very low compared to the adsorption density of OLA at the same temperature (57%). However, heating increased the adsorption density substantially, to 64% for the d-STA layer at 100°C, and it was more thermally stable. For BO+d-STA+ZDDP, the adsorption density was almost zero, and eventually, the metal surface dissolved. For BO+d-PLA, its adsorption density gradually increased with temperature, from 64% at 25°C to 79% at 100°C. For BO+d-PLA+ZDDP, although the adsorption density of d-PLA at 25°C (71%) was higher than that without d-PLA alone (64%), it decreased to 62% at 50°C and the surface dissolved at 75°C. For BO+ZDDP, the layer thickness and SLD were zero at all temperatures because ZDDP is not deuterated, and NR cannot observe ZDDP.

Table 2–2. Analysis results obtained using Motofit analysis package

| **Oil mixtures** | | **25°C** | **50°C** | **75°C** | **100°C** |
|---|---|---|---|---|---|
| BO+d-OLA | Thickness [nm] | 2.1 | 1.9 | 1.6 | d-OLA layer desorbed |
| | SLD [$\times 10^{-6}$Å$^{-2}$] | 3.9 | 4.3 | 5.0 | |
| | Density | 57% | 63% | 73% | |
| BO+d-OLA+ZDDP | Thickness [nm] | 2.1 | Metal surface dissolved | | |
| | SLD [$\times 10^{-6}$Å$^{-2}$] | 0.6 | | | |
| | Density | 9% | | | |
| BO+d-STA | Thickness [nm] | 1.7 | 1.7 | | 1.8 |
| | SLD [$\times 10^{-6}$Å$^{-2}$] | 1.3 | 2.5 | | 4.5 |
| | Density | 19% | 36% | | 64% |
| BO+d-STA+ZDDP | Thickness [nm] | No d-STA adsorbed layer | | | Metal surface dissolved |
| | SLD [$\times 10^{-6}$Å$^{-2}$] | | | | |
| BO+d-PLA | Thickness [nm] | 2.2 | 2.1 | 2.1 | 1.9 |
| | SLD [$\times 10^{-6}$Å$^{-2}$] | 4.4 | 4.9 | 5.3 | 5.5 |
| | Density | 64% | 71% | 77% | 79% |
| BO+d-PLA+ZDDP | Thickness [nm] | 1.9 | 1.6 | Metal surface dissolved | |
| | SLD [$\times 10^{-6}$Å$^{-2}$] | 4.9 | 4.3 | | |
| | Density | 71% | 62% | | |
| BO+ZDDP | Thickness [nm] | The ZDDP layer is undetectable. | | | |
| | SLD [$\times 10^{-6}$Å] | The metal surface was not dissolved. | | | |

The adsorption density was calculated by dividing the SLD value obtained in the analysis by the theoretical value

## 4. Discussion

This study combined AFM-based friction experiments and NR-based interfacial analysis to investigate the relationship between interfacial adsorption of fatty acid molecules and friction reduction with the presence or absence of ZDDP in PAO.

The results when fatty acids and ZDDP were used separately suggest that the adsorption of fatty acids plays a vital role in friction reduction when added to PAO alone. All three fatty acids formed adsorbed films on the metal surface at 25°C, and thus their friction coefficients were much lower than that of BO and BO+ZDDP. As shown in Figure 2–19, the friction coefficients were approximate with the lubrication of the three fatty acids, indicating that the fatty acids all exert similar lubricating effects after reaching a critical adsorption density. On the other hand, the contact increase in pressure diminished the lubricating effect of fatty acids. However, for NOS, although we could not test it in NR, the increase in pressure did not diminish its lubricating effect. Accordingly, NOS forms a chelate-liking structure at the metal interface to enhance NOS adsorption [98], thus lubricating and protecting the friction surface. As a result, although the friction coefficient was higher with NOS than with other fatty acids at 150 MPa, it maintained the lowest friction coefficient overcoming subsequent pressure increases.

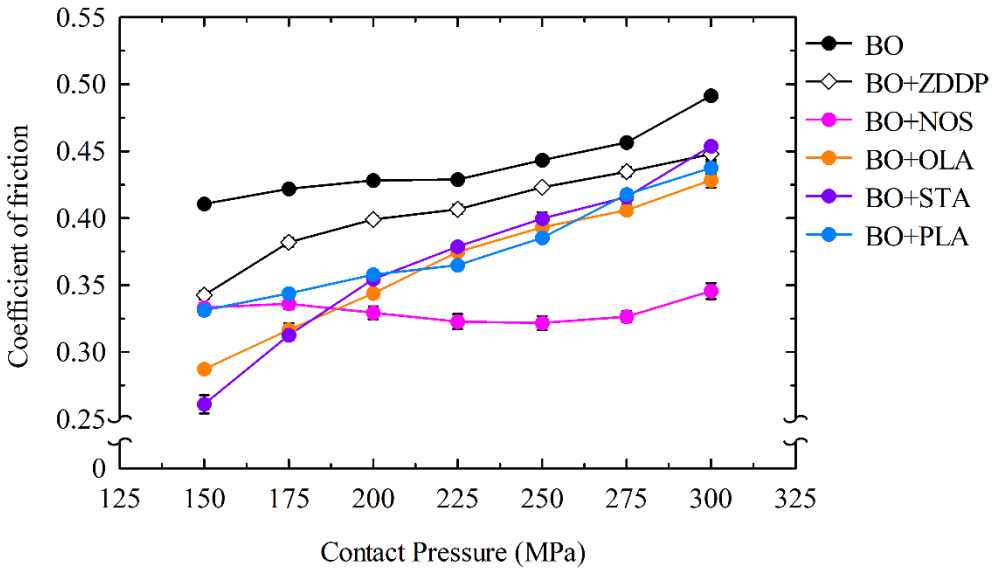


Figure 2–19. The friction coefficient of fatty acids at 25°C

On the other hand, as shown in Figure 2–20, the friction coefficient with BO+OLA was almost the same as that with BO at 100°C, whereas the friction coefficient with BO+STA and BO+PLA was much lower than that of BO. The results of NR also associate with the results of the friction experiment, where at 100°C, d-OLA desorbed from the substrate surface and therefore no longer showed lubricating ability; in contrast, d-STA and d-PLA maintained their dense adsorption layer,

thus reducing friction. The substrate and the BO+d-OLA oil after the NR measurement is shown in Figure 2-21, the lubricating oil turned from clear to light blue, indicating that at 100°C, the oleic acid has desorbed from the interface and the copper ions have dissolved into the lubricant. The friction coefficient with NOS was close to that with STA and PLA. This suggests that NOS adsorbed film did not desorb from the surface and thus still reduced friction. In Campen's previous study, i.e., in fatty acid-hexadecane solutions, the initial friction coefficient was higher for STA-hexadecane solution than for OLA-hexadecane solution at low temperatures [90]. This may also be because OLA forms a higher density adsorbed films than STA at low temperatures and therefore exhibits a lower friction coefficient, although subsequent friction reverses their magnitude relationship, which will be discussed in the next chapter. In addition, in another fatty acid study by Campen, the friction coefficient for OLA-hexadecane solution was higher than that for STA-hexadecane solution when heated to 100°C [111]. These results agree with the AFM and NR measurements of this study, i.e., OLA desorbed at 100°C, while STA maintained a dense friction-reducing layer.

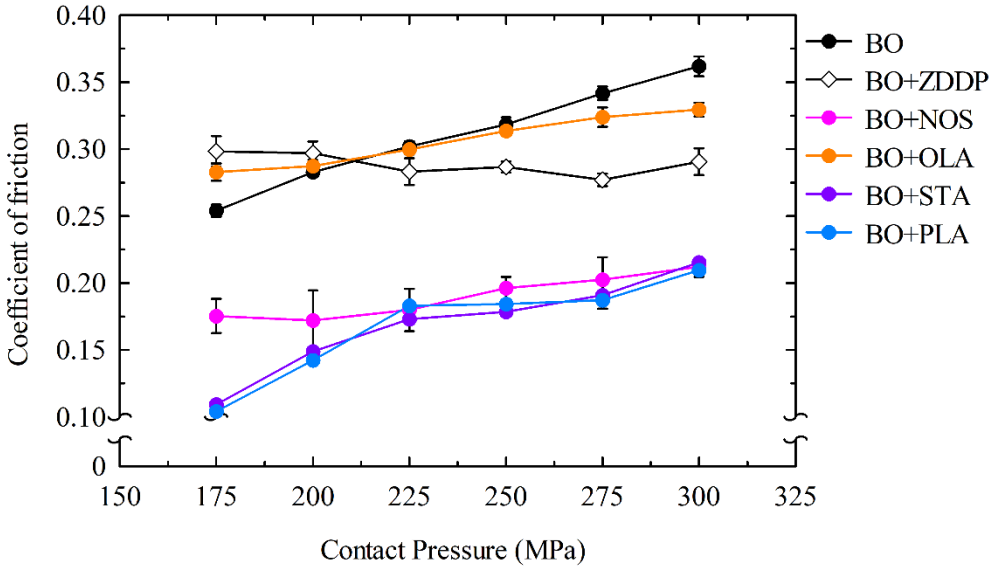


Figure 2–20. The friction coefficient of fatty acids at 100°C

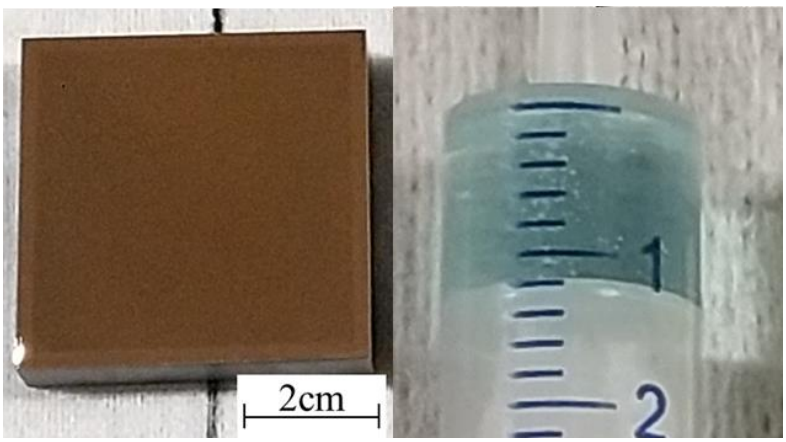


Figure 2-21. The substrate and the BO+d-OLA oil after the NR measurement.

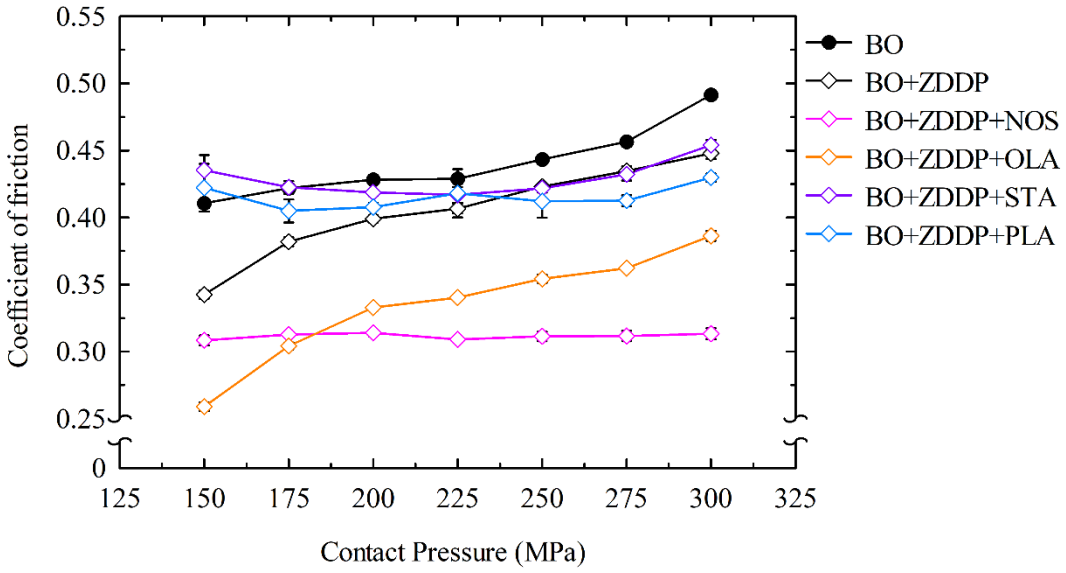


Figure 2–22. The friction coefficient of fatty acids-ZDDP at 25°C

However, the adsorption and tribological properties of fatty acids changed with the addition of ZDDP. Figure 2–22 shows that at 25°C, the friction coefficient with BO+STA+ZDDP was between BO and BO+ZDDP at almost all contact pressures. Also, no adsorption layer of d-STA was observed in the NR measurements. This may be because of the high melting point of stearic acid (69.3 °C); however, d-STA adsorbed on the metal surface and demonstrated a friction-reducing effect when it was added to BO alone. The above results suggest that the friction-reducing effect was lost because of the interaction between STA and ZDDP or because of the competitive adsorption. The friction coefficient with BO+PLA+ZDDP was close to that with BO+STA+ZDDP. Their loss of the friction-reducing effect may be due to the same mechanism. However, an increase in d-PLA adsorption density was observed in the NR test. Like STA, PLA and ZDDP may react with each other; however, the difference is that the new substance formed by the reaction of PLA and ZDDP remained adsorbed on the substrate. In comparison, the friction coefficient with BO+OLA+ZDDP was the smallest of the three, despite the low adsorption density of d-OLA (only 9%).

The results at 100°C were the opposite of those at 25°C. As shown in Figure 2–23, at 100°C, BO+STA+ZDDP and BO+OLA+ZDDP both exhibited synergistic effects, while BO+OLA+ZDDP had a limited friction-reducing effect. In the NR test, all three lubricants resulted in the dissolution of the substrate metal. The difference was that for BO+d-OLA+ZDDP, dissolution of the substrate most likely occurred at 25 °C and the base material exposed at 75°C; dissolution of the substrate due to BO+d-PLA+ZDDP occurred after 50°C, while BO+d-STA+ZDDP led to only a slight interfacial dissolution at 100°C. The substrate and the BO+d-OLA+ZDDP oil after the NR measurement is shown in Figure 2-24, the lubricating oil turned

from clear to light yellow, and the copper on the surface of the substrate is dissolved, exposing the underlying silicon layer. Similar corrosion behaviors were reproduced in the laboratory (using undeuterated additives) in the absence of neutron irradiation. If left for a long enough time (12 hours), the dissolution of the copper layer was observed even at 25°C. However, only complete dissolution of the copper layer occurred; the iron layer was not completely dissolved because iron is less chemically active than copper. These results suggest that when both fatty acids and ZDDP are added to BO, the slight dissolution of the substrate surface contributes to reducing friction.

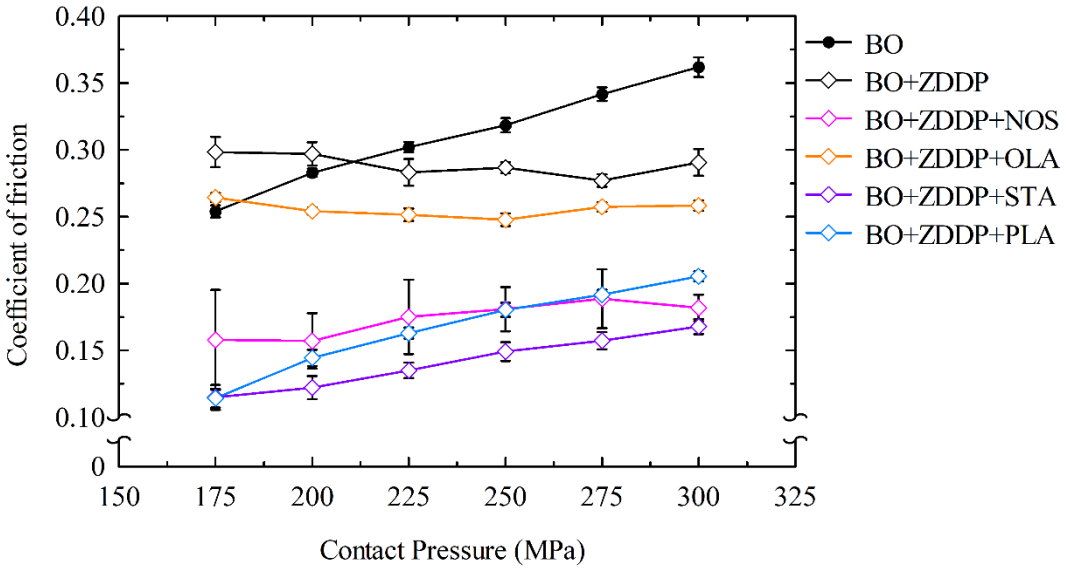


Figure 2–23. The friction coefficient of fatty acids-ZDDP at 100°C

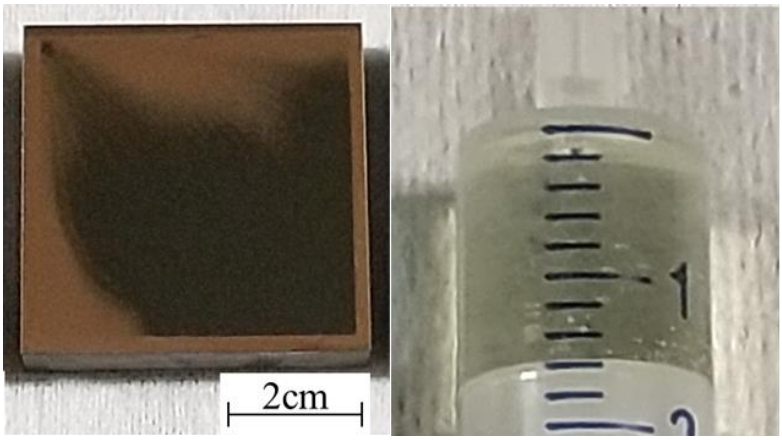


Figure 2-24. The substrate and the BO+d-OLA+ZDDP oil after the NR measurement.

Unlike the aforementioned model OFM, NOS demonstrated good friction reduction at both temperatures. At 25°C, the friction coefficient was the lowest among all lubricating oils at most contact pressures and did not vary with pressure. At 100°C, although the friction coefficient was slightly higher than BO+STA+ZDDP and BO+OLA+ZDDP, it was still very low compared to BO.

When fatty acids were used together with ZDDP, the friction coefficient and the adsorption behavior of fatty acids changed considerably. Although the results suggest that the friction coefficient of the fatty acid-ZDDP mixture is affected by the fatty acid adsorption state, it is neither a simple correlation nor competitive adsorption. Based on many findings to date, this reduction in friction is a reaction between OFM, ZDDP, and metal at the interface, resulting in the formation of a low-friction metallic soap layer on the sliding surface. In addition, as the corrosion was intensified at higher temperatures, a thermochemical reaction may occur. Oleic acid reacts with ZDDP to form zinc soap, producing dialkyl dithiophosphate, which reacts more actively on copper than fatty acids. Although ZDDP decomposes by heating and displaces with copper, ZDDP is not corrosive in this experimental line, as shown in Figure 2–18. The fatty acids accelerate this process, and different fatty acids exhibit different characteristics. For BO+OLA+ZDDP, at 25 °C, both OLA and metallic soap were adsorbed on the surface, and a similar pressure dependence was seen for it as for BO+OLA. On the other hand, at 100 °C, the adsorption capacity of OLA decreased, and the intense metallic soap reaction limited the friction-reducing effect. Furthermore, it is quite reasonable to expect that BO+STA+ZDDP and BO+PLA+ZDDP also reduce friction through the same mechanism, but BO+STA+ZDDP forms a more stable metal soap that does not cause metal dissolution. Although BO+PLA+ZDDP dissolves copper, it is less corrosive compared to BO+OLA+ZDDP, so the metal soap formation is also relatively stable between PLA, ZDDP, and iron. Moreover, since PLA is more polar than the other two fatty acids, it is likely to adsorb on the surface of iron during friction test as well, although dissolution at the interface in the NR measurement makes d-PLA unobservable.

## 2.5 Conclusion

This chapter investigates the frictional properties of lubricating oils containing OFM, ZDDP, or both. The interfacial adsorption density of OFM in them was measured to clarify the relationship between OFM adsorption and friction reduction. The results are concluded below.

1. NR measurements showed that the adsorption density of fatty acids was correlated with the friction coefficient. For BO+OLA, the desorption of OLA at 100°C resulted in a friction coefficient similar to that of BO.

2. Different mixtures of fatty acids with ZDDP exhibited different effects. Among them, saturated fatty acids-ZDDP antagonized each other at room temperature, while unsaturated fatty acids-ZDDP exhibited good friction-reducing effects. Moreover, the contact pressure dependence of the friction coefficient for the OLA-ZDDP mixture was similar to that of OLA alone, suggesting that OLA contributes significantly to the friction reduction even in the mixture.

3. At 100°C, the metallic soap formation promoted by the fatty acid-ZDDP mixture dominated the frictional properties. In the STA-ZDDP mixture, the stable metallic soap reduced the friction, whereas PLA-ZDDP and OLA-ZDDP dissolved the interface. Moreover, the intense metal soap formation reaction in the OLA-ZDDP mixture limited its friction-reducing effect.

4. Among the four OFMs tested, the NOS-ZDDP mixture exhibited considerable friction reduction at different temperatures, and similar absolute values were seen at different contact pressure conditions which suggests the synergistic tribological effects between NOS and ZDDP.

# Chapter 3. Tribological characteristics of tribofilms formed by various ZDDP-OFM mixtures with colloidal probe AFM

## 3.1 Introduction

The previous chapter discussed the relationship between the interfacial adsorption of the additives and their frictional properties. However, as presented in the results, although the initial frictional properties of the OFM-PAO solutions were greatly affected by their adsorption properties, chemical reactions occurred when OFM and ZDDP were both added to PAO. In addition, as reported by Campen [90], even for the OFM solution in hexadecane, the friction coefficient with oleic acid was lower than that of stearic acid in the early stages of friction tests (due to the higher adsorption density of oleic acid according to the results in chapter 2). However, the friction coefficient with oleic acid overtook that of stearic acid as the friction proceeds.

Many other studies have reported that OFMs require friction to initiate or complete their friction reduction. As for the reasons, Spikes concluded the following three possibilities [5]:

*(1) that rubbing "activates" the adsorption/reaction process in some way*
*(2) that it accelerates adsorption by forcing convection*
*(3) that it helps "order" the film in a similar fashion to the "ironing" process used to form liquid crystal display surfaces.*

Previous studies have compared the frictional behavior of oleic, stearic, and elaidic acids [111], where elaidic acid is a trans-oleic acid and, unlike oleic acid, elaidic acid possesses a linear configuration. Their results show that stearic and elaidic acids had very low friction at low speeds and increased approximately linearly with log sliding speed. However, oleic acid exhibited very different behavior, and the friction remained almost constant with speed and higher than the fatty acids with linear configurations. The molecules with linear and non-linear structures produced different lubricating films under rubbing, and their frictional properties were quite different. In addition to macroscopic experiments, a microscopic experiment performed with FM-AFM has investigated the effect of rubbing on the growth of fatty acid-adsorbed films [112]. As observed by FM-AFM, the layer thickness of palmitic acid was only 2.8 nm immediately after the hexadecane solution of palmitic acid was dropped on the copper surface. However, after 2 hours of continuous scanning, the thickness of the boundary layer grew to nearly 20 nm. In addition, the scanned area exhibited a considerable decrease in friction compared to the unscanned area.

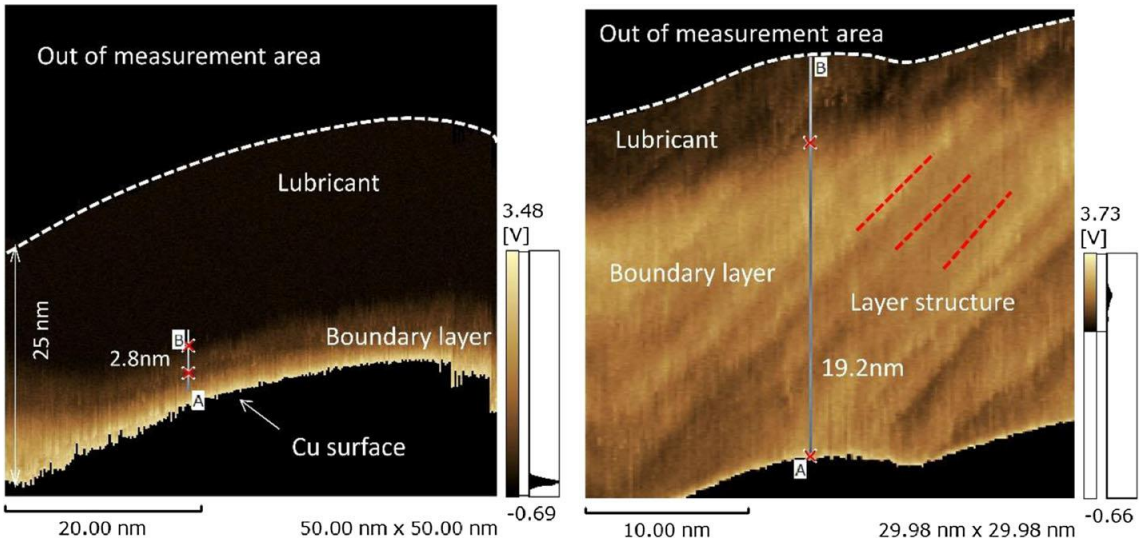


Figure 3-1. Growth of layer thickness of PLA on Cu substrate after rubbing, cited from [112].

Although much has been done to clarify the effect of rubbing on the friction behavior of fatty acids, there is not enough literature to describe how ZDDP interacts with the OFM solution [2]. As introduced in Chapter 1, ZDDP is known to form tribofilms on rubbing surfaces. Miklozic described two ways to investigate the impact of OFMs on ZDDP [113]:

*(1) by examining the effect of OFMs on the film formation rate and friction of ZDDP-containing oils using mixtures containing both additives*
*(2) by studying the effect of OFMs on the friction and durability of pre-formed tribofilms.*

For the first way, it has been found that the GMO-ZDDP mixture resulted in thinner tribofilms, but the frictional effect depended on the substrate material, where it was limited for steel but better for DLC [40], [74], [85], [89]. The amine-ZDDP mixture exhibited synergistic effects on both friction and wear [83–84]. For the second way, it has been found that some amines could reduce the thickness and friction coefficient of the pre-formed tribofilm [82], [85], [113].

Either way, previous studies have focused on the effect of OFM on ZDDP tribofilm thickness. The friction tests were mainly performed in the rolling or rolling-sliding condition, where the tribofilm was formed in the hydrodynamic lubrication regime, and the complete Stribeck curve was later obtained by varying the entrainment speed. This study, however, focuses on boundary lubrication. A recent study has investigated the ZDDP tribofilm formation by single-asperity sliding contact [37]. This study enabled the imaging of ZDDP tribofilms and clarified the mechanism of ZDDP tribofilm growth, and the results suggest that the film growth was activated by compressive stress, shear stress, and heating [37–38]. On the other hand, as mentioned above, film growth under friction was also observed for the fatty acids. Therefore, this chapter's research

interest and objective are to clarify how OFM interacts with ZDDP under boundary lubrication, what kind of tribofilms are formed by the mixture, and how the mixture alters friction. A tribofilm film was first formed by rubbing with a colloidal probe, and then friction experiments were performed on the film to investigate its tribological effects.

## 3.2 Experimental

### 3.2.1 Testing oils and substrates

The same substrates and additives in chapter 2 were used. STA was not tested due to its low solubility at the same concentration that the laser light from AFM cannot be completely reflected. The information on lubricating oils is given in Table 3–1.

Table 3–1. Lubricating oil mixtures

| **Base oil + additive(s)** | **Content** |
|---|---|
| BO | PAO4 |
| BO+ZDDP | ZDDP (P 700 ppm) in PAO4 |
| BO+OLA | OLA (0.3 wt%) in PAO4 |
| BO+OLA+ZDDP | ZDDP (P 700 ppm) and OLA (0.1 wt%) in PAO4 |
| BO+PLA | PLA (0.3 wt%) in PAO4 |
| BO+PLA+ZDDP | ZDDP (P 700 ppm) and PLA (0.1 wt%) in PAO4 |
| BO+NOS | NOS (0.3 wt%) in PAO4 |
| BO+NOS+ZDDP | ZDDP (P 700 ppm) and NOS (0.1 wt%) in PAO4 |

### 3.2.2 Experimental procedure

The experiments were performed at 25°C and 100°C, respectively. The testing areas in the following steps are shown in Figure 3–2.

Step 1: **[Substrate preparation]** Drop lubricating oil on substrates 3 hours before the test and keep the substrates at testing temperature.

Step 2: **[Hertzian contact pressure calculation]** Measure the adhesion force to obtain the force curve. Hertzian contact pressure was calculated based on this force curve. The approaching and releasing speeds were 200 nm·s-1.

Step 3: **[Surface profiling]** Scan a 10×10 μm area (Area A) to obtain the surface profile before rubbing.

Step 4: **[Rubbing]** Rub a 2×2μm area (Area C) for 2 hours under 300 MPa. The scan speed was 8 μm·s-1.

Step 5: **[Friction measurement]** Perform friction tests in the area oulined by the red dotted line.

The friction coefficient was calculated based on the data in the blue patterned area. The measurement was performed 6 times at each contact pressure. The scan speed during the measurement was 10 μm·s$^{-1}$.

Step 6: **[Surface profiling]** Scan area A to obtain the surface profile after rubbing.

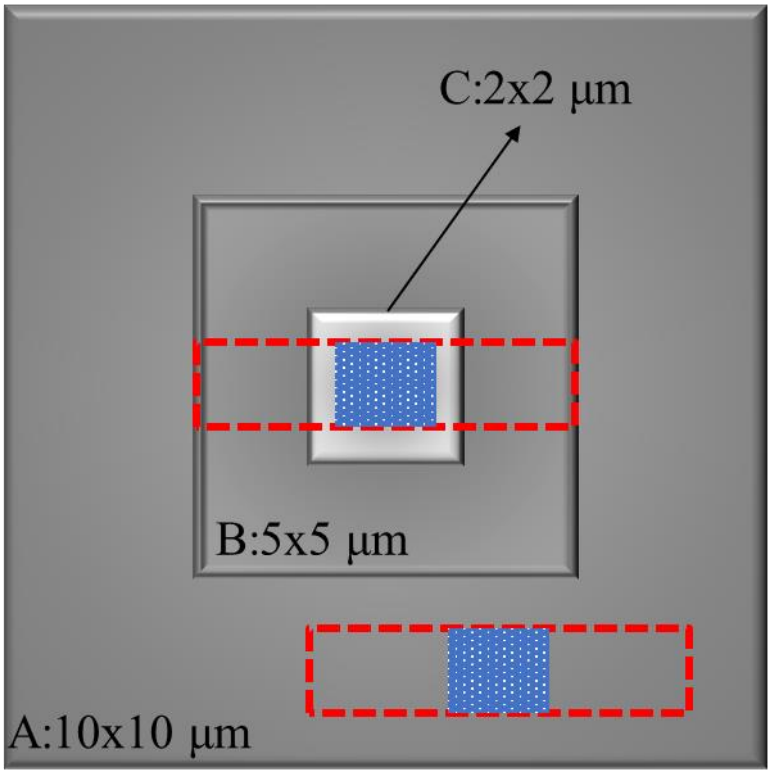


Figure 3–2. Testing areas on the substrate. Area A is the surface profiling area. Area C is the rubbing area. The area framed in red is the friction test area. The coefficient of friction was calculated based on the data in the blue patterned area.

## 3.3 Results

### 3.3.1 ZDDP and its tribofilm formation

BO and BO+ZDDP were tested first to confirm the tribofilm formation of ZDDP by colloidal probes. As shown in Figure 3–3, tribofilm formed by ZDDP was observed at both 25°C and 100°C; the formation was more active at 100°C. The tribofilm formation reduced friction, and its friction coefficient was lower than that of BO under almost all contact pressures at both temperatures. In addition, the friction coefficient did not change with contact pressure at both temperatures.

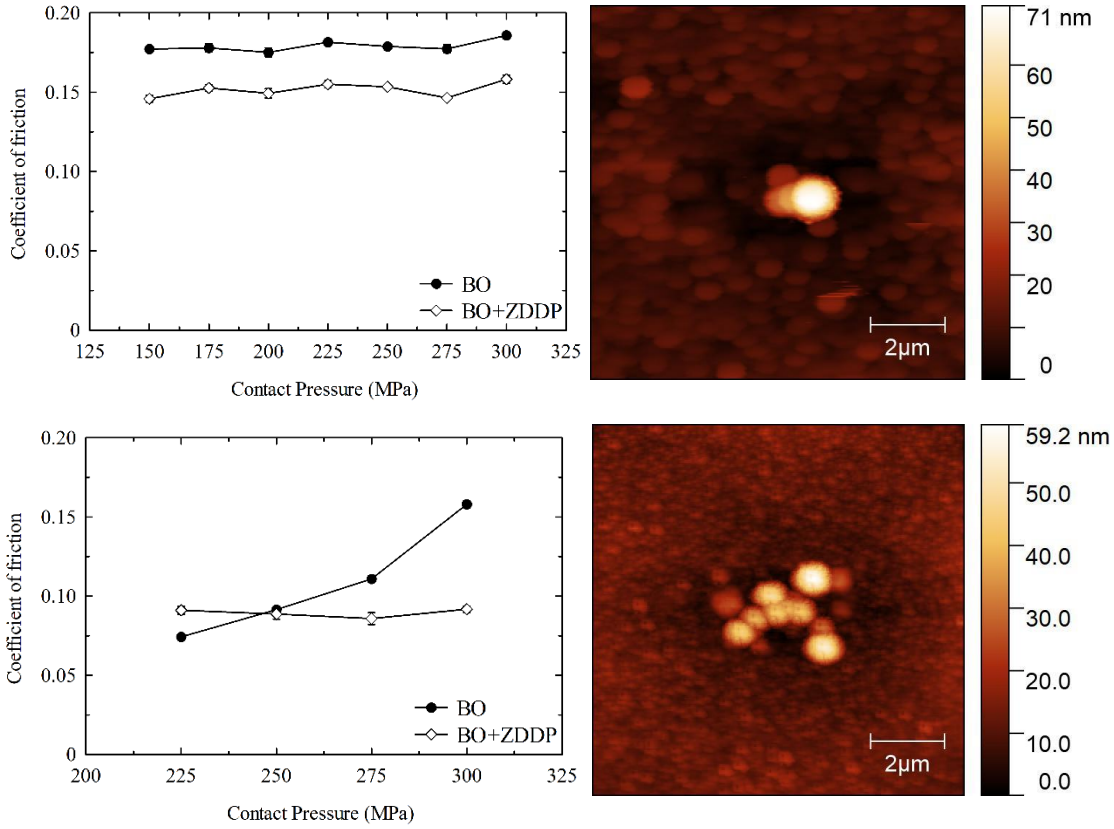


Figure 3–3. The friction coefficient of ZDDP tribofilm at 25°C (upper) and 100°C (lower).

### 3.3.2 The tribological property of the surface rubbed with OFM alone

The addition of OFMs to PAO resulted in lower levels of friction coefficients. As shown in Figure 3–4, for all tested lubricating oils, the friction coefficients of the rubbing surfaces increased with increasing contact pressure after being rubbed for two hours. BO+NOS exhibited the lowest friction coefficient in the contact pressure range from 150 MPa to 225 MPa. BO+PLA exhibited the lowest friction from 250 MPa to 300 MPa. BO+OLA exhibited a slightly higher friction coefficient than BO+PLA and BO+NOS, and even higher than BO at 300 MPa. The results suggest that the linear configuration of PLA enables them to pack on the surface closely, thus exhibiting a lower friction coefficient at relatively high contact pressures due to the better load capacity.

The unsaturated OFM exhibited a different tribological effect at 100°C than at 25°C. As shown in Figure 3–5, the friction coefficients of BO+OLA and BO+NOS were higher than those of BO. Since AFM measures the shear of rubbing surfaces, this result indicates that unsaturated OFM formed a high shear boundary film by rubbing at 100°C. In addition, since both OLA and NOS contain cis-structured carbon-carbon double bonds, this causes their molecules to be unable to be

aligned regularly on the rubbing surface, which may be one of the reasons for the higher friction coefficients. In contrast, the saturated PLA exhibited better friction reduction than BO. As revealed by NR in chapter 2, higher polarity enables PLA to form a denser boundary film than OLA, which leads to a lower friction coefficient.

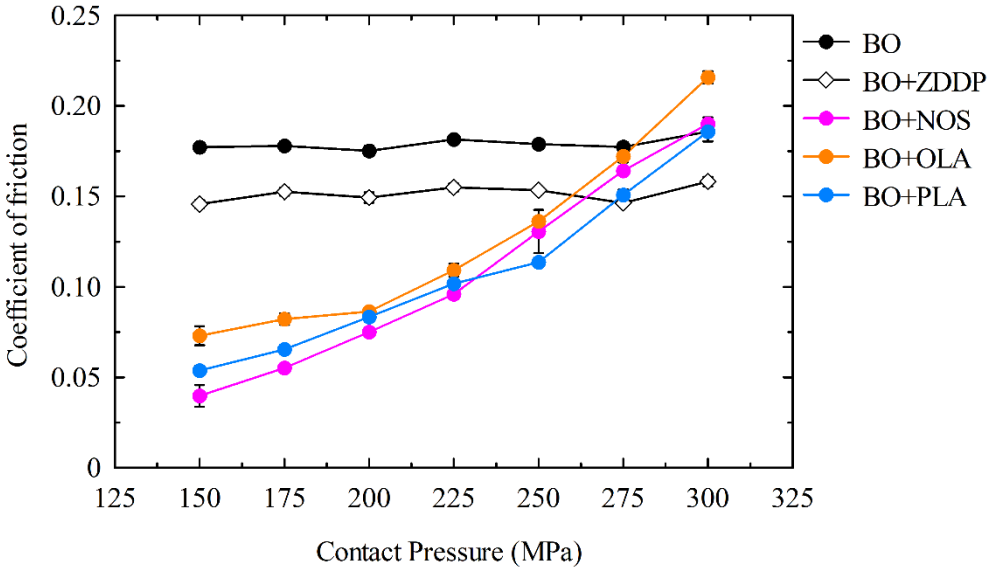


Figure 3–4. The friction coefficient of OFMs in BO at 25°C.

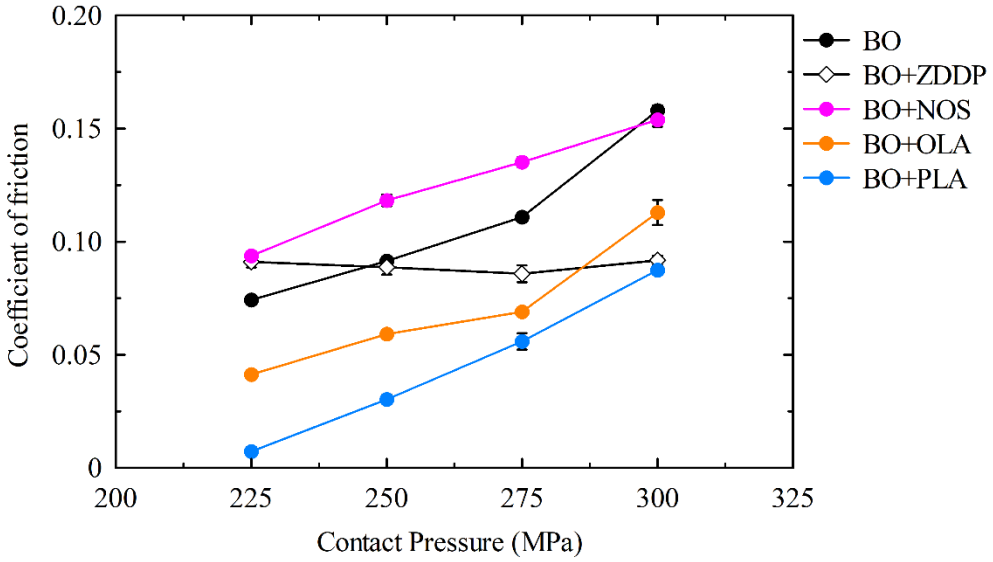


Figure 3–5. The friction coefficient of OFMs in BO at 100°C.

### 3.3.3 The tribological property of the surface rubbed with the OFM-ZDDP mixture

The friction coefficients with the lubrication of each lubricating oil at 25°C are shown in Figure 3–6. BO+PLA+ZDDP exhibited a high friction coefficient, and the average value at each contact

pressure lay between BO and BO+ZDDP. In contrast, both BO+OLA+ZDDP and BO+OS+ZDDP exhibited friction reduction capability. In addition, as shown in Figure 3–7, a similar tribofilm was observed when lubricated with BO+PLA+ZDDP. It suggests that although PLA adsorbed on the surface with the presence of ZDDP, the continuous rubbing desorbed them while promoting the reaction of ZDDP. However, the thickness of the tribofilm differed from that shown in Figure 3–3. The friction property was also different which suggests that although PLA cannot prevent tribofilm formation by ZDDP, the composition changed and thus exhibited different tribological behavior.

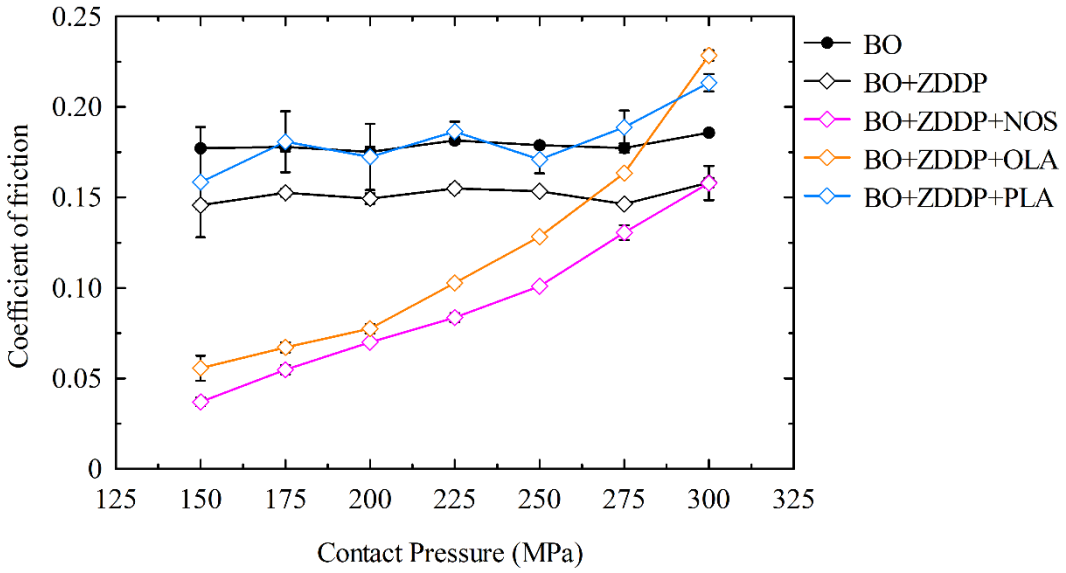


Figure 3–6. The friction coefficient of OFM-ZDDP mixtures in BO at 25°C.

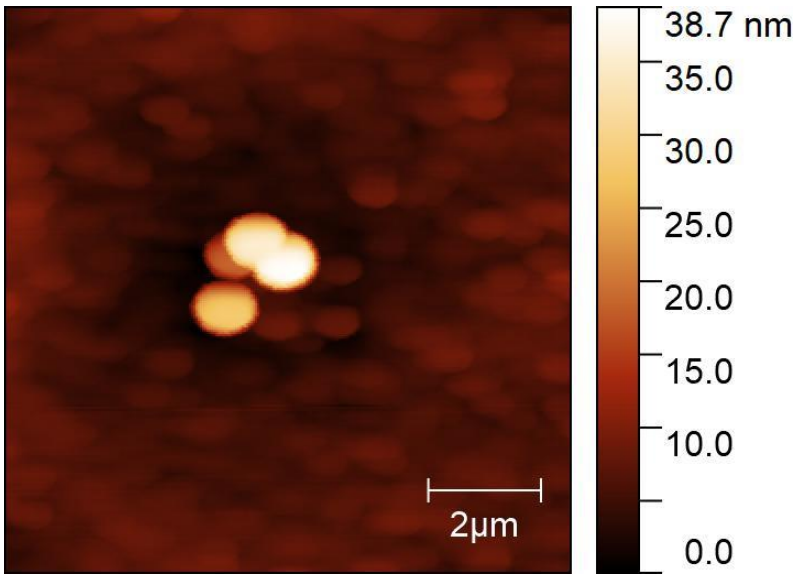


Figure 3–7. Tribofilm observed with BO+PLA+ZDDP lubrication at 25°C.

However, the PLA-ZDDP mixtures exhibited the lowest friction coefficient when heated at 100°C. Although they did not exhibit a friction-reducing effect at room temperature, they were effective in reducing friction when heated. Combined with the results of NR measurements in Chapter 2, it suggests that ZDDP reacted preferentially with the surface by rubbing to form tribofilm at 25°C. At 100°C, as the interfacial dissolution observed in NR, the fatty acid, the ZDDP, and the metal reacted with each other to form a low-friction metallic soap on the interface. On the other hand, for OLA-ZDDP mixtures, the friction coefficient was close to but larger than that of ZDDP at all contact pressures, as shown in Figure 3–8. The results of NR in the previous chapter suggest that the OLA the ZDDP and substrate metal reacted and formed a metallic soap that reduced friction at 25°C. However, heating accelerated this reaction, causing it to lose its effect eventually. In addition, as shown in Figure 3–9, the observed image of AFM showed an apparent depression in the rubbing area, which suggests that the iron layer has been removed during rubbing, resulting in ZDDP adsorbed on the bare silicon. Hence, its friction coefficient was similar to that of ZDDP.

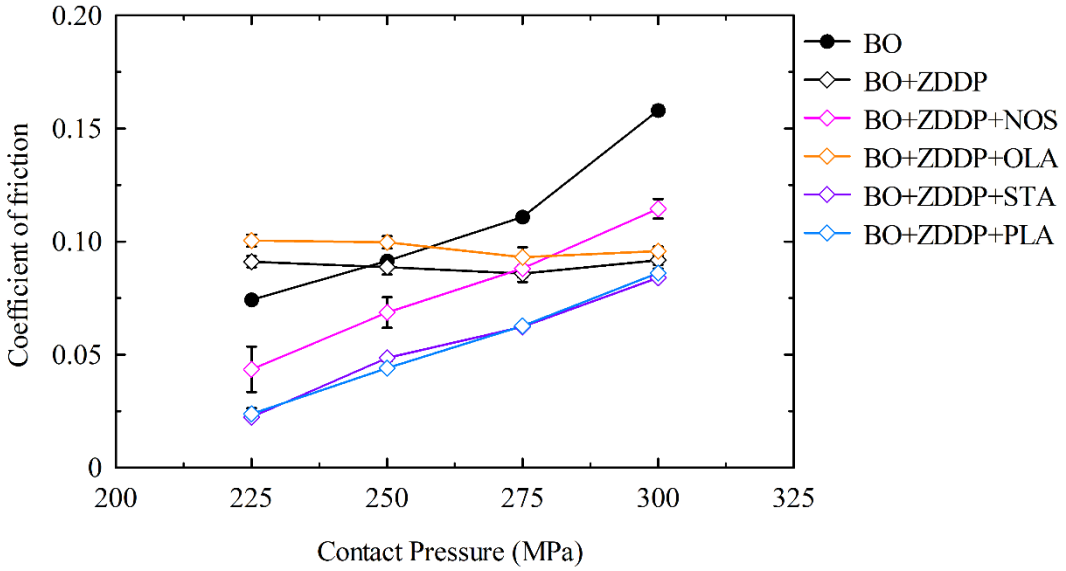


Figure 3–8. The friction coefficient of OFM-ZDDP mixtures in BO at 100°C.

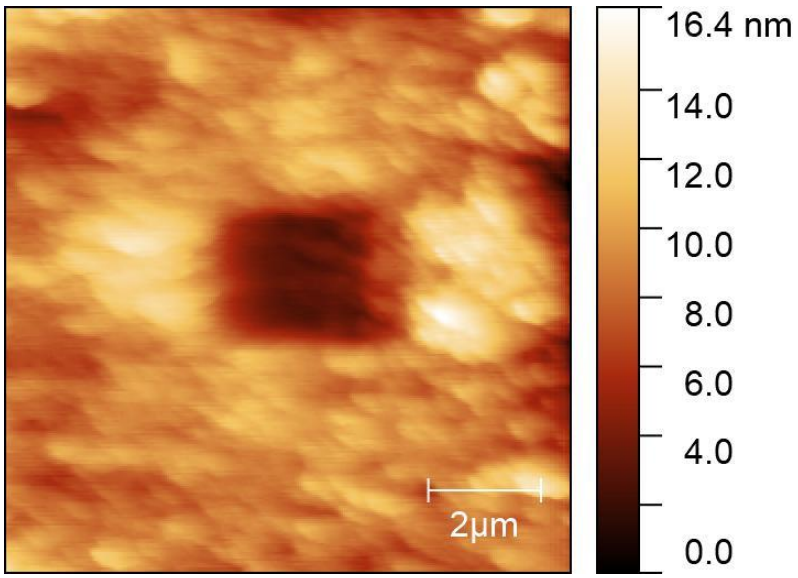

Figure 3–9. Depression in the rubbing area with BO+OLA+ZDDP lubrication at 100°C.

## 3.4 Discussion

In this chapter, friction tests were performed with the AFM. Regarding the advantages of the AFM, it enables ZDDP to form tribofilms in boundary lubrication and to perform in-situ friction tests on the tribofilm simultaneously. The results suggest that ZDDP forms tribofilms on the rubbing surface regardless of temperature. These tribofilms have a good load capacity, and the friction coefficient was almost the same at different contact pressures. At room temperature, the friction coefficients of the tribofilms were lower than that with BO lubrication, but at 100°C, it exhibited a higher friction coefficient below 250 MPa. However, the tribofilm formation at 100°C reduced friction noticeably compared to the unrubbed area lubricated with ZDDP. These findings agree with the outcomes of previous ZDDP studies, which concluded that tribofilm formation is accompanied by high friction under boundary lubrication and mixed lubrication.

The formation of tribofilms by OFMs was also studied. Unlike ZDDPs, OFMs do not form tribofilms that bulge upward. Although the formation and film thickness could not be observed with AFM, by comparing the results of the rubbed and unrubbed areas, we can glimpse the tribological property of the film. As shown in Figure 3–10, for the saturated PLA, the results suggest that rubbing promoted the growth of boundary films and ordered their molecules at the interface. The surfaces exhibited extremely low friction coefficients on the rubbed area compared with BO at both temperatures. In contrast, the PLA-ZDDP mixture exhibited an antagonistic effect at 25°C but a synergistic effect at 100°C. The observation of ZDDP tribofilm with PLA+ZDDP lubrication at 25°C suggests that although PLA was adsorbed on the surface, rubbing removed the adsorbed layer, which allowed ZDDP to interact with the interface metal to form tribofilm preferentially. However, heating led to the formation of metallic soap on the interface, as shown

in Figure 3–11; its friction coefficient was lower than that of the unrubbed area lubricated with BO+PLA. In contrast, the friction coefficient of the PLA-ZDDP mixture was higher than that of PLA on the rubbed areas. Although the metallic soap exhibited considerable friction reduction ability, the results suggest that the effect was still worse than the aligned PLA by rubbing.

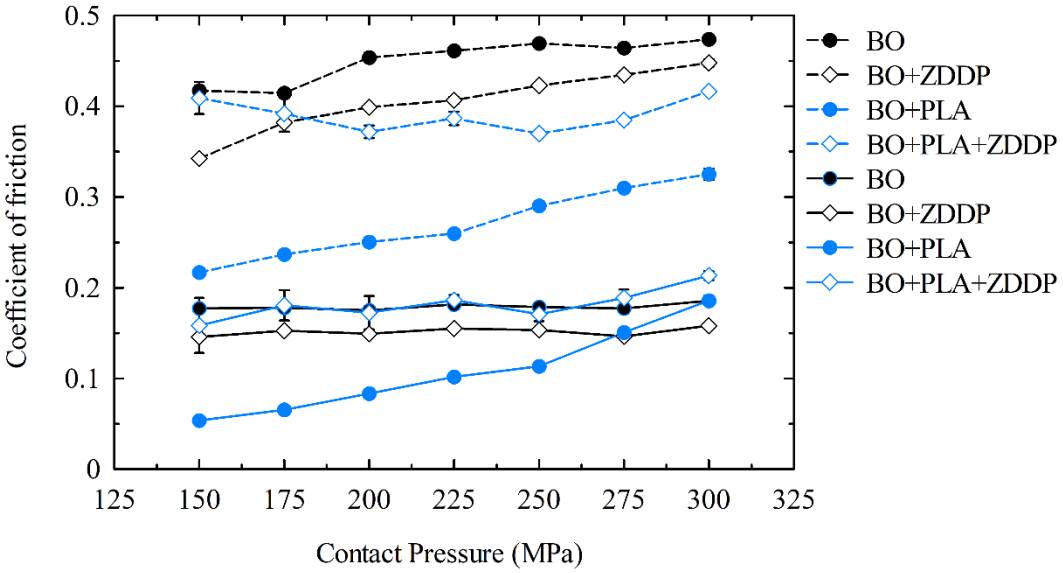


Figure 3–10. Comparison of the rubbed and unrubbed area lubricated at 25°C.

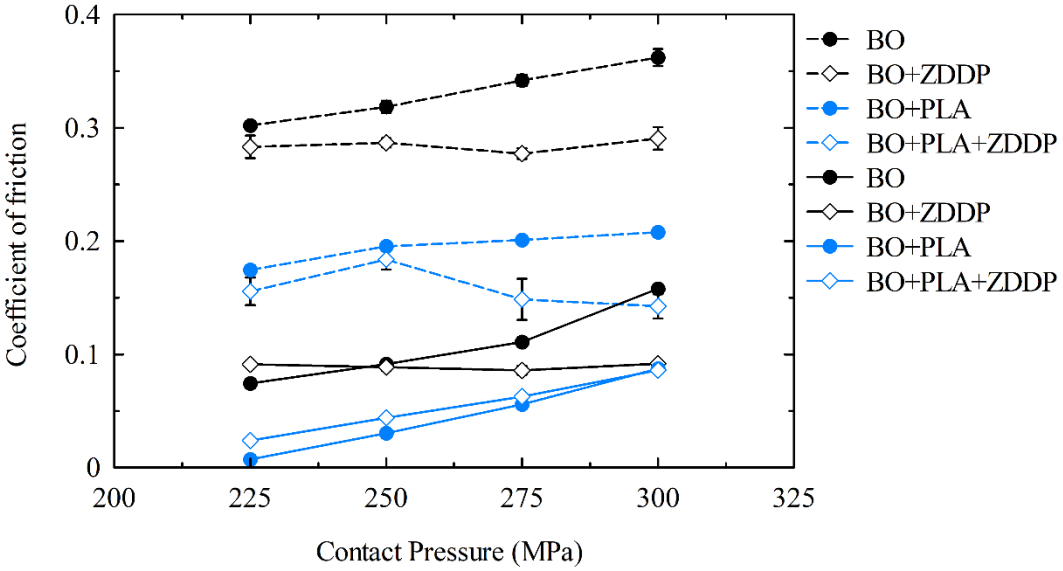


Figure 3–11. Comparison of the rubbed and unrubbed area at 100°C.

The cis unsaturated carbon bonds in the OLA give it different tribological properties than PLA. As described in the introduction, one of the main differences is that the carbon bond limits the alignment of the OLA molecular. It is remarkable at 100°C as shown in Figure 3–13; the friction coefficient on the rubbed area lubricated with BO+OLA was higher than the rubbed area

lubricated with BO. The low friction by BO lubrication is because of the viscosity reduction and surface familiarity associated with heating, while the unaligned OLA boundary has a higher shear force. Another difference is that rubbing has a limited effect on the friction reduction of the OLA and OLA-ZDDP mixture compared to the PLA and its mixture with ZDDP. As shown in Figures 3–12 and 3–13, OLA and the OLA-ZDDP mixture exhibited very low friction coefficients in the unrubbed areas. In addition, the rubbed and un-rubbed areas lubricated with the OLA-ZDDP mixture exhibited similar friction coefficient levels at 100°C. It suggests that the metallic soap was formed even without rubbing.

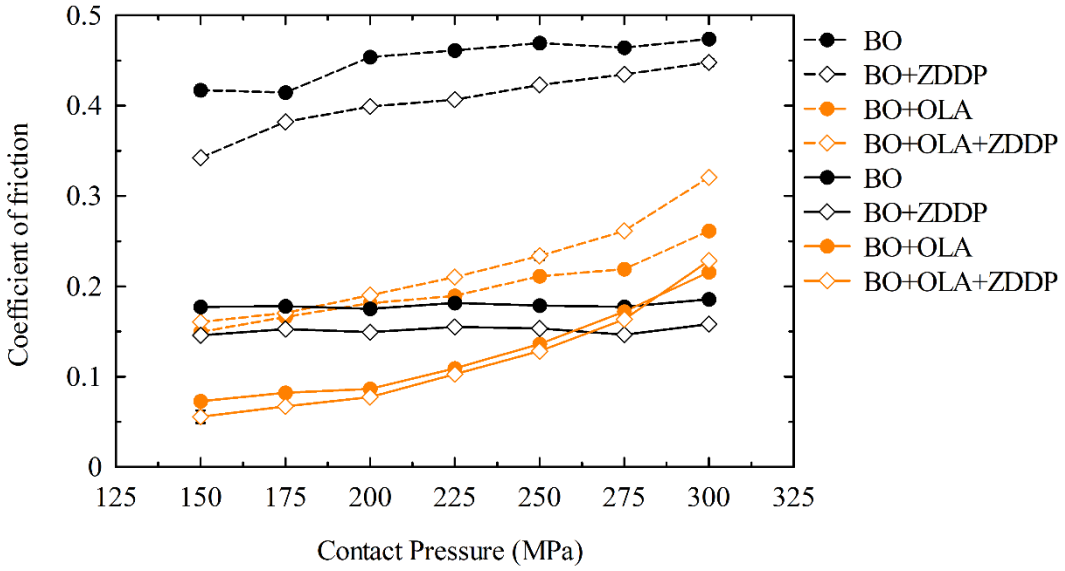


Figure 3–12. Comparison of the rubbed and unrubbed area lubricated at 25°C.

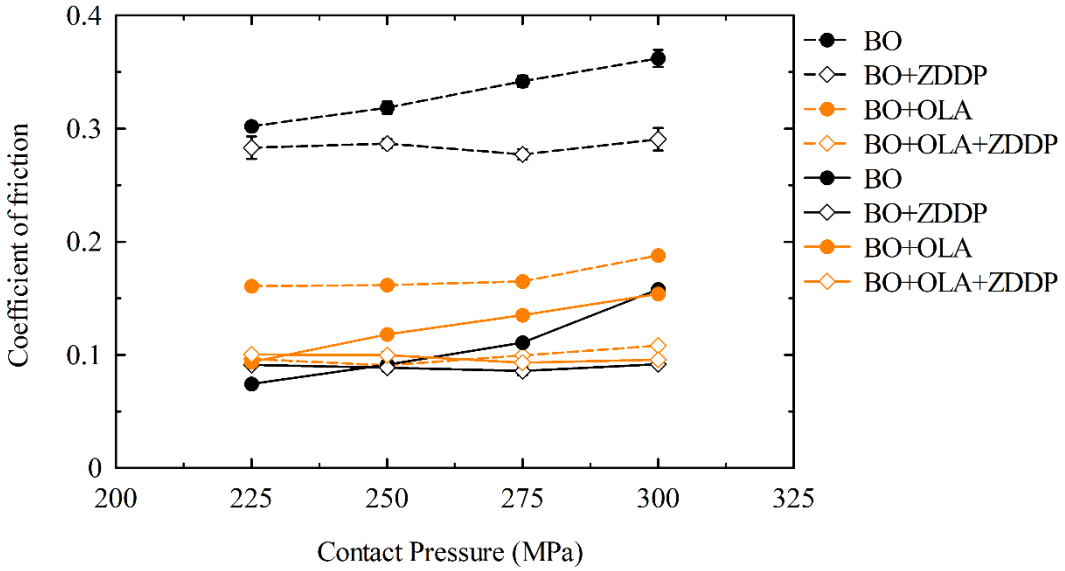


Figure 3–13. Comparison of the rubbed and unrubbed area lubricated at 100°C

The NOS exhibited different outcomes from the model OFMs. As shown in Figure 3–14, the friction coefficient did not increase with increasing contact pressure in the unrubbed area but rather showed better friction reduction at higher pressures, such as 275 MPa and 300 MPa at 25°C. However, in the rubbed area, its friction coefficient became larger with the increasing contact pressure. It is also the same for the NOS-ZDDP mixture. As shown in Figure 3–15, at 100°C, the friction coefficient of unrubbed areas lubricated with NOS and NOS-ZDDP was lower than that of BO, while on the rubbed area, the friction coefficient with NOS turned out to be higher, while the NOS-ZDDP mixture remained a lower friction coefficient than that of BO. In addition, the NOS-ZDDP mixture exhibited a similar contact pressure dependency to the NOS rather than ZDDP at both temperatures. All these results suggest that in the OFM-ZDDP mixture, the OFM dominated the frictional behavior. Rubbing and ZDDP mixing can enhance NOS's tribological performance.

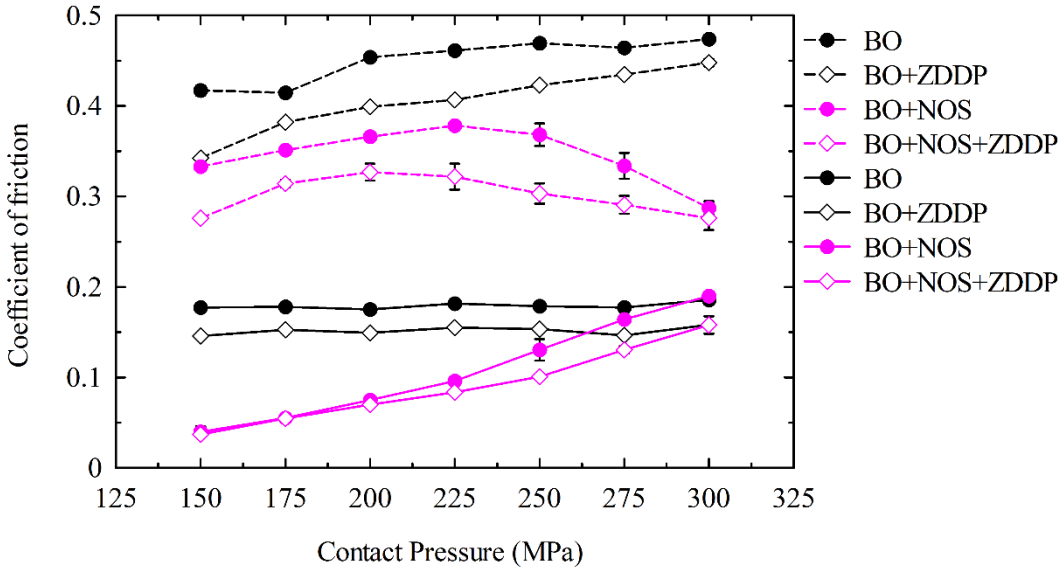


Figure 3–14. Comparison of the rubbed and unrubbed area at 25°C.

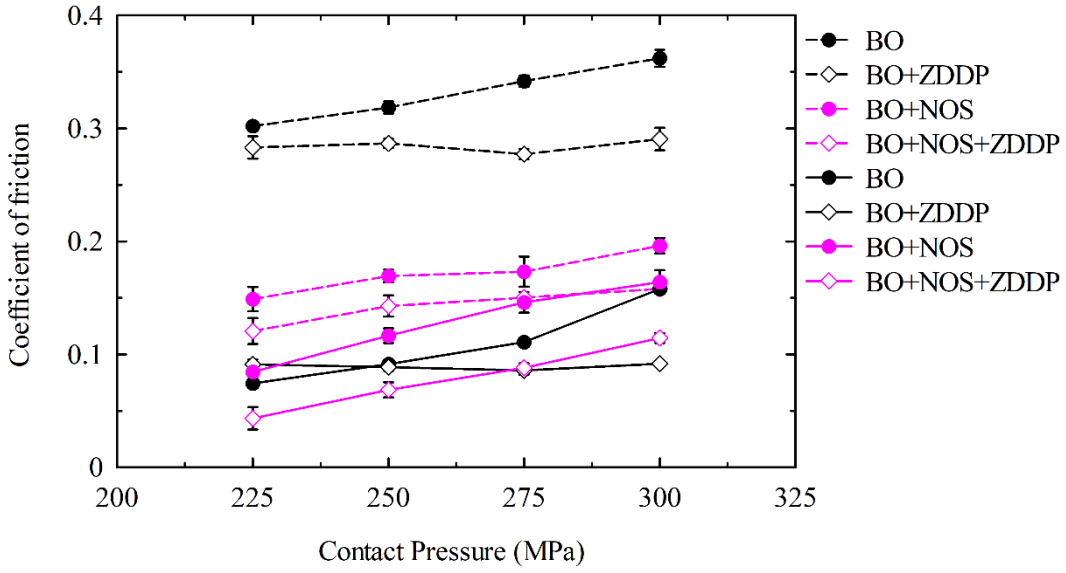


Figure 3–15. Comparison of the rubbed and unrubbed area at 100°C.

## 3.5 Conclusion

This chapter investigated the effects of rubbing on the tribological properties of OFMs and OFM-ZDDP mixtures. The friction coefficients of the rubbed and unrubbed areas under lubrication were measured with AFM and compared. The results are summarized as follows.

1. Rubbing the substrates immersed in BO+ZDDP led to ZDDP tribofilm formation at both 25°C and 100°C. The friction coefficient of the tribofilm was lower than the unrubbed area, but the friction reduction was limited.

2. The friction reduction ability of the PLA-ZDDP mixture depends on temperature. At 25°C, the friction coefficient on the rubbed area was comparable to that of ZDDP tribofilm. In comparison, at 100°C, the friction coefficient on the rubbed area was considerably reduced, although still higher than that of PLA.

3. The lubrication of the OLA-ZDDP mixture exhibited a lower friction coefficient on the unrubbed area than other additive combinations, but the friction reduction benefit from rubbing was limited. In addition, the mixture led to a similar friction coefficient on the rubbed and unrubbed area at 100°C and was close to the friction coefficient of ZDDP tribofilm. It may be due to the intense metallic soap formation resulting in the dissolution of the iron layer and the adsorption of ZDDP on the bare silica surface, thus showing a friction coefficient close to that of ZDDP tribofilm.

4. Different from model OFMs, the NOS-ZDDP mixture exhibited synergistic effects in friction reduction at both 25°C and 100°C. At 25°C, the friction coefficient did not show contact pressure dependence in the unrubbed area but showed pressure dependence in the rubbed area. This suggests that rubbing changed the property of the boundary film formed by the mixture. In addition, at 100°C, the addition of ZDDP effectively reduced the high friction coefficient of NOS due to the irregular alignment.

5. Because AFM enables the formation of tribofilms under boundary lubrication and the friction coefficient measurement while observing the rubbing surface, AFM was chosen for friction testing in this section. However, there are also some limitations in this chapter. First, AFM is limited to additives that do not form convex tribofilms. AFM cannot accomplish molecular-level observations, so a great deal of the discussion in this paper is based on the results of previous studies and the friction reduction concept with OFM summarized by Spikes. Second, the rubbed area is tiny in AFM tests, and the prior technical means cannot perform compositional analysis of the rubbed area. Therefore, the discussion on the formation of metallic soaps and the role of boundary films is still insufficient. These will be described in the following two chapters using macroscopic tests.

# Chapter 4. Mechanisms of the synergistic effect of ZDDP-N-Oleoyl sarcosine in friction-reducing and anti-wear performance

## 4.1. Introduction

In the past decades, a large number of studies have investigated the interaction between the anti-wear additive ZDDP and the FMs to reduce the high friction caused by the ZDDP tribofilm while maintaining its original anti-wear properties [5], [14], [40], [56–59], [68–69], [72–73], [80–83], [85], [89], [92–95], [113–118]. Among them, there are reactive friction reducers represented by MoDTC [56–59], [68–69], [72–73], [114–117], organic additives represented by GMO [40], [80–81], [89], [92–95], and amines/amides [14], [80], [82–85], [113], [118].

MoDTC forms a low-friction $MoS_2$ layer by chemical reaction under rubbing conditions [42–46]. It has been shown that ZDDP provides sulfur in the tribochemical reaction to promote the formation of $MoS_2$, which reduces the friction coefficient while retaining its anti-wear properties to the maximum extent [57–59]. However, it has still been noted in some studies that MoDTC reduces the anti-wear performance of ZDDP tribofilms and that lubrication with MoDTC-ZDDP mixtures results in greater wear on sliding surfaces compared to lubrication with ZDDP alone [72], [114]. In addition, the frictional performance of the tribofilm formed by the MoDTC-ZDDP mixture is related to the composition of the tribofilm, and different temperatures lead to different composition ratios in the tribofilm [73]. However, as the reaction between MoDTC and ZDDP is not the main theme of this paper, it will not be discussed further here.

In this paper, we focus on another class of friction modifiers, the OFMs, which, unlike MoDTC, do not require a chemical reaction to "activate" their friction-reducing effects. OFMs form single or multi-layer films on sliding surfaces by adsorption, which reduces wear and friction by preventing direct contact [52], [119]. Among them, GMO is a representative industrial OFM. GMO consists of an oleoyl tail, a carboxyl group, and two hydroxyl groups. Some studies suggest that GMOs are hydrolyzed to oleic acid and glycerol during sliding [86–87]. The hydrolysis products form aggregates and micelles that bind better to the metal, thus reducing the coefficient of friction [88], [120–121]. However, the synergistic effect of friction reduction and wear reduction in the GMO-ZDDP mixture is not clear. It was shown that at the Fe/Fe interface, the addition of GMO to ZDDP-containing oil leads to a thinner reaction film and that GMO delays the friction increase caused by ZDDP, but its effect can only last for a limited time [40]. At the DLC/DLC interface, the GMO-ZDDP mixture reduces friction to the same level as GMO alone, but no additional friction reduction is achieved, or anti-wear reaction film formation is observed [89], [94–95]. In addition to the GMO, the tribological effects of amine/amide and ZDDP mixtures have been extensively studied. The addition of saturated amines, especially monoamines, into

ZDDP results in a synergistic effect on friction reduction and anti-wear properties [83–84], but the effect is dependent on the molar ratio of the additives [84]. The addition of oleylamine to ZDDP results in limited friction reduction and slightly negative anti-wear properties [81-82], whereas the addition of oleamide to ZDDP results in a synergistic effect on friction reduction on the steel surface but limited synergistic effects in terms of anti-wear properties [80]. The mechanism of the synergistic effect of the amine/amide-ZDDP mixture may originate from the differences in the complex formation of the additives. It has been shown that the addition of the GMO together with basic fatty acids results in the formation of neutral ZDDP complexes, whereas the addition of amines results in the formation of basic ZDDP complexes [79]. In addition to GMO and amine compounds, fatty acids are also a typical class of OFM. However, there is little research on the synergistic effects of fatty acids-ZDDP mixtures. The reason for this, the author think, is that acids are inherently corrosive, which leads to their limited use in industry. Although friction reduction is important in environmental protection, energy conservation, and emission reduction, as Holmberg points out, wear seems to be more important than friction because it can lead to catastrophic failures and operational breakdowns with negative effects on productivity and costs [122].

In addition to the OFM mentioned above, this study focuses on the tribological properties of NOS and its performance when mixed with ZDDP. NOS is an oleic acid derivative with a sarcosine head consisting of an oleoyl tail, a carboxyl group, and an amide group. The sarcosine head forms a chelate-liking structure on the metal surface [96], while the C=C double bond of the oleoyl tail enhances the adsorption [90], [123]. Because of the strong adsorption of NOS to metal surfaces, it has been suggested to act as an OFM in engine oils [98] though it was first used as a rust inhibitor [96–97]. NOS inhibits boundary friction and improves oil retention through its strong adsorption film [98]. In Chapters 2 and 3, we tested the adsorption film of NOS and NOS-ZDDP mixtures and the friction coefficient of the boundary film formed under rubbing with those lubrications, respectively. The results indicate that when mixed with ZDDP, the mixture is highly likely to suggest a synergistic effect to reduce friction. Therefore, the main purpose of this study is to clarify the tribological properties of NOS and its performance when mixed with ZDDP.

In this chapter, ball-on-disk friction tests were performed to investigate the tribological properties of NOS and NOS+ZDDP additive mixtures. After that, the chemical composition of the reaction film and the mechanism of their synergistic effects were studied using XPS.

## 4.2 Experimental

### 4.2.1 Materials

SUJ2 disks and balls were used in this study. The disks were purchased from Standard Test Piece

Co., Ltd. The original size of the disks was 15×15 mm, and the thickness was 4mm. The surface of the substrate was vacuum hardened. The surface roughness was up to 0.04μm Ra, and the hardness was 58-60 HRC. To facilitate the experiment, the disks were cut into small pieces 10 mm square by wire-cut electrical discharge machining. The balls were purchased from Tsubaki Nakashima Co., Ltd. The balls were 3/16 inches in diameter. The roughness of the balls was up to 0.05μm Ra, and the hardness was 62-67 HRC. The balls and disks were ultrasonically cleaned with acetone for 10 minutes before the tribotests. The testing oils used in this chapter were the same as those mentioned: ZDDP in PAO4, NOS in PAO4, and ZDDP-NOS mixture in PAO4. The information about the testing oils is shown in Table 4-1.

Table 4–1 Lubricating oils

| Lubricating oil | Additive |
|---|---|
| PAO (poly-α-olefin) | none |
| PAO+ZDDP | ZDDP (700 ppm P) |
| PAO+NOS | NOS (0.3 mass%) |
| PAO+ZDDP+NOS | NOS (0.3 mass%) and ZDDP (700 ppm P) |

### 4.2.2 Friction tests

The tribotest was performed using a ball-on-disc device (FPR-2100, RHESCA, Japan, refer to Figure 4–1). The test conditions are listed in Table 4–2. The friction tests were performed in the linear reciprocating mode under boundary lubrication conditions with a lubricating oil volume of 60 μl. Each test was repeated three times to check reproducibility and to obtain the average friction coefficient. The steady-state friction coefficient was defined as the average friction coefficient for the last 200 of the 1800 cycles. The steady-state friction coefficient was used as an index to compare the tribological performance of each oil. After the test, the worn balls were rinsed with acetone and hexane and dried with $N_2$ gas. The discs were cleaned with the same detergents. Microscopic images of the worn state of the balls and discs at the same magnification were taken to compare the morphological features of the tribofilms and the anti-wear effects of the different oils. An ultra-high-magnification USB microscope (NSH130CS-R, SHODENSHA, Inc., Japan) was used to evaluate the wear condition of the balls and disks after the tribotests under 5 N load. The widths of the wear tracks on the disks and the wear areas on the balls were measured for anti-wear evaluation.

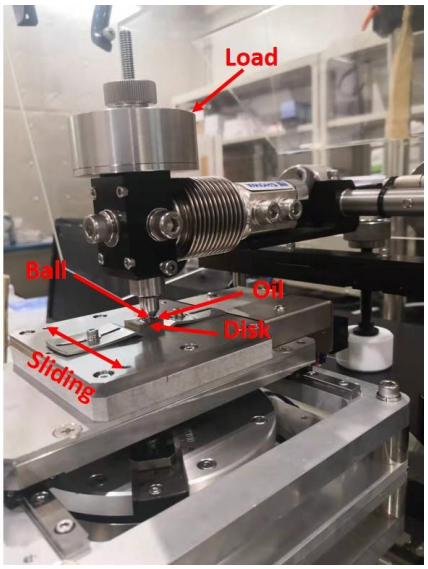


Figure 4–1. Ball on disk tribo-meter FPR-2100

Table 4–2 Tribo-test conditions

| Parameter | Values |
|---|---|
| Sliding speed (mm/s) | 10 |
| Stroke length (mm) | 5 |
| Normal load (N) | 1, 3, 5 |
| Test duration (s) | 1800 |
| Maximum pressure (MPa) | 764, 1102, 1306 |
| Average pressure (MPa) | 509, 734, 871 |
| Temperature (°C) | 25 |

### 4.2.3 Chemical composition analysis

XPS analyses were performed using a PHI 5000 VersaProbe2 X-ray Photoelectron Spectroscope (ULVAC Equipment Sales, Inc., Japan). The excitation source was a monochromatized Al Kα X-ray beam. The beam size was 100-µm diameter, and the pass energy was set to 117.4-eV. The worn disks after the tribotests at 5 N were analyzed. The analysis points inside and outside the wear areas were selected using secondary X-ray images of the substrate surfaces. An example image is shown in Figure 4-2. Data processing was performed using CasaXPS software (version 2.3.24, Casa Software Ltd., UK). After subtracting the Shirley background, the spectra were fitted using the product of Gaussian and Lorentzian functions.

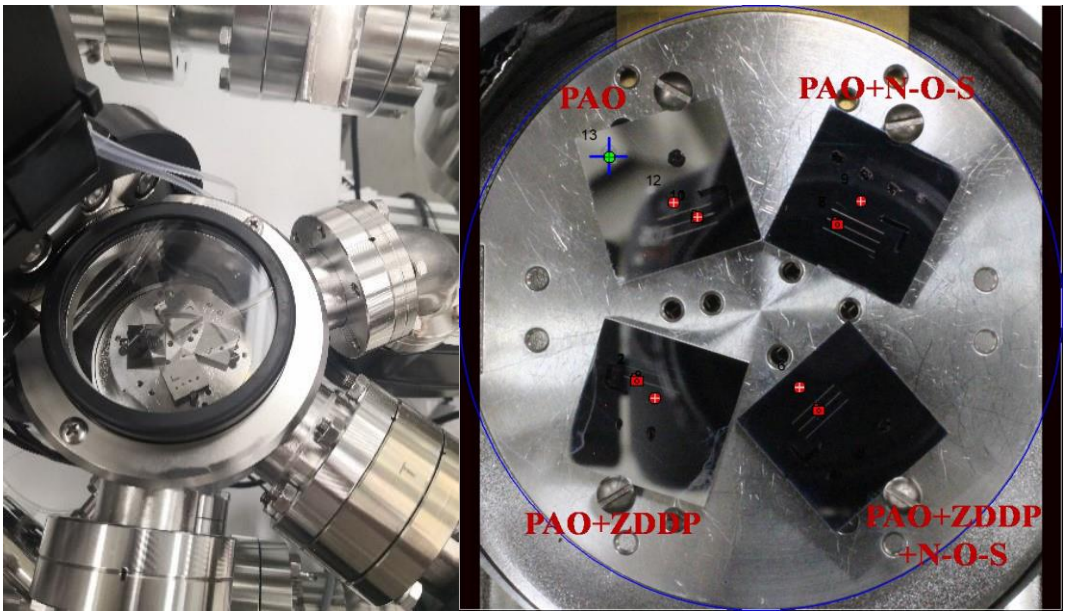


Figure 4–2. XPS measurement on the disks

## 4.3 Results and discussion

### 4.3.1 Tribological behavior

#### 4.3.1.1 Friction coefficient

Figures 4–3, 4–4, and 4–5 show the friction coefficients under 1N, 3N, and 5N loads, respectively. In these figures, a clear trend between the friction coefficient and the sliding cycle number was observed. The friction coefficient with PAO+NOS lubrication was the lowest for the first few hundred cycles, then slightly exceeded that with PAO+ZDDP+NOS lubrication and stabilized. The friction coefficient with PAO+ZDDP lubrication initially increased, gradually decreasing after reaching a peak, and then slowly increasing again. Moreover, the trends of the friction coefficients for the three additive mixtures were very similar for all applied loads.

With PAO+NOS lubrication, the friction coefficient decreased to a minimum value of 0.078 after about 300 cycles when the load was 1 N and increased to 0.104 after about 660 cycles and remained stable. When the load was 3N, the friction coefficient stabilized within only 430 cycles and only 260 cycles at 5N. With PAO+NOS lubrication, the applied load increase shortened the time for the friction coefficient to stabilize. However, with PAO+ZDDP and PAO+ZDDP+NOS lubrication, the load increase extended the running-in stage. With a load of 1 N, the friction coefficient stabilized after only 300 cycles. At a load of 3N, 380 cycles were required. The threshold for stabilization at 5N was difficult to define because the friction coefficient increased continuously with PAO+ZDDP lubrication.

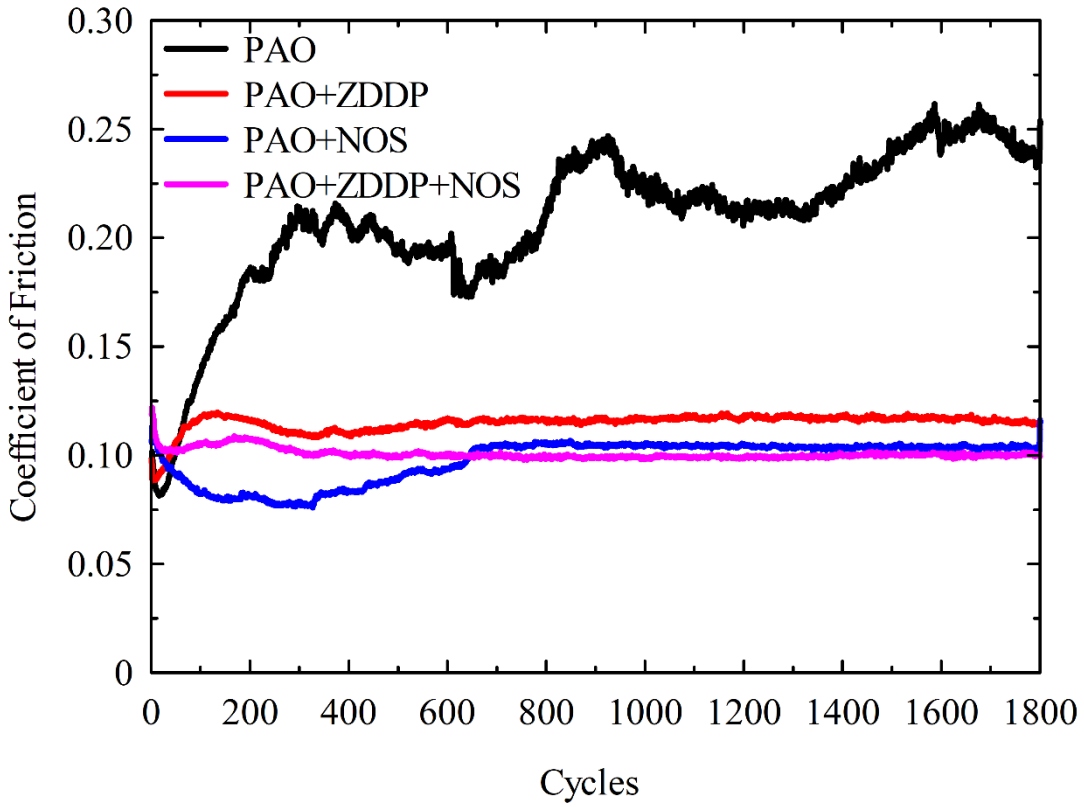


Figure 4–3. Friction coefficient at 1N

The trend of the friction coefficient with PAO+ZDDP lubrication and PAO+ZDDP+NOS lubrication was very similar. The friction coefficient showed a decreasing-increasing-decreasing trend under the lubrication of both oils, taking the results for the load of 5N as an example. However, with PAO+ZDDP lubrication, it took 20 cycles for the friction coefficient to start increasing, while only 10 cycles were required with PAO+ZDDP+NOS lubrication. On the other hand, the maximum friction coefficient was 0.123 with PAO+ZDDP lubrication, while with PAO+ZDDP+NOS, the maximum value was only 0.109. The friction coefficient with PAO+ZDDP+NOS lubrication stabilized after 350 cycles. In contrast, with PAO+ZDDP lubrication, the friction coefficient decreased to 0.11 after 350 cycles and began to rise slowly, as evidenced in Figure 4–5. By comparing the results of PAO+ZDDP and PAO+ZDDP+NOS, it suggests that during the running-in stage, the change in friction coefficient originating from the formation of the ZDDP reaction film exhibited a significant effect on the performance of the NOS-ZDDP mixture. However, during the steady state, the NOS in the mixture effectively reduced friction and kept the friction coefficient stable.

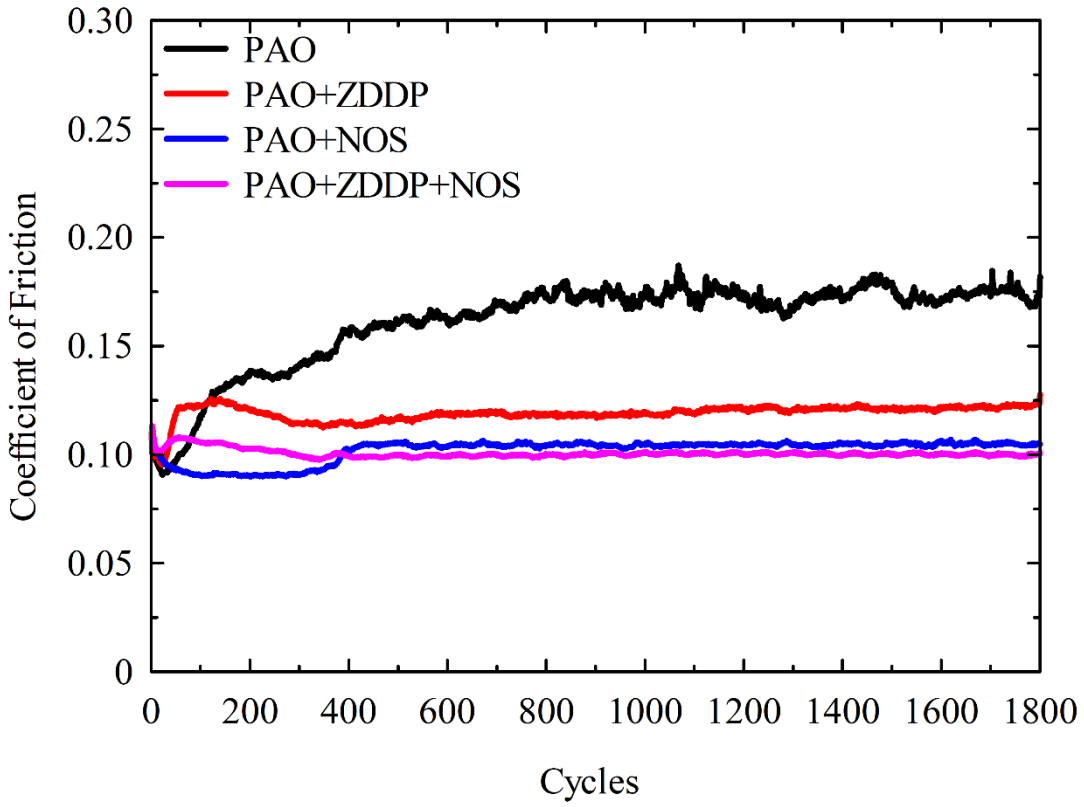


Figure 4–4. Friction coefficient at 3N

The steady-state friction coefficients for each lubricating oil at different loads are shown in Figure 4–6. The black dashed line in Figure 4–6 marks the steady-state friction coefficient with PAO+ZDDP+NOS lubrication at a load of 5N as a reference. As the load increased, the steady-state friction coefficient with PAO lubrication gradually decreased. In contrast, the steady-state friction coefficient for all lubricating oils containing additives increased slightly with increasing load. In contrast, the steady-state friction coefficient with PAO+ZDDP+NOS lubrication was the smallest at all loads.

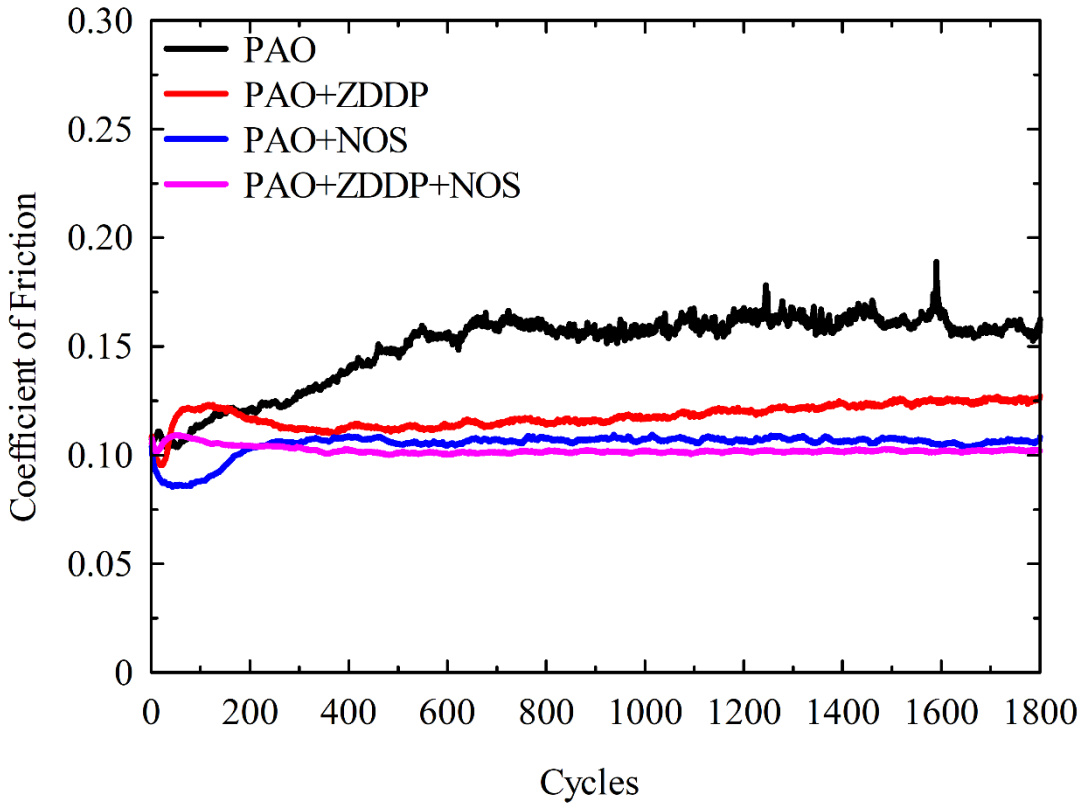


Figure 4–5. Friction coefficient at 5N

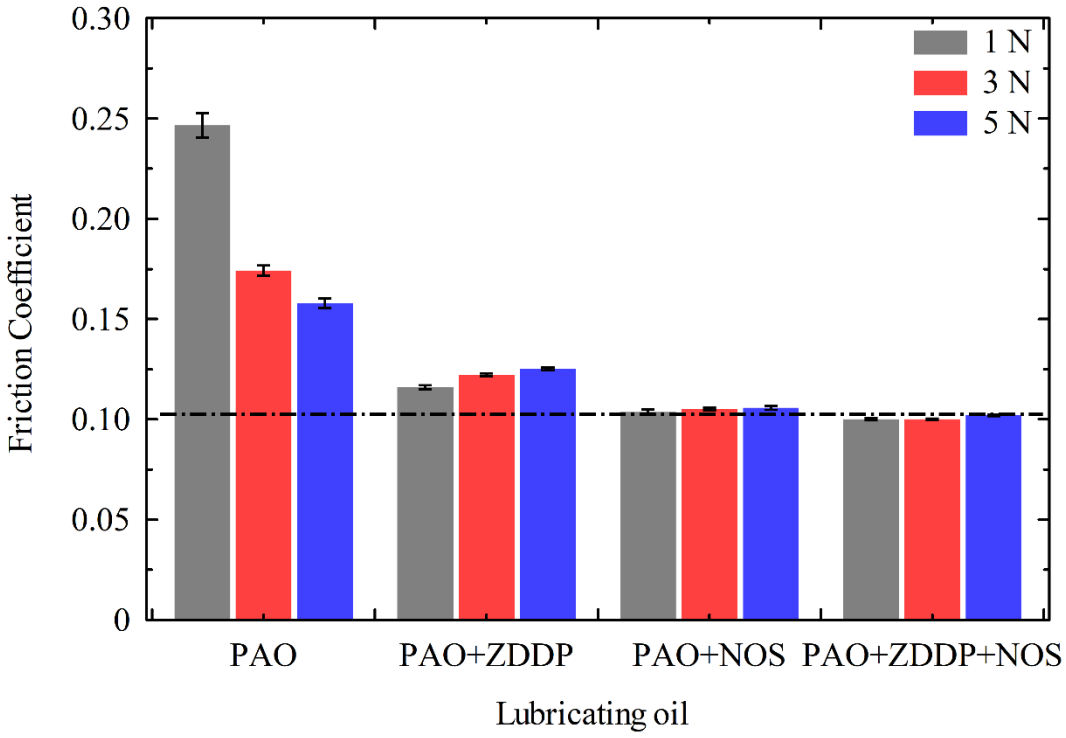


Figure 4–6. Steady-state Friction coefficient

#### 4.3.1.2 Wear state analysis

Figures 4–7a, 7b, 7c, and 7d show the imaging of the wear state of the balls and disks lubricated with PAO, PAO+ZDDP, PAO+NOS, and PAO+ZDDP+NOS respectively, after 1800 sliding cycles under 5N load condition. The direction of the arrow in Figure 4–7a indicates the sliding direction. As seen from the images, the wear diameter of the balls was consistent with the wear width of the disks. Among those balls, the PAO-lubricated ball exhibited an adhesive-wear-like feature. Figure 4–7a shows that some dislodged particles were attached to the ball surface, even in the noncontact area. This is because the contact surfaces were in direct contact with each other, so the adhesion points were sheared and transferred to the ball surface during the sliding process. At the same time, groove-like scars were seen in the contact area because the base oil did not protect the sliding surface sufficiently.

On the other hand, adding additives to PAO effectively improved wear resistance. As shown in Figure 4–7b, the tribofilm on the ball also exhibited grooved wear scars when lubricated with PAO+ZDDP, but the degree of wear was noticeably lower than that when lubricated with PAO. With PAO+NOS lubrication (Figure 4–7c), the tribofilm was relatively uniform over the entire ball surface contact area, and there was a clear grooved wear feature on the disk surface. When lubricated by PAO+ZDDP+NOS (Figure 4–7d), it is obvious that there were only dotted marks on the surface of the ball instead of groove-like wear. The dotted marks may be the key reason for the synergistic effect in terms of friction reduction and wear resistance. Also, on the disc, the wear under PAO+ZDDP+NOS lubrication was extremely light (Figure 4–7d), while PAO+ZDDP (Figure 4–7b) and PAO+NOS (Figure 4–7c) showed similar levels of wear.

Figure 4–8 shows the relative wear diameters of the balls with different lubricating oils and at different load conditions. The relative wear diameters were calculated using that for PAO at 5N as 1.0. As the load increased from 1N to 5N, the wear diameters of all balls became larger. Among them, the wear diameter of the ball with PAO+ZDDP+NOS lubrication was the smallest at each load, which is consistent with its lowest friction coefficient. When the load was increased from 3N to 5N, the increase in wear diameter of the PAO-lubricated ball was the largest, and the PAO+ZDDP+NOS-lubricated ball was the smallest. These results suggest that the NOS-ZDDP additive mixture promoted positive wear resistance.

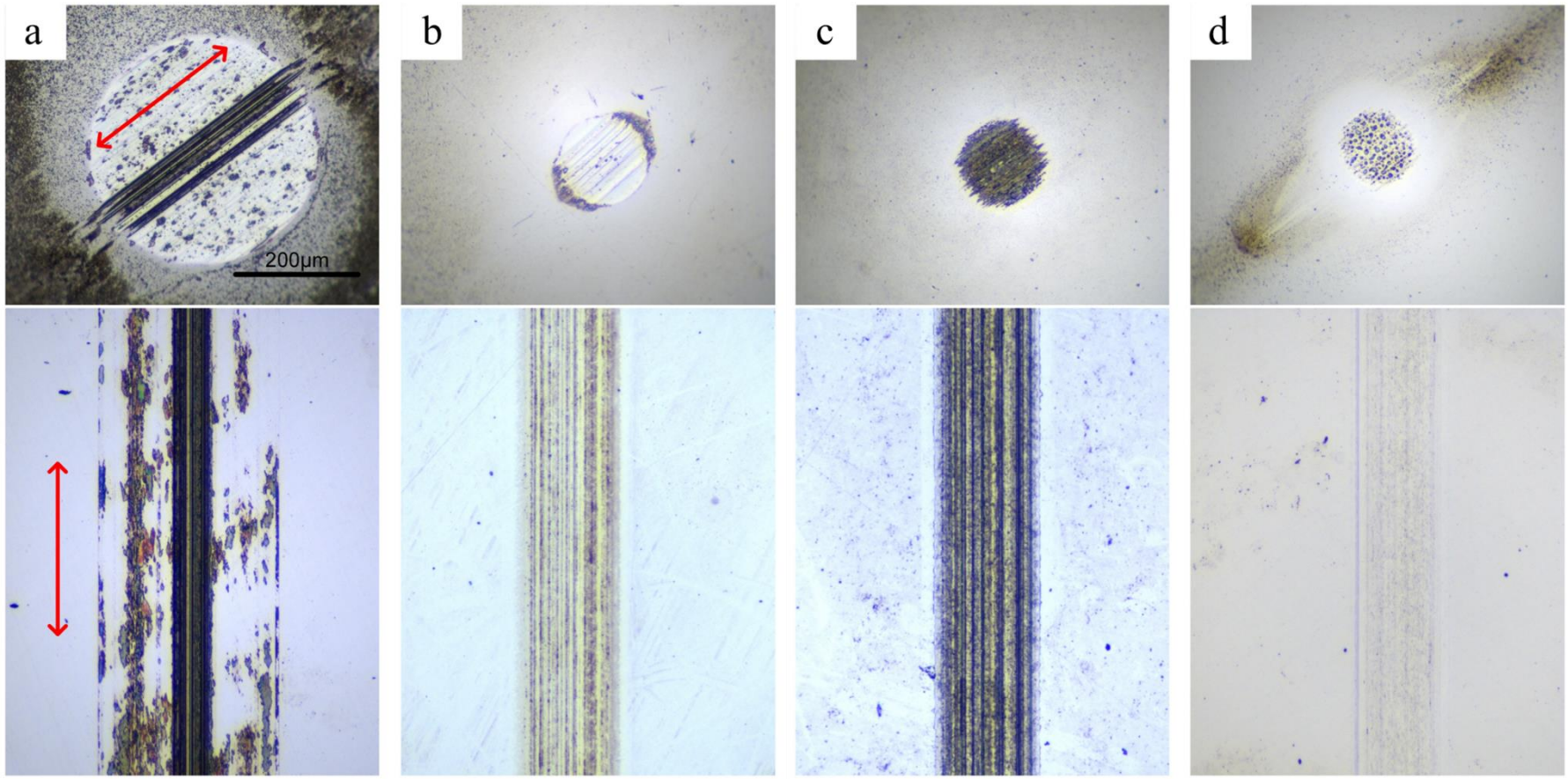


Figure 4–7. The imaging of the wear state of the balls and disks lubricated with each lubricating oil

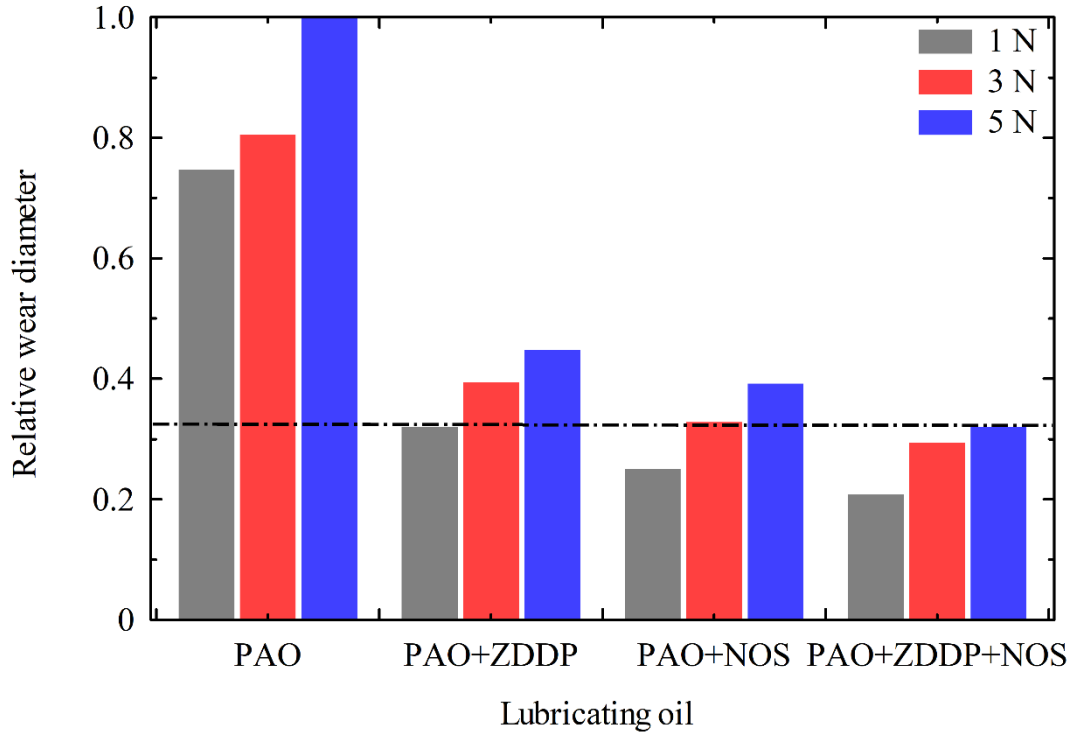


Figure 4–8. Relative wear diameters of the balls.

#### 4.3.1.3 Tribo-film formation process

Figure 4–9 is an enlarged version of Figure 4–5, showing the friction coefficient for the first 600 cycles under a 5N load. In Figure 4–9, the difference in the running-in stage for the tribological performance with various lubricating oils was observed. With PAO+NOS lubrication, the lowest friction coefficient was observed in the first 200 cycles, which indicates that a sufficient NOS adsorption layer between the ball and the disk effectively reduces the friction. After that, the friction coefficient increased as the test cycle proceeded. With PAO+ZDDP lubrication, the friction coefficient started to increase after the $20^{th}$ cycle, which may be related to the formation of the ZDDP tribofilm. The friction coefficient reached the maximum after 40 cycles and then decreased. In the case of PAO+ZDDP+NOS lubrication, the friction coefficient in the first 40 cycles was higher than that with the lubrication of the other two kinds of oil. However, the change in the friction coefficient with the number of cycles was smaller.

The contact area of the balls at the points on the friction coefficient curves marked in Figure 4–9 was imaged to clarify the relationship between tribofilm morphology and friction coefficient variation. For PAO+NOS, these points were marked at the $60^{th}$, $200^{th}$, and $600^{th}$ cycles, as $A_1$, $A_2$, and $A_3$, respectively. For PAO+ZDDP, they were marked at the $20^{th}$, $75^{th}$, and $600^{th}$ cycles ($B_1$, $B_2$, and $B_3$); for PAO+ZDDP+NOS, they were marked at the $10^{th}$, $200^{th}$, and $600^{th}$ cycles ($C_1$, $C_2$, and $C_3$). The results are shown in Figure 4–10. In this experiment, each point corresponds to the

contact area of each ball. For example, $A_1$ shows the contact area of a ball rubbed after 60 test cycles, while $A_2$ is the contact area of another completely different ball after 200 test cycles. These contact areas were enlarged to the same size to make them easier to see. As the number of cycles increased, the characteristics of the tribofilm in the contact area became more and more obvious.

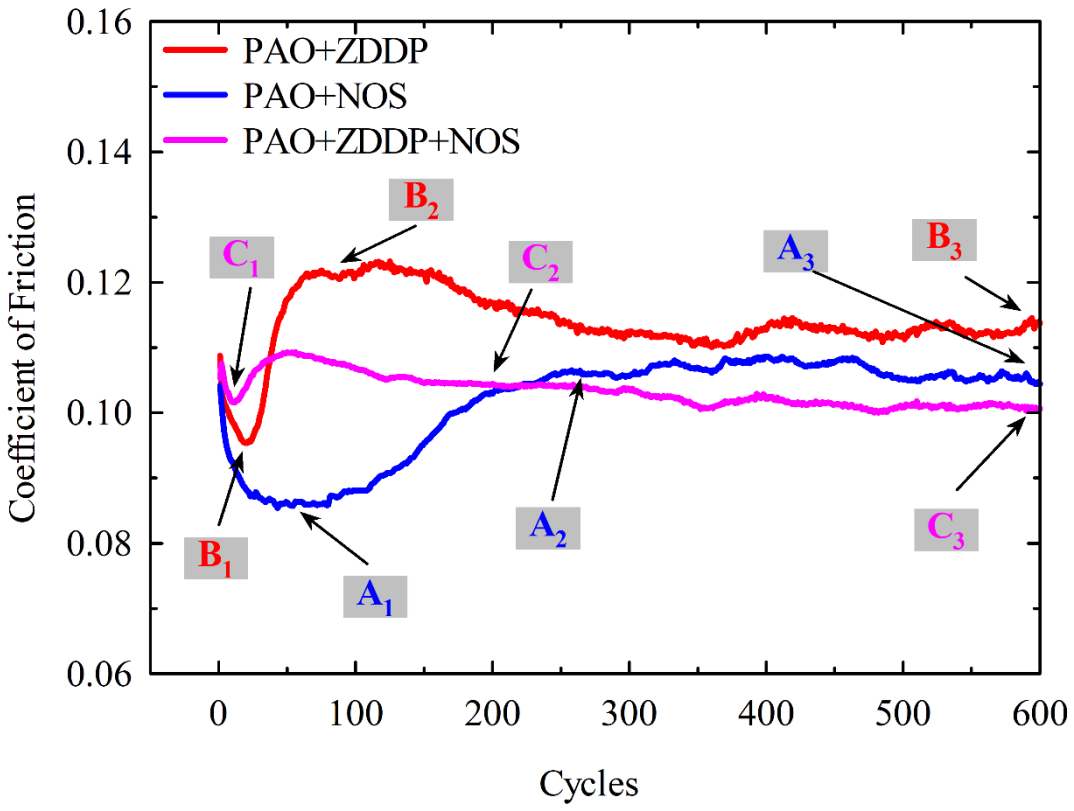


Figure 4–9. Enlarged view of the friction coefficient of the first 600 cycles.

With PAO+NOS (Figure 4–10a), slightly dotted structures were seen in the contact area at $A_1$, where the friction coefficient was the lowest. Previous studies have reported an increase in NOS density in the contact area under boundary lubrication conditions, resulting in a very low friction coefficient [124]. The low friction of PAO+NOS in the running-in stage in this study may be based on the same mechanism. At $A_2$, the dotted structures grew larger and more pronounced, and the friction coefficient exceeded that of PAO+ZDDP+NOS at the same cycle. At $A_3$, the dotted structures were no longer observed but were replaced by friction-induced abrasion marks, indicating that the previously formed NOS friction film had been physically broken. Similar wear marks were seen in the contact area at the end of the 1800$^{th}$ cycle. However, the PAO+NOS still exhibited good tribological performance, and the damage to the NOS tribofilm did not lead to a further increase in the friction coefficient.

With PAO+ZDDP (Figure 4–10b), barely any lubricating film was evident at B1, where the friction coefficient was the lowest. The wear area was scorched yellow with obvious groove-like

structures at B2, with the highest friction coefficient. The color change on the ball and the increase in friction coefficient indicates that under sliding conditions, B1 to B2 represented the transition from ZDDP adsorption to ZDDP decomposition. Then, from B2 to B3, the friction coefficient decreased again as the tribofilm was fully formed. After the 1800th cycle, a clear groove-like wear scar was seen on the contact area, which indicates the destruction of the tribofilm under sliding conditions. The groove-like wear scars may be the reason for the slow increase in the friction coefficient from 600 to 1800 cycles with the lubrication of PAO+ZDDP, as shown in Figure 4-7c.

With PAO+ZDDP+NOS (Figure 4–10c), the tribofilm had characteristics of both the NOS tribofilm and the ZDDP tribofilm. At $C_1$, the central area exhibited a slight groove-like feature, similar to that seen in $B_1$, while the lateral region exhibited a dotted feature, similar to that seen in $A_1$. This suggests that the adsorption of ZDDP limited the friction-reducing ability of NOS during the first 40 cycles, resulting in a higher friction coefficient. As the cycle number increased, the dots and grooves coupled together and grew gradually from $C_2$ to $C_3$ in the direction normal to the sliding direction. The morphology of the tribofilm seen on the contact area indicates that NOS changed the high frictional nature of the ZDDP tribofilm so that the increase in friction coefficient from C1 was not as drastic as the increase with PAO+ZDDP. In the steady state, NOS continuously inhibited the formation of the high-friction ZDDP tribofilm and inherited the advantages of ZDDP's anti-wear properties. As a result, it subsequently exhibited a stable friction coefficient and efficient wear resistance. In the $1800^{th}$ cycle, the coupled tribofilm fulfilled the entire contact area.

Through the morphological analysis above, the relationship between tribofilm formation and friction coefficient change can be summarized as follows. With PAO+NOS lubrication, although the friction coefficient was low at the initial stage, the formation of the tribofilm led to an increase in the friction coefficient, but the friction coefficient tends to stabilize after the full tribofilm formation as observed at $A_2$. With PAO+ZDDP lubrication, the friction coefficient and contact area size increased with the formation of ZDDP tribofilm. The friction coefficient increased slowly during the friction cycle after full tribofilm formation, as observed at $B_3$. In the case of PAO+NOS+ZDDP lubrication, dotted structures similar to $A_2$ can be seen at $C_2$, $C_3$, and $C_4$. This suggests that the mixture of ZDDP also could not completely prevent the reaction of NOS and the formation of NOS-derived tribofilm. However, it took more sliding cycles for NOS in the mixture to form a tribofilm (at least 600 cycles) than the NOS alone (200 cycles). In addition, after 1800 cycles, the groove-like abrasion marks, as shown in $B_4$, could no longer be observed in the contact area, indicating that the NOS effectively improved the wear-resistance properties of the tribofilm.

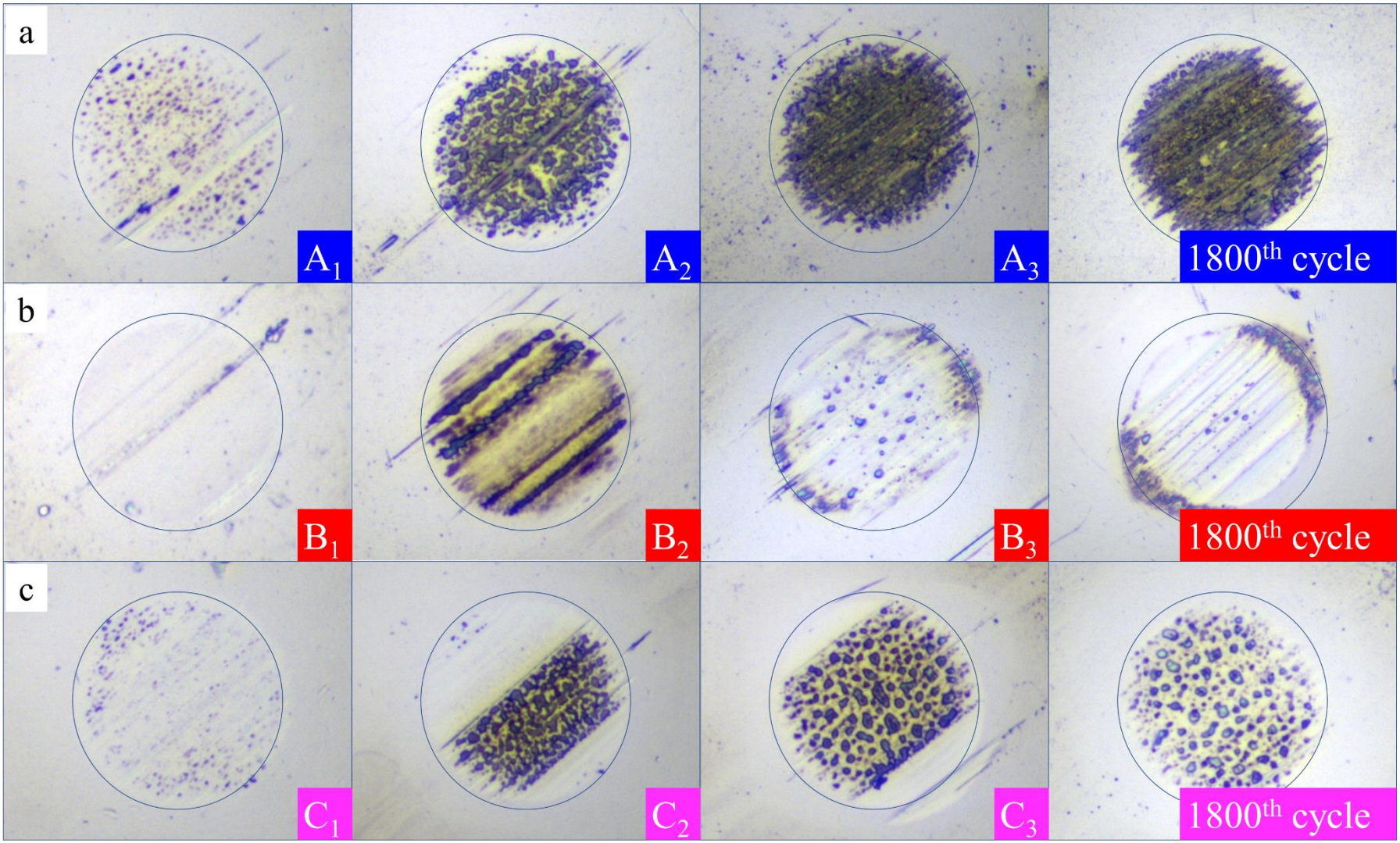


Figure 4–10. Tribofilm on the contact area at marked cycle

### 4.3.2 XPS analysis

#### 4.3.2.1 XPS spectra in friction tracks

Figure 4–11 to Figure 4–22 show the XPS spectra of C1s, N1s, O1s, P2p, S2p, Fe2p3, and Zn2p3 and the peak distribution of C1s and O1s recorded inside the friction tracks. The X-ray beam size was φ100 μm to ensure that only the inner area of the friction track was analyzed to shave off the contribution of the unrubbed area to the analytical results. In the analysis, all signals were fitted using Gaussian/Lorentzian peaks. The binding energies of the photoelectron peaks are listed in Table 4–3 as a numerical result.

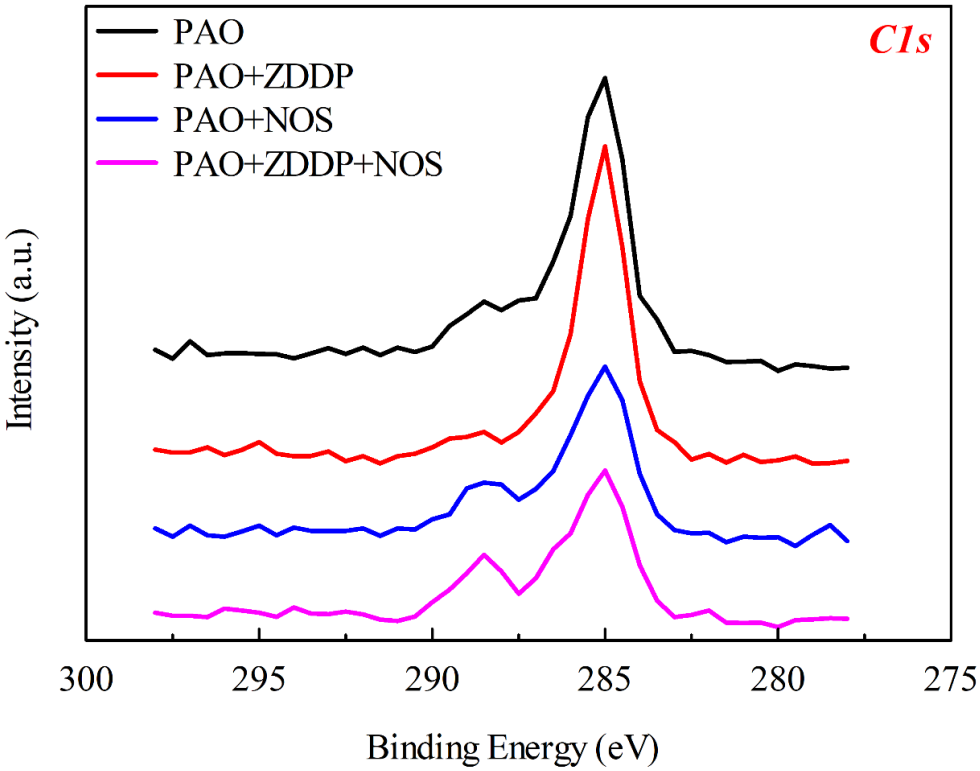


Figure 4–11. C1s spectra inside the friction tracks.

**C1s spectra:** The C1s spectra are shown in Figure 4–11, and the peak distribution with PAO+NOS and PAO+ZDDP+NOS are shown in Figure 4–12 and Figure 4–13, respectively. The friction tracks corresponding to all lubricating oils recorded a strong signal around 285.0 eV, which is due to the aliphatic C (C-C, C-H) bonds [125]. The fit results indicate furtherly that a small amount of signal was recorded around 286.5 eV, on all friction tracks. These signals correspond to the C-O bond and may be due to oxidation brought by sliding. In addition, the third peak near 288.5 eV was recorded in the friction marks lubricated by PAO+NOS (Figure 4–12) and PAO+ZDDP+NOS (Figure 4–13). As these peaks were only recorded when the NOS was used, they may originate from the carboxyl groups in the NOS. The appearance of this peak in the track lubricated with

PAO+ZDDP+NOS suggests that NOS-derived tribofilm was formed even in the additive mixture. This agrees with the morphological results shown in Figure 4–10c that the tribofilm formed by PAO+ZDDP+NOS exhibited synergistic properties of PAO+ZDDP and PAO+OS.

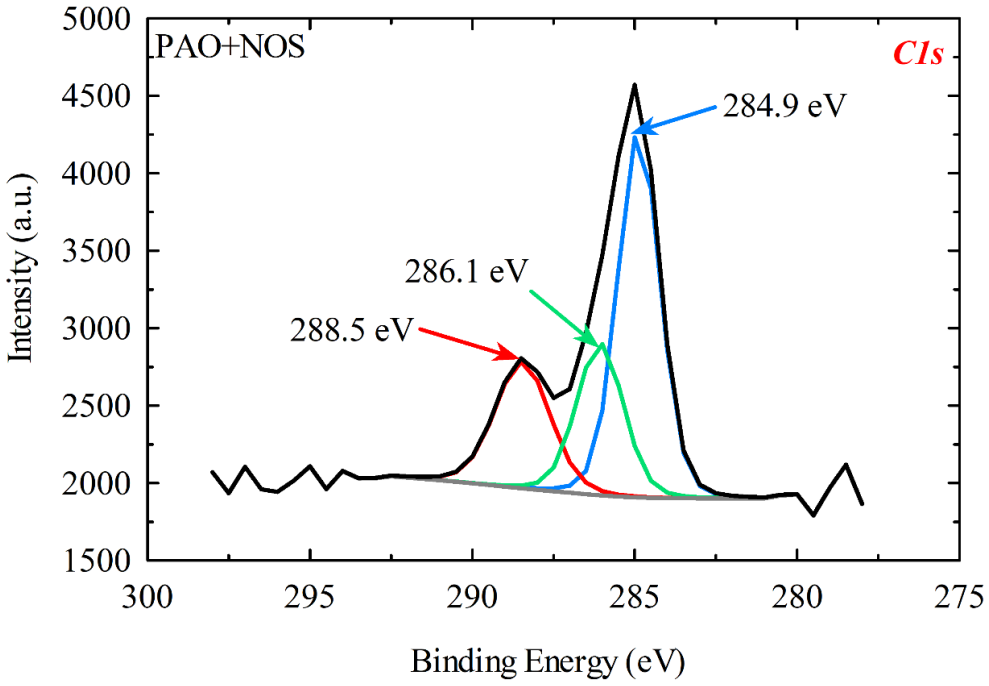


Figure 4–12. C1s peak distribution with PAO+NOS.

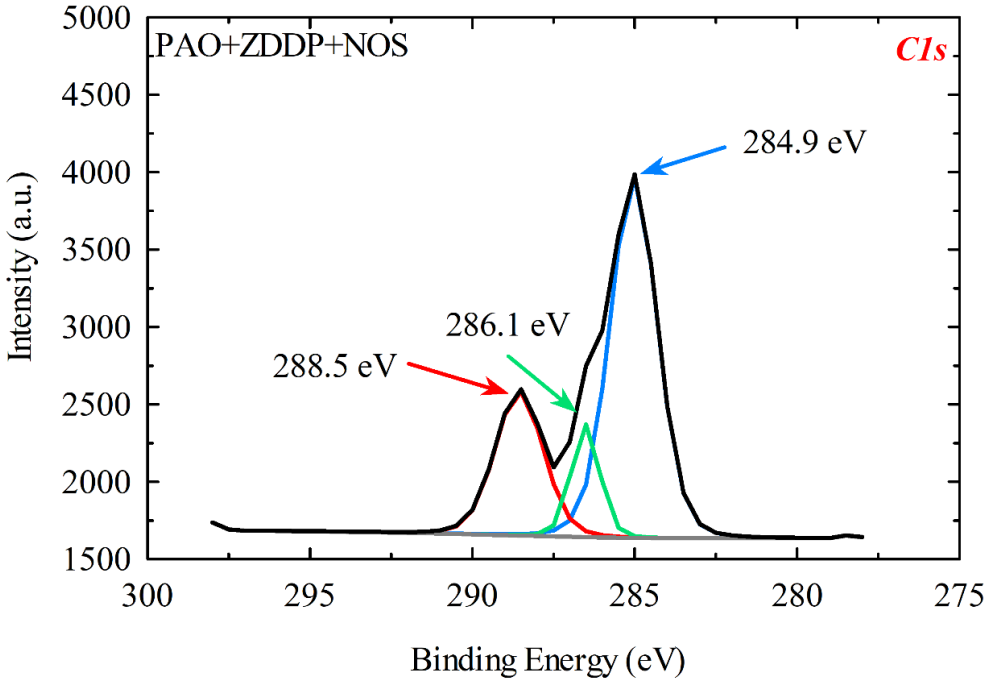


Figure 4–13. C1s peak distribution with PAO+ZDDP+NOS.

**N1s spectra:** The N1s spectra are shown in Figure 4–14. An intense N1s signal peak at 400.2 eV was recorded in the friction tracks with PAO+NOS and PAO+ZDDP+NOS. It originated from the nitrogen in NOS. A very weak N1s signal peak was recorded in the friction tracks with PAO and PAO+ZDDP at 400.2 eV. These signals were detected because of the nitriding process in the substrate fabrication.

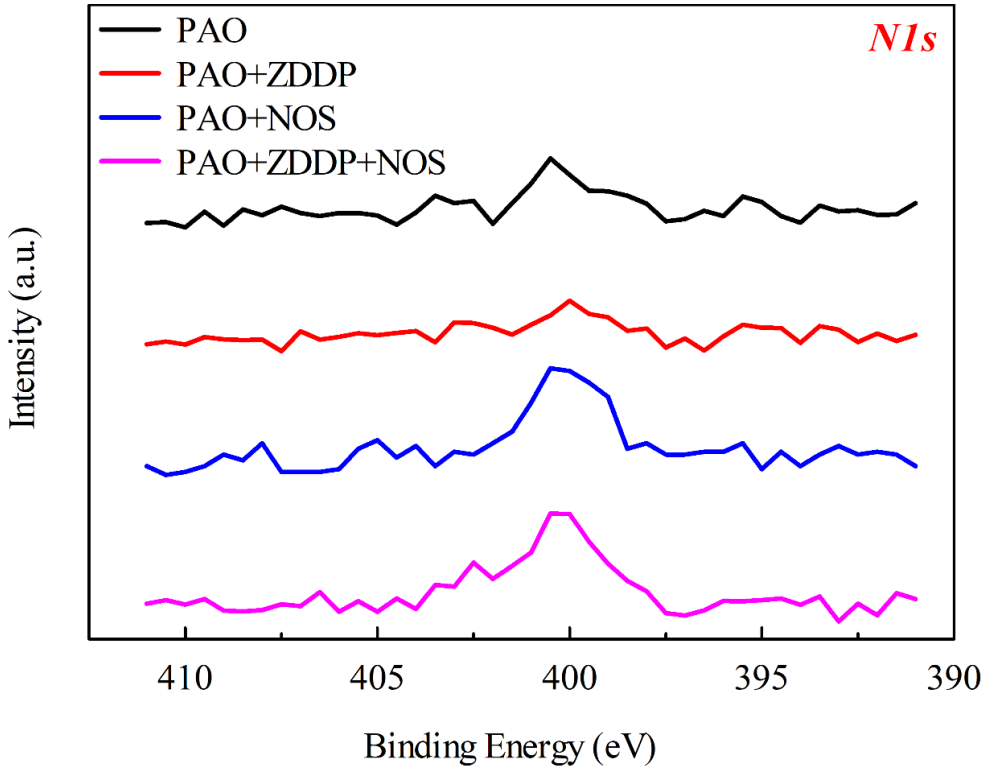


Figure 4–14. N1s spectra inside the friction tracks.

**O1s spectra:** The O1s spectra are shown in Figure 4–15, and the peak distribution with PAO+NOS, PAO+ZDDP, and PAO+ZDDP+NOS are shown in Figure 4–16, Figure 4–17, and Figure 4–18 respectively. Two peaks were recorded in the friction marks with each lubricating oil. For PAO, PAO+OS, and PAO+ZDDP+NOS, there was a common signal peak recorded around 531.2 eV corresponding to non-bridging oxygen. Another signal peak was recorded at around 529.9 eV. Whereas, as shown in Figure 4–17, the two signal peaks recorded in the friction track corresponding to PAO+ZDDP were around 531.4 eV and 533.8 eV. The main peak at 531.4 eV is attributed to non-bridging oxygen in the poly-phosphate chains, and considering the composition of ZDDP, this peak can also be attributed to other oxygen-containing groups in the polyphosphate chain, such as sulfate, carbonate, and hydroxide [126-127]. Another small peak of 533.8 eV corresponds to the bridging oxygen in FePO4 [128], which was not detected in the PAO+ZDDP+NOS track (Figure 4–18). In addition, the 529.9 eV peak corresponds to a higher

percentage in the friction track with PAO+NOS+ZDDP lubrication compared to that with PAO+NOS lubrication (Figure 4–16). This may be due to the difference in the proportion of NOS-derived components in the tribofilm.

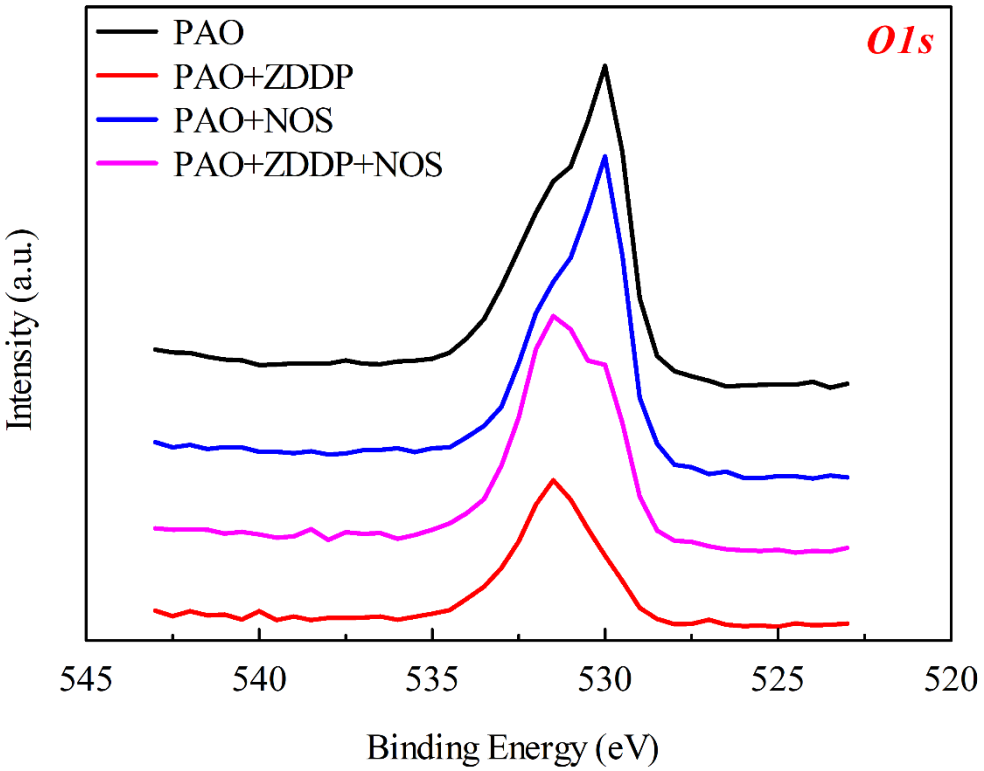


Figure 4–15. O1s spectra inside the friction tracks.

**P2p spectra:** The P2p spectra are shown in Figure 4–19. A P2p signal peak was recorded at 133.5 eV in the friction tracks corresponding to PAO+ZDDP and PAO+ZDDP+NOS. This signal is consistent with the signal of phosphate in the literature, which was around 133.4-133.8 eV [29], [129]. Another signal peak was recorded at 139.9 eV, which was derived from Zn3s, and this signal peak has been detected in previous studies of ZDDP tribofilms [125], [128]. These suggest that even lubricated with the ZDDP-NOS mixture, a tribofilm similar to the ZDDP tribofilm was formed by rubbing. Since the S2p intensity was very low, this signal peak may originate from the compounds of Zn and P. The tribofilm formed by the NOS-ZDDP mixture was different from that formed by the amine-ZDDP mixture [84], [130], which was rich in Zn and poor in phosphate [131-132]. The high Zn content may be induced by the hydrolysis of neutral ZDDP to basic ZDDP induced by amines [14], [113], [118]. However, this hydrolysis did not occur with NOS-ZDDP lubrication because the composition of the ZDDP-NOS tribofilm was more similar to that of the ZDDP tribofilm. NOS may also prevent the removal of the ZDDP tribofilm.

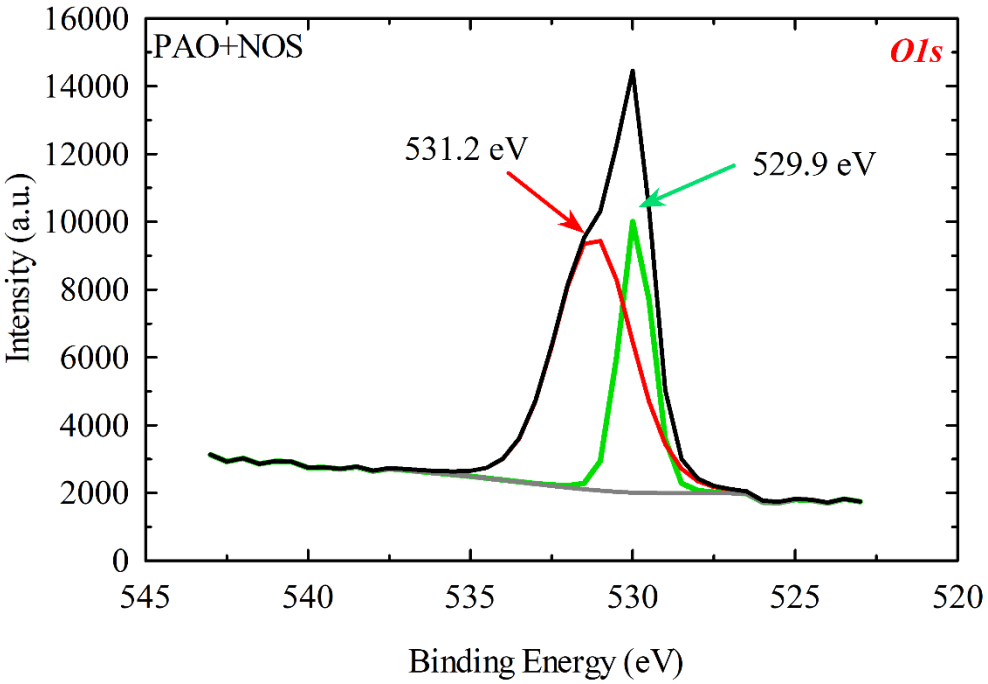


Figure 4–16. O1s peak distribution with PAO+NOS.

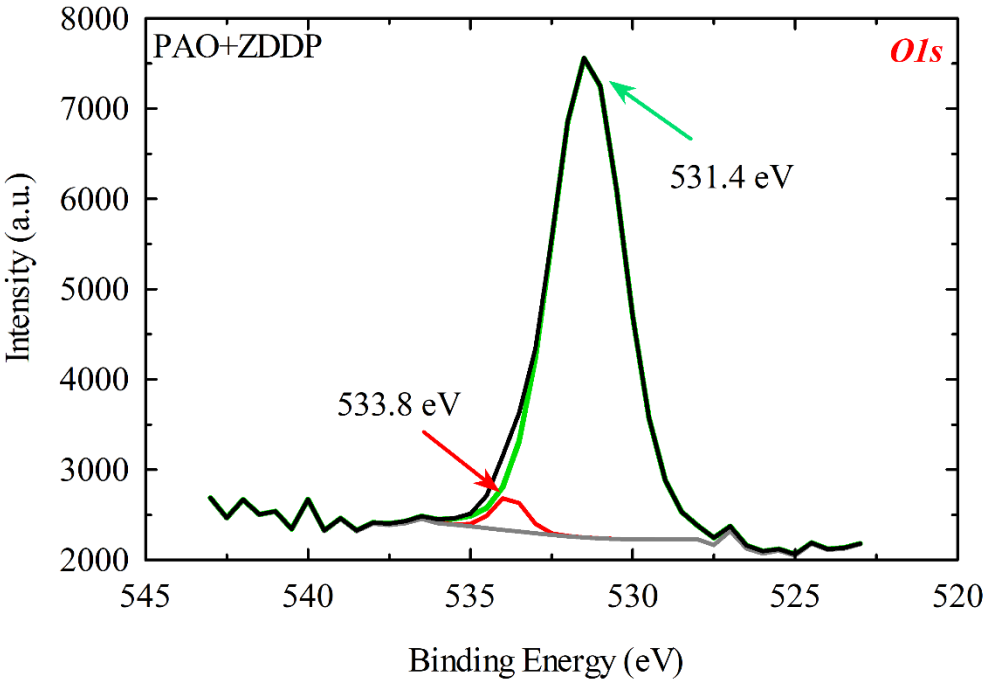


Figure 4–17. O1s peak distribution with PAO+ZDDP.

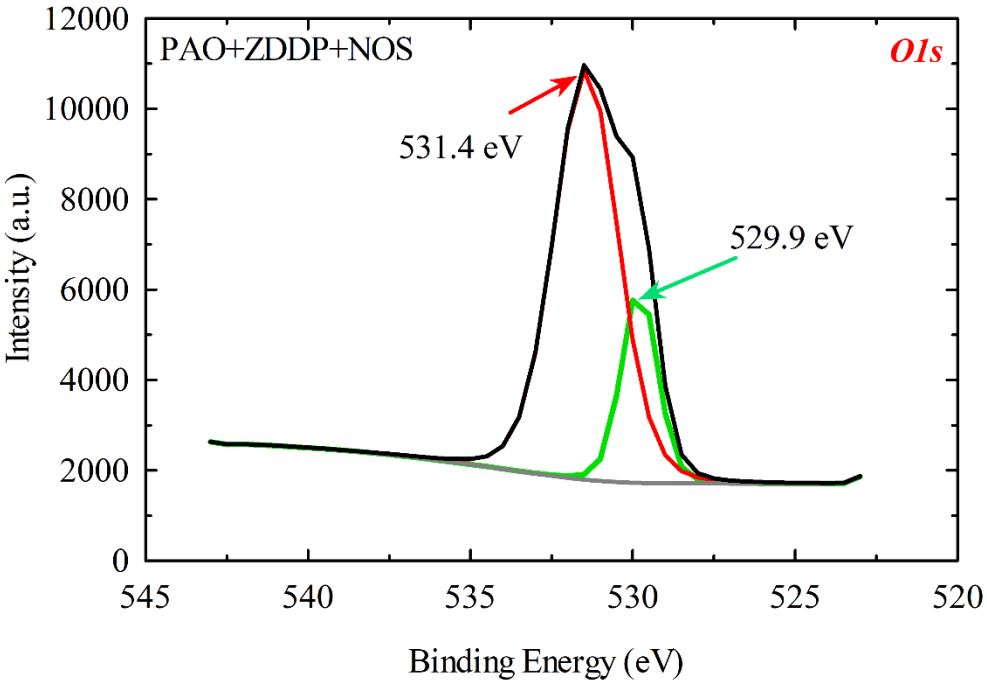


Figure 4–18. O1s peak distribution with PAO+ZDDP+NOS.

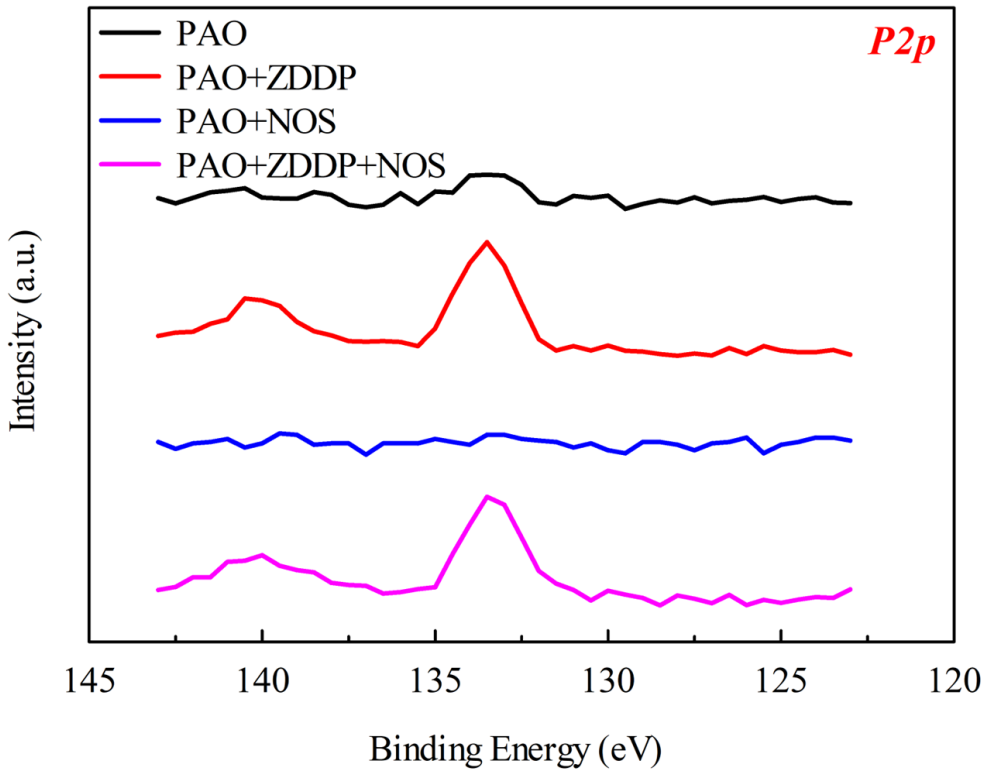


Figure 4–19. P2p spectra inside the friction tracks.

**S2p spectra:** The P2p spectra are shown in Figure 4–20. The main S2p signal peak was recorded at 162.5 eV only in the friction track with PAO+ZDDP. The peak can be assigned to zinc sulfide. Sulfur was also detected in the friction track with PAO+ZDDP+NOS; however, the signal was not intense enough for a proper fit.

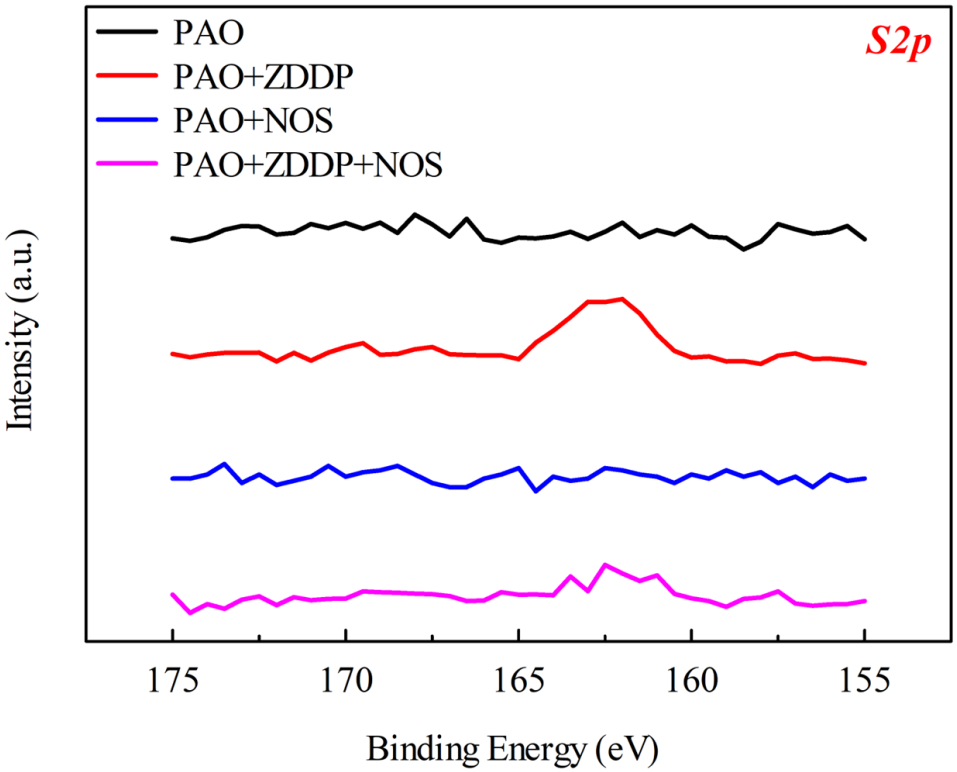


Figure 4–20. S2p spectra inside the friction tracks.

**Fe2p3 spectra:** The Fe2p3 spectra are shown in Figure 4–21. Similar signal peaks were recorded near 711.0, 714.5, and 724.5 eV for all friction tracks for FeO, Fe2O3, and Fe3O4. The most intense signal peak at 711.0 eV is considered to be FeO. The intensity of the signal may suggest the thickness of the tribofilm because it is more difficult for XPS, an outermost surface analysis technique, to detect an intense Fe2p3 signal where a thick tribofilm covers the iron. The Fe2p3 spectra in the friction track corresponding to PAO+ZDDP were weaker in intensity than the other friction tracks, which suggests that a thick tribofilm was formed in the track. In addition, the tribofilm formed with PAO+ZDDP+NOS was thinner than the ZDDP tribofilm because its intensity was stronger than the intensity recorded on the PAO+ZDDP substrate . This suggests that NOS inhibited the growth of ZDDP friction film.

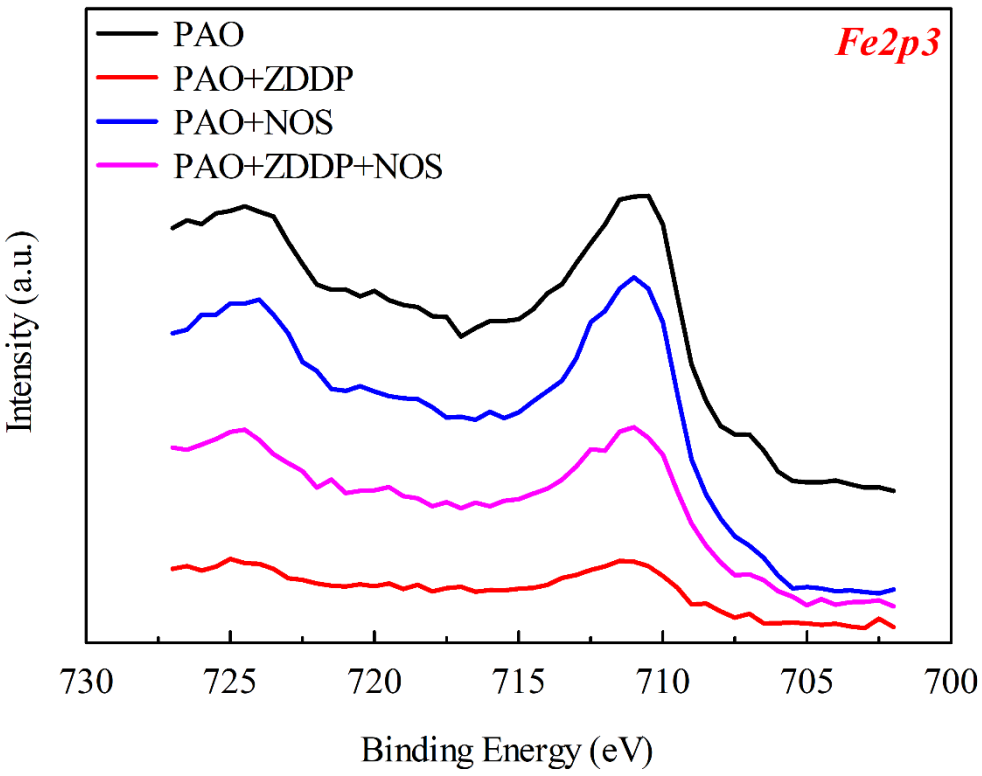


Figure 4–21. Fe2p3 spectra inside the friction tracks.

**Zn2p3 spectra:** The Zn2p3 spectra are shown in Figure 4–20. The Zn2p3 signal was detected on all the friction tracks. A strong signal peak at 1022.0 eV was recorded in the friction tracks corresponding to PAO+ZDDP and PAO+ZDDP+NOS, which can be assigned to zinc sulfide. A weak signal peak at 1022.0 eV was also recorded in the friction tracks corresponding to PAO and PAO+NOS. Since these oils did not contain zinc, this signal could be traceable amounts of zinc introduced during the wire-cut electrical discharge machining because the wire contained 47% of zinc.

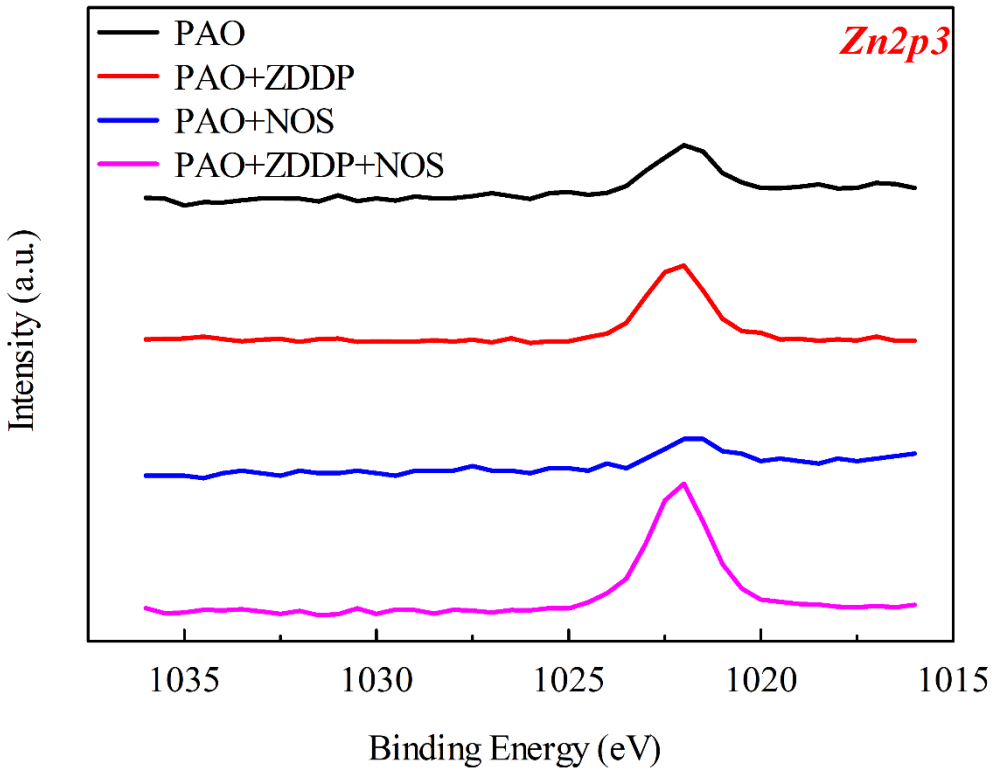


Figure 4–22. Zn2p3 spectra inside the friction tracks.

Table 4–3 Binding energies of photoelectron peaks measured in friction tracks for reference compounds. The standard deviation is 0.1–0.2 eV for all values listed.

| | *C1s* | *O1s* | *Zn2p3* | *Fe2p3* | *P2p* | *S2p* | *N1s* |
|---|---|---|---|---|---|---|---|
| PAO | 285.1<br>286.7 | 529.9<br>531.4 | 1022.0 | 711.0<br>714.5<br>724.0 | --- | --- | 400.2 |
| PAO+ZDDP | 285.0<br>286.2 | 531.4<br>533.8 | 1022.2 | 711.2<br>714.4<br>724.4 | 133.5<br>140.0 | 162.5 | --- |
| PAO+NOS | 284.9<br>286.1<br>288.5 | 529.9<br>531.2 | 1021.8 | 711.0<br>714.6<br>724.0 | --- | --- | 400.1 |
| PAO+ZDDP+NOS | 285.0<br>286.5<br>288.5 | 529.9<br>531.4 | 1022.0 | 711.0<br>713.9<br>724.3 | 133.3<br>139.9 | --- | 400.2 |

#### 4.3.2.2 XPS spectra outside friction tracks

The XPS spectra recorded outside the friction tracks are shown in Figure 4–23 to Figure 4–29, and the fitted peak information is listed in Table 4–4. The signal distributions of C1s (Figure 4–23), N1s (Figure 4–24), and Fe2p3 (Figure 4–28) outside the friction tracks were the same as those in the friction tracks. Zn2p3 (Figure 4–29) was detected on all substrates because of the contamination by wire-cut electrical discharge machining.

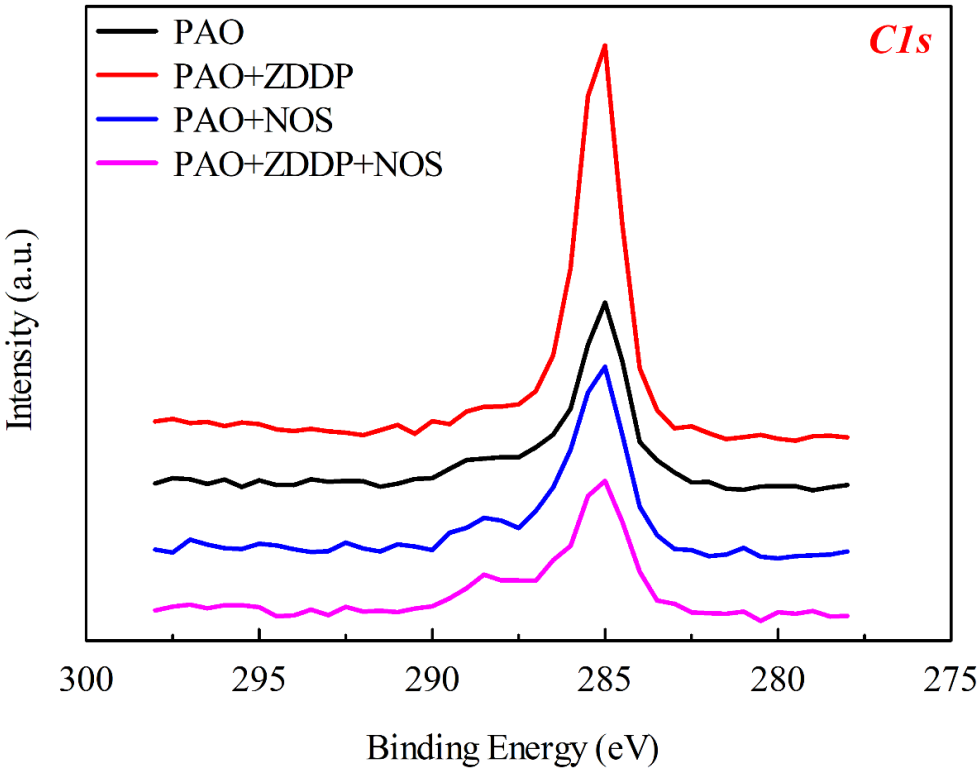


Figure 4–23. C1s spectra outside the friction tracks.

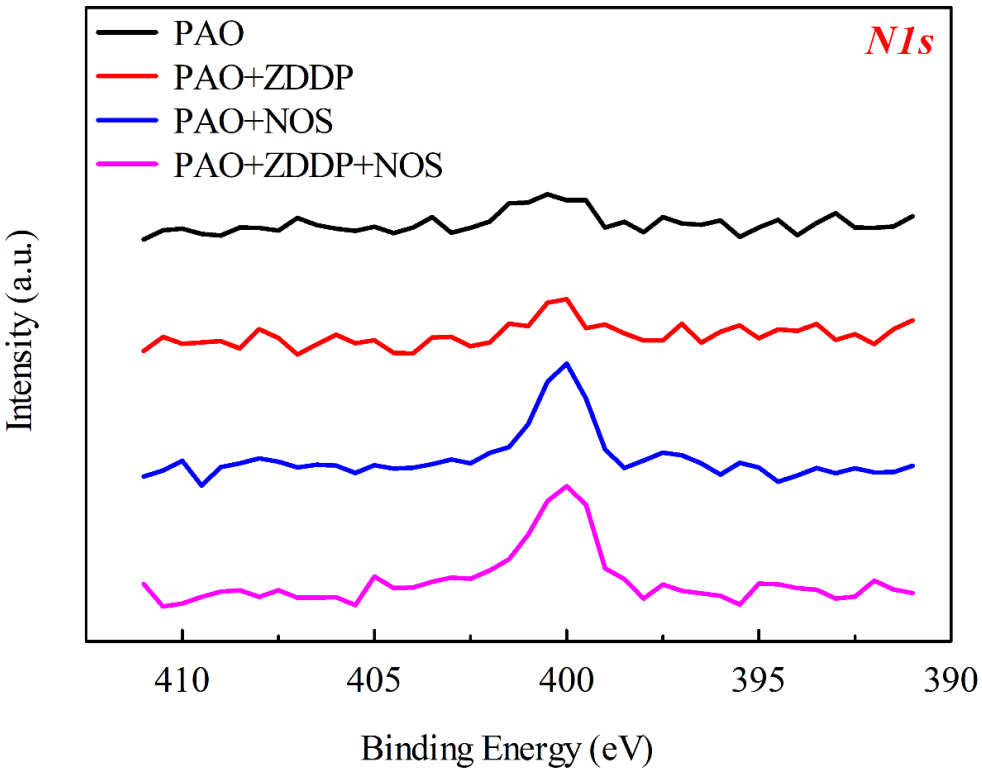


Figure 4–24. N1s spectra outside the friction tracks.

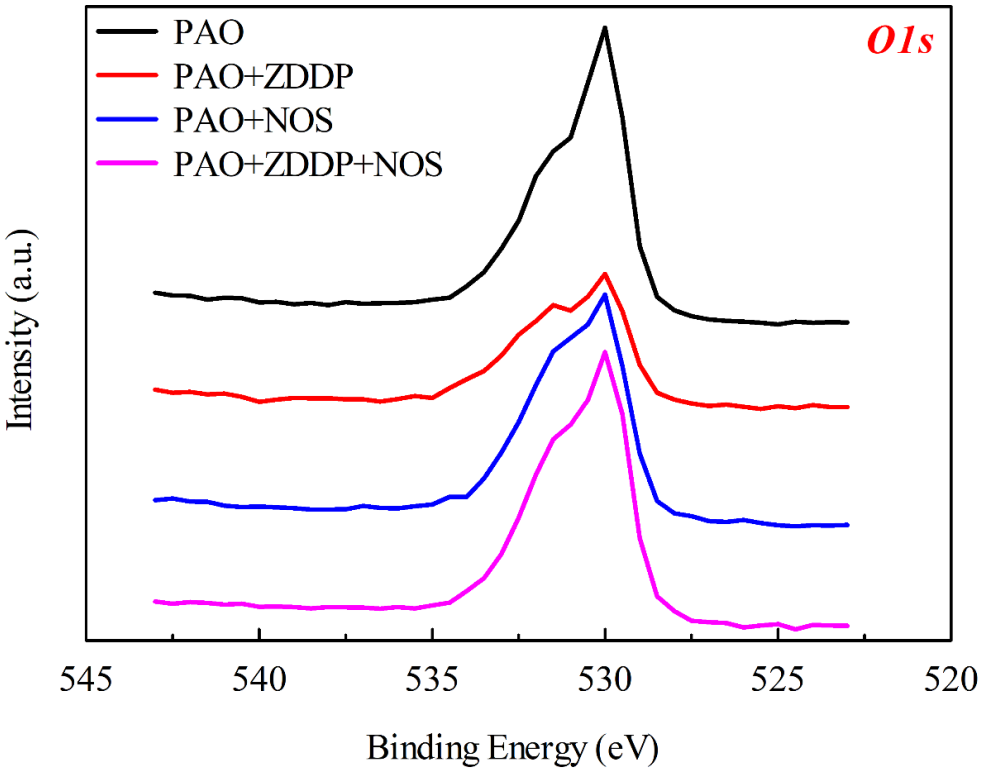


Figure 4–25. O1s spectra outside the friction tracks.

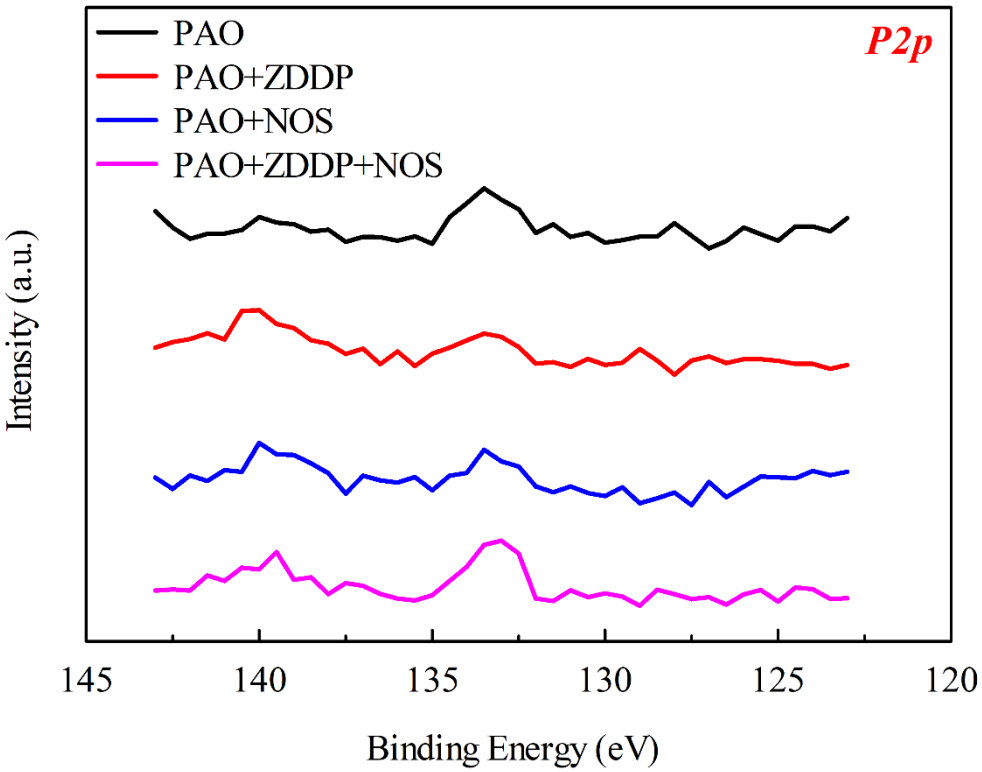


Figure 4–26. P2p spectra outside the friction tracks.

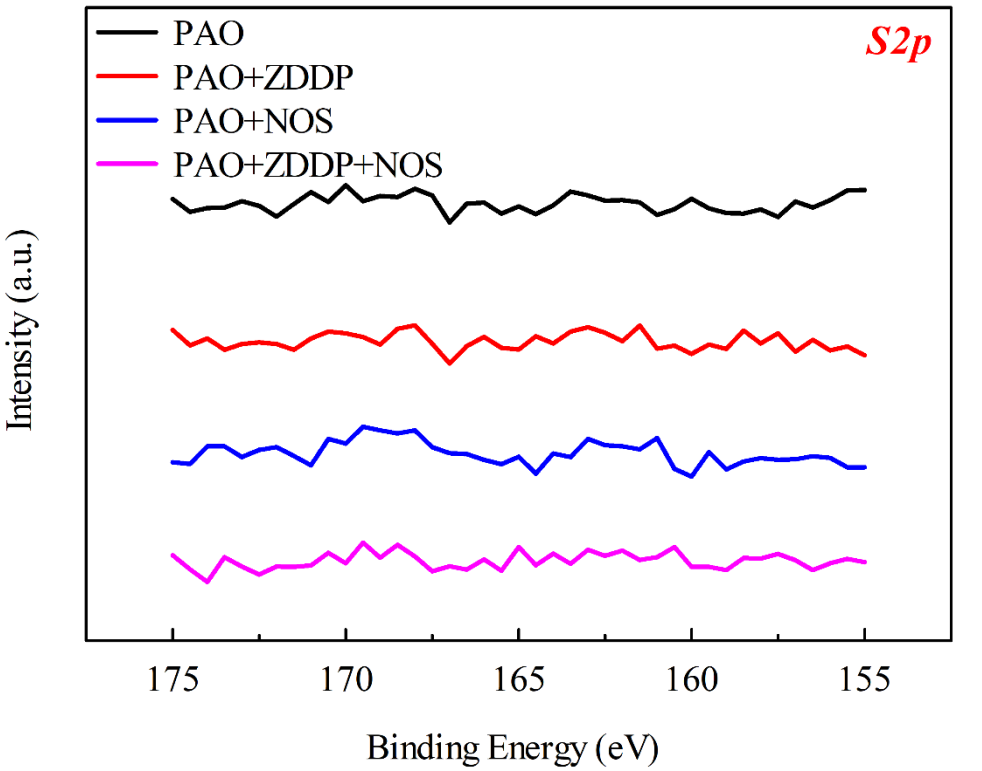


Figure 4–27. S2p spectra outside the friction tracks.

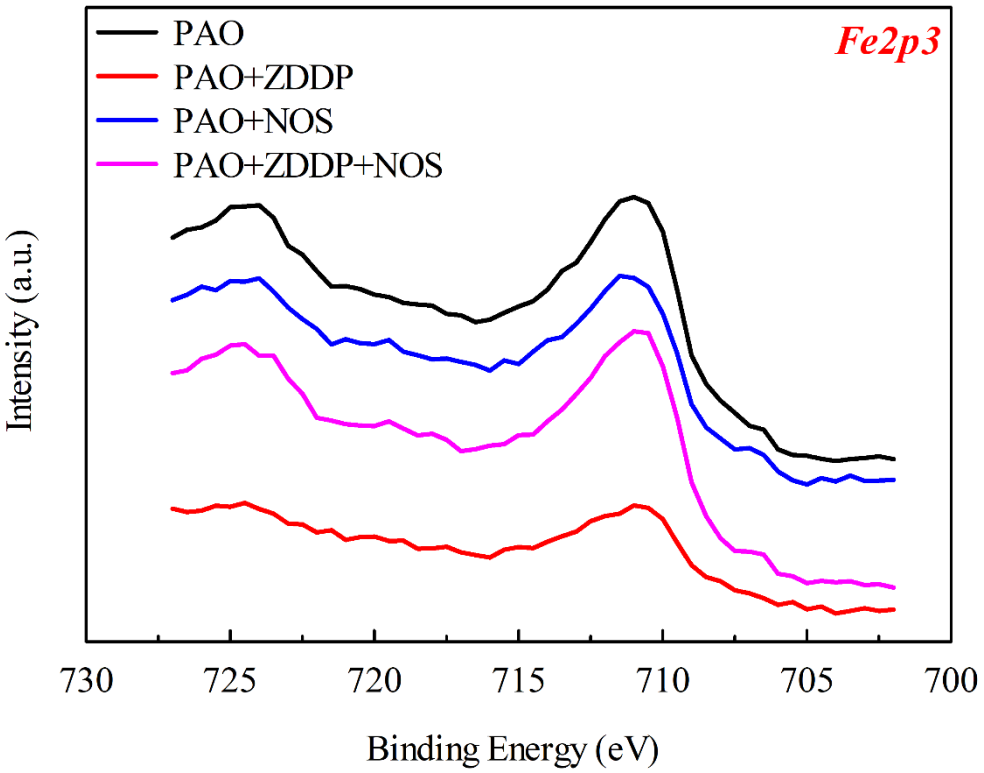


Figure 4–28. Fe2p3 spectra outside the friction tracks.

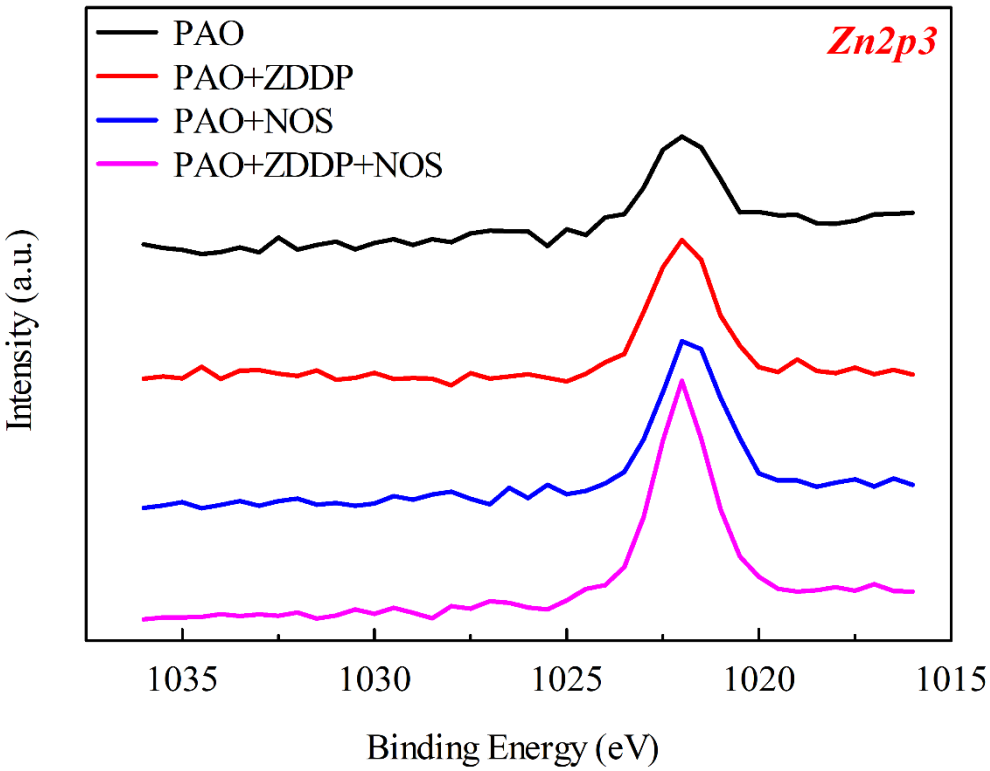


Figure 4–29. Zn2p3 spectra outside the friction tracks.

The O1s (Figure 4–25), S2p (Figure 4–26), and P2p (Figure 4–27) signal differed. The peak distribution of O1s with PAO+NOS, PAO+ZDDP, and PAO+ZDDP+NOS are shown in Figure 4–30, Figure 4–31, and Figure 4–32, respectively. The O1s signals that were recorded on PAO+NOS (Figure 4–30) and PAO+NOS+ZDDP (Figure 4–32) substrates were at 529.9 eV and 531.3 eV, which were the same as those recorded inside the friction tracks. However, the O1s peak recorded outside the friction tracks (Figure 4–31) differed from that inside the friction tracks with PAO+ZDDP lubrication (Figure 4–17). As shown in Figure 4–31, non-bridging oxygen near 529.9 eV was only recorded outside the friction tracks, and the signal peak corresponding to $FePO_4$ was not recorded. This indicates that the tribofilm was not formed in the non-contact area. On the other hand, with NOS+ZDDP lubrication, although the peak distribution was the same inside and outside the friction tracks, the intensities were different. As shown in Figure 4–30, the signal intensity near 531.1 eV is lower than that shown in Figure 4–16. This indicates that the rubbing-induced tribofilm had a different composition than the adsorbed film with PAO+ZDDP+NOS lubrication.

Another difference between the inside and outside of the friction tracks was observed in the S2p (Figure 4–27) and P2p (Figure 4–26) signals. First, peaks originating from S2p were not detected in either signal. Second, P2p signals with lower binding energy were detected in both signals; however, the peaks were not large enough for proper fitting. This is because no tribofilm is formed in the unrubbed region, and ZDDP was not decomposed into sulfides and phosphides.

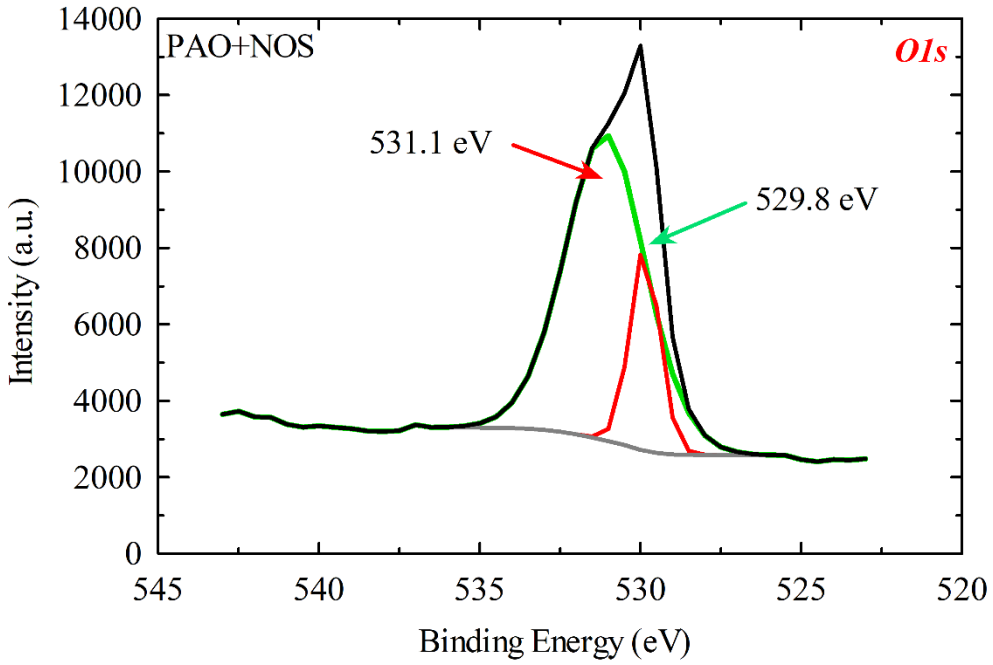


Figure 4–30. O1s peak distribution with PAO+NOS.

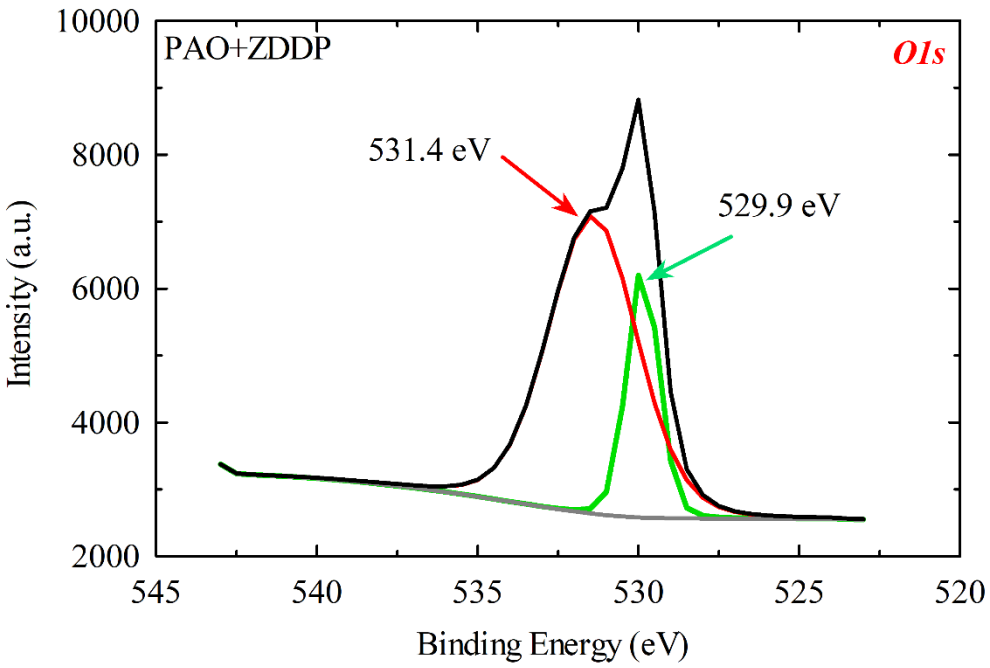


Figure 4–31. O1s peak distribution with PAO+ZDDP.

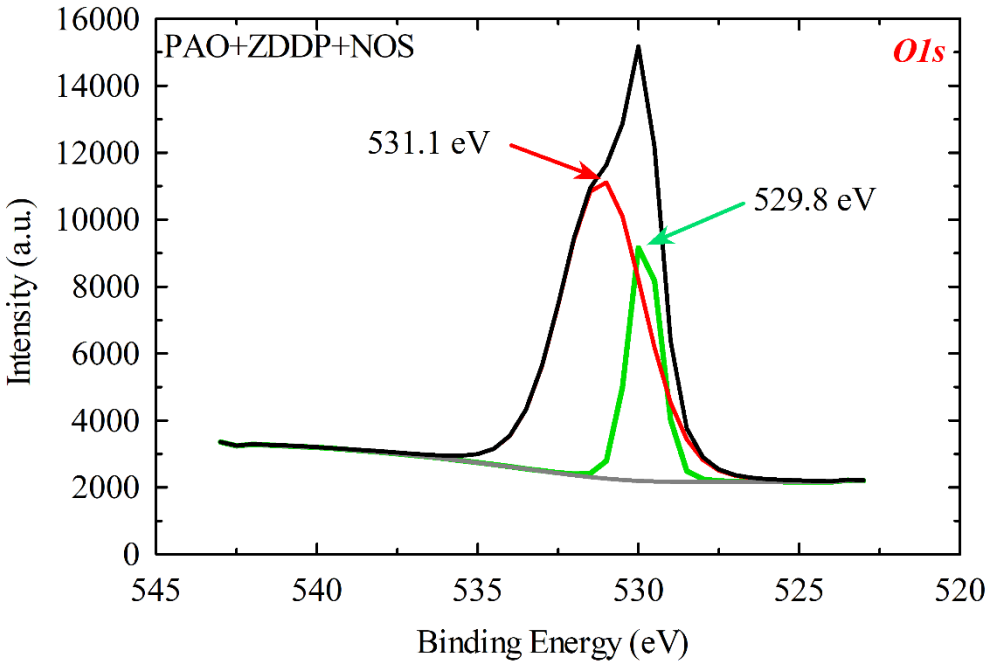


Figure 4–32. O1s peak distribution with PAO+ZDDP+NOS.

Table 4–4 Binding energies of photoelectron peaks measured outside friction tracks for reference compounds. The standard deviation is 0.1–0.2 eV for all values listed.

| | *C1s* | *O1s* | *Zn2p3* | *Fe2p3* | *P2p* | *S2p* | *N1s* |
|---|---|---|---|---|---|---|---|
| PAO | 285.0<br>285.4 | 529.9<br>531.3 | 1022.0 | 711.0<br>714.8<br>723.9 | --- | --- | --- |
| PAO+ZDDP | 285.1<br>286.2 | 529.9<br>531.4 | 1022.0 | 711.0<br>714.2<br>724.0 | --- | --- | --- |
| PAO+NOS | 285.1<br>286.5<br>288.4 | 529.6<br>531.1 | --- | 711.1<br>714.9<br>724.0 | --- | --- | 400.2 |
| PAO+ZDDP+NOS | 285.1<br>286.6<br>288.3 | 529.8<br>531.1 | 1022.0 | 711.0<br>714.9<br>724.1 | --- | --- | 400.2 |

## 4.4 Conclusion

In Chapters 2 and 3, NR-based adsorption film observation and AFM-based friction experiments provided preliminary insight into the relationship between additive adsorption film, rubbing-induced tribofilm formation, and friction performance. The results suggest that the NOS-ZDDP mixture exhibit synergistic tribological effects on anti-wear and friction-reducing. In this chapter, friction tests, morphological characterization, and surface analysis were performed to elucidate the lubrication mechanism with the NOS-ZDDP additive mixture. The results can be summarized as follows.

1. The NOS+ZDDP mixture exhibited enhanced friction-reducing and wear-resistance at 25°C.

2. The tribofilm formation process of the ZDDP+NOS mixture exhibited the features of both individual additives. Although the friction coefficient was initially high, it decreased and stabilized as the ZDDP-derived tribofilm encased the NOS-derived tribofilm so that the friction-reducing properties of NOS were maintained.

3. The wear diameters of balls with ZDDP+NOS lubrication were the smallest under each load, suggesting that this mixture had the best load capacity.

4. The surface analysis results suggest a mechanism for the NOS+ZDDP mixtures. First, unlike the reported amino-group-containing additives, NOS does not induce hydrolysis of neutral ZDDP to basic ZDDP. In addition, NOS probably does not remove the ZDDP tribofilm as other amines do. During the running-in cycles, NOS and ZDDP competitively adsorb onto the metal, resulting in a slightly higher friction coefficient compared to the case with individual additive lubrication. The tribofilm is then formed by sliding. However, NOS inhibits the formation of sulfide and $PO_4^{3-}$ species in the ZDDP tribofilm. At the same time, ZDDP retards the film formation of NOS and increases its durability. Eventually, the tribofilms formed by the NOS-ZDDP mixtures exhibit synergistic tribological effects over a wide range of loads.

# Chapter 5. Tribological characteristics of ZDDP-N-Oleoyl sarcosine mixture at engine operating temperature

## 5.1 Introduction

The previous chapter discussed the possibility of NOS as an engine oil additive by evaluating its friction-reducing and anti-wear ability when used alone or with ZDDP. XPS studies were carried out to clarify the mechanism of the NOS-ZDDP mixture at room temperature conditions. The results suggested that NOS has a good lubricating ability and, when used with ZDDP, NOS maintains its low-friction and reduces the high friction caused by ZDDP by forming a coupled tribofilm with ZDDP. However, on the other hand, the actual internal combustion engine operating temperature is much higher than the room temperature. A gasoline engine's operating temperature is generally between 90 and 105°C, and in some extreme cases, can reach about 140°C. The increase in oil temperature can lead to a decrease in oil viscosity, which can cause a reduction in oil film thickness and even wear on the sliding surfaces. Therefore, in this study, it is important to investigate the frictional characteristics of NOS and NOS+ZDDP at high temperatures.

Heating reduces the oil viscosity and affects the performance of OFM. Bowden and Tabor [53] noted that the addition of oiliness additives to paraffin leads to higher friction coefficients at high temperatures. This may be because as the temperature increases, the solid-like boundary-lubricating film melts into a liquid-like film and breaks away from the surface [133]. Also, as reported in Chapter 2, the OLA desorbed from the sliding surface at 100°C resulted in a friction coefficient as high as the base oil. In contrast, in the study by Bowden and Tabor [53], the friction coefficients of the extreme pressure additives were lower at high temperatures. Extreme pressure additives such as ZDDP are more likely to form a tribofilm at high temperatures, which protects the sliding surface and reduces wear and friction. However, ZDDP will form a thermal film on the sliding surface when heated, which may affect the adsorption of NOS.

Therefore, this chapter focuses on the tribological performance of NOS, ZDDP, and NOS-ZDDP mixture at 100°C. As in Chapter 4, ball-on-disk reciprocating friction tests were performed to compare the tribological characteristics of each lubricating oil. SEM analysis was also performed to evaluate the anti-wear performance. In addition, to understand each additive's film formation at 100°C, EDX mapping was used to visualize the distribution of elements on the ball surfaces after the test.

## 5.2 Experimental

### 5.2.1 Friction tests

The substrates and lubricating oils used in this chapter were the same as in the previous chapter. The tribotests were carried out using a reciprocating ball-on-disk machine (FPR-2100, RHESCA Co. Ltd., Japan) while heated at 100°C. A schematic diagram of the ball-on-disk setup, including the heating unit, is shown in Figure 5-1. Before starting the test, the disc and lubricant were heated to 100°C. The tests were performed three times after the temperature stabilized. The normal loads were 1, 3, 5, and 8 N. The test conditions are summarized in Table 5–1.

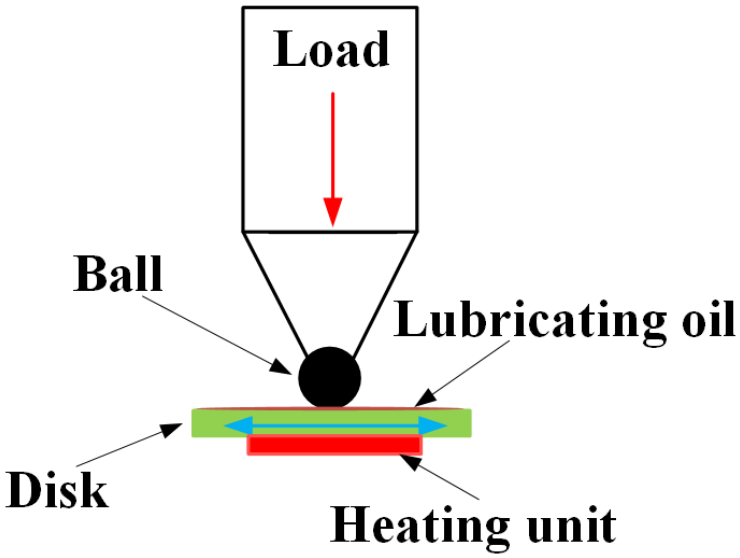


Figure 5–1. A schematic diagram of the ball-on-disk

Table 5–1. Tribo-test conditions

| ***Parameter*** | ***Values*** | | | |
|---|---|---|---|---|
| Frequency (Hz) | 1 | | | |
| Sliding speed (mm/s) | 10 | | | |
| Stroke length (mm) | 5 | | | |
| Normal load (N) | 1 | 3 | 5 | 8 |
| Test duration (s) | 1800 | | 5400 | |

### 5.2.2 Surface morphology observation

A three-dimensional laser microscope (OLS4000-SAT, Olympus Corporation, Japan) was used

in this experiment to image the ball contact area after the friction test to determine the size of the wear marks.

### 5.2.3 Tribofilm composition analysis

Prior to testing, the balls were rinsed with hexane and blown with $N_2$ gas to avoid contamination. The tribofilm on the ball surface was imaged using SEM (SU6600, HITACHI Co. Ltd., Japan), and the chemical composition of the tribofilm was resolved using EDX (E-MAX20, Oxford Instruments plc). In the EDX test, each ball was scanned 45 times, automatically accumulated, and normalized to obtain the elemental mapping results.

## 5.3 Results and discussion

### 5.3.1 Friction measurement results under different loads and durations

The friction coefficients at loads of 1, 3, and 5 N are shown in Figure 5–2, 5–3, and 5–4, respectively, with the test durations of 1800 s.

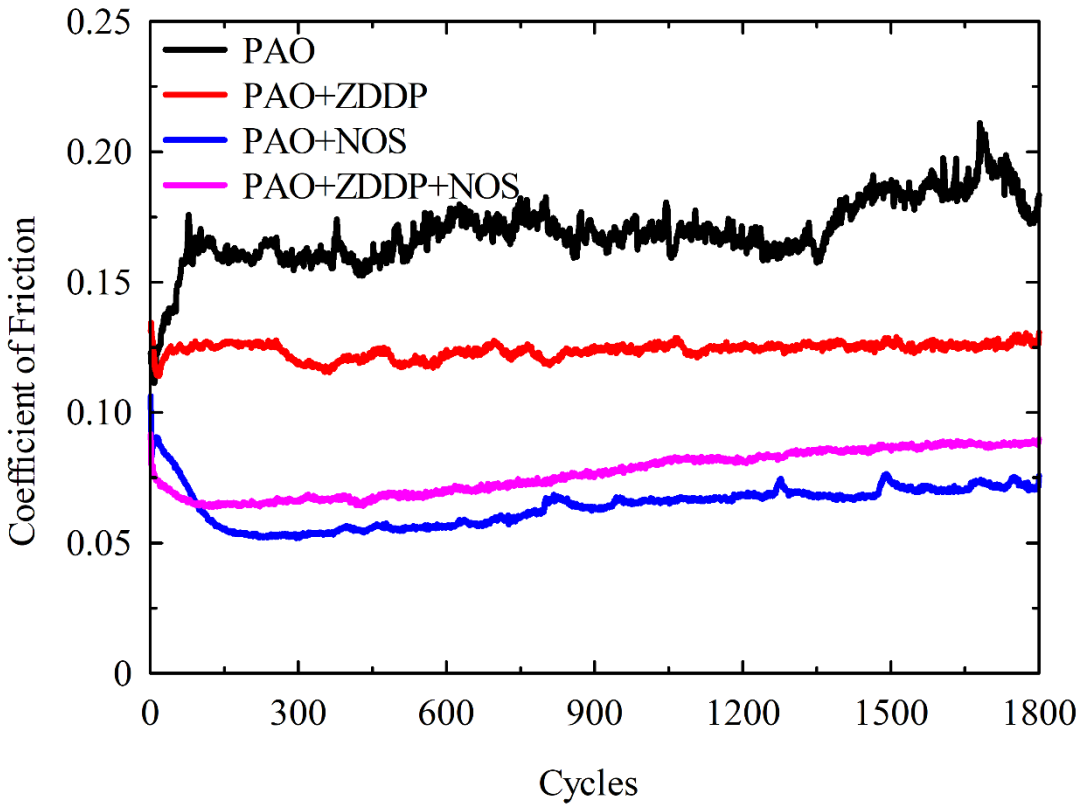


Figure 5–2. Friction coefficient with each lubricating oil at 1N for 1800 cycles

When lubricated with PAO+ZDDP lubrication, the friction coefficient gradually approached that with PAO lubrication as the load increased. The results showed that with PAO+ZDDP lubrication, the friction coefficient was about 0.12 at 1 N and between 0.13 and 0.15 at 3 N, which was always lower than the friction coefficient of 0.16 with PAO lubrication. The friction coefficient with PAO+ZDDP lubrication was between 0.14 and 0.16 at 5 N, which was very close to the friction coefficient with PAO lubrication. In addition, the friction coefficient-cycle number curves with PAO+ZDDP lubrication were noticeably unsettling compared to the case with other lubricating oils. For example, under a 5N load, as shown in Figure 5–4, the friction coefficient fluctuates continuously and never reaches a steady state. This fluctuation may be due to the formation and destruction of the glassy tribofilm during the sliding cycle. The wear resistance of the ZDDP tribofilm stems from the isolation of the sliding surfaces. Although this tribofilm effectively protects the surfaces under sliding, the ZDDP tribofilm was worn under boundary lubrication. It may be the reason why its friction coefficient is fluctuating. In addition, as mentioned in Chapter 1, the high friction of ZDDP tribofilm may be due to the lack of lubrication on its surface, which leads to the stick-slip phenomenon, which may aggravate the wear of the tribofilm under the boundary lubrication.

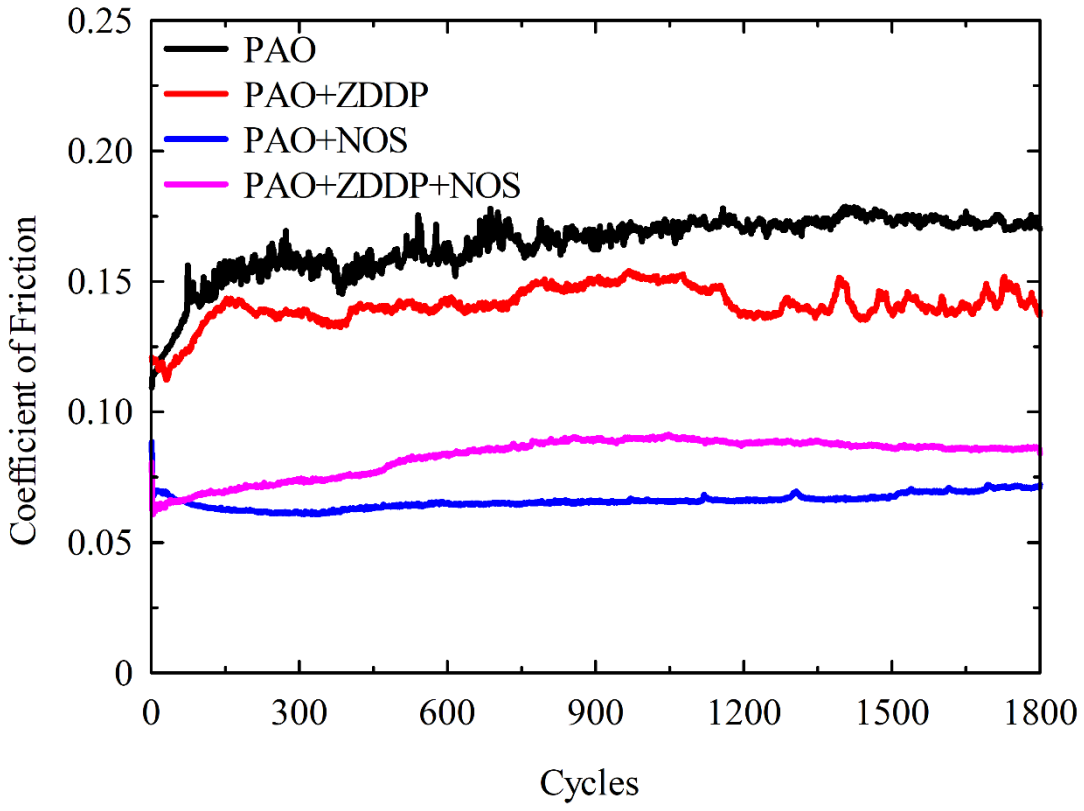


Figure 5–3. Friction coefficient with each lubricating oil at 3N for 1800 cycles

The friction coefficient was minimized with PAO+NOS lubrication. When the applied load was increased from 1 N to 5 N, PAO+NOS exhibited a stable friction coefficient of about 0.06 for fewer sliding cycles. The friction coefficient-cycle number curve showed noticeable fluctuations at a load of 1 N, the same as with PAO+ZDDP lubrication. Although the reason for this fluctuation cannot be clearly explained, it can be speculated that the increased surface adsorption of NOS and the disordered nature of its molecules in the heated state led to an increase in viscous resistance of its adsorbed layer. At 1 N load, this viscous resistance may have led to fluctuations in the friction coefficient. However, the fluctuation decreased with increasing load. Especially at 5 N, the friction coefficient was very stable. It indicates that although the NOS adsorbed layer exhibits a higher shearing resistance, sliding at higher loads can order the molecules. This adsorbed film can effectively protect the friction surface in boundary lubrication and make the friction coefficient more stable by preventing direct contact and wear.

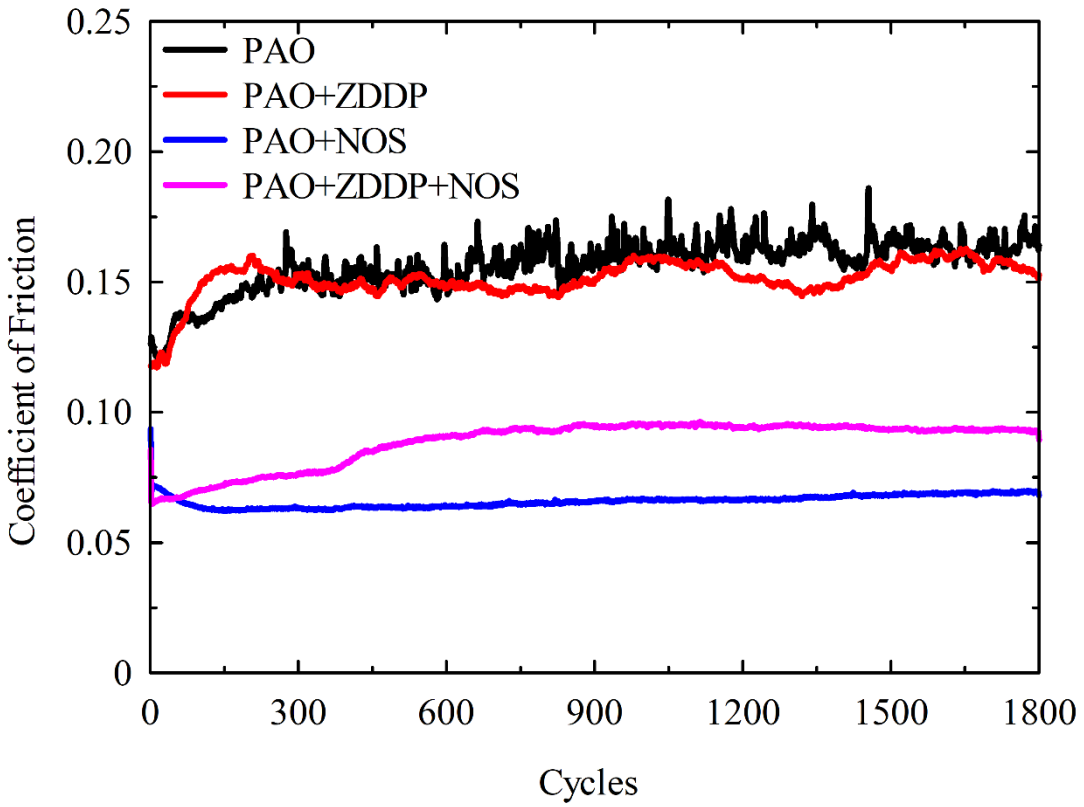


Figure 5–4. Friction coefficient with each lubricating oil at 1N for 1800 cycles

The friction coefficient was the lowest in the running-in stage with PAO+ZDDP+NOS lubrication under all applied loads. However, this low friction was not sustained, and as the test proceeded, its friction coefficient exceeded that with PAO+NOS lubrication. In addition, the friction coefficient-cycle number relationship showed different trends at different loads. As shown

in Figure 5–2, at a load of 1 N, the friction coefficient variation was similar to that of PAO+NOS lubrication, decreased at the running-in stage, and then stabilized. This indicates that NOS contributed more to the frictional behavior in the ZDDP-NOS mixture. However, the friction coefficient increased and stabilized at heavier loads, following the same trend as PAO+ZDDP. This suggests that the load increase may accelerate the decomposition of ZDDP and the formation of its tribofilm, which may cause an increase in the friction coefficient. However, the NOS in the mixture contributed to the stability of the friction coefficient. Its friction coefficient curve was as smooth as that of PAO+NOS and less fluctuating than that of PAO+ZDDP. The results indicate that the tribofilm formed by the mixture effectively improves the high friction of the ZDDP tribofilm. Therefore, the friction coefficient with PAO+ZDDP+NOS finally stabilized between that of PAO+ZDDP and PAO+NOS.

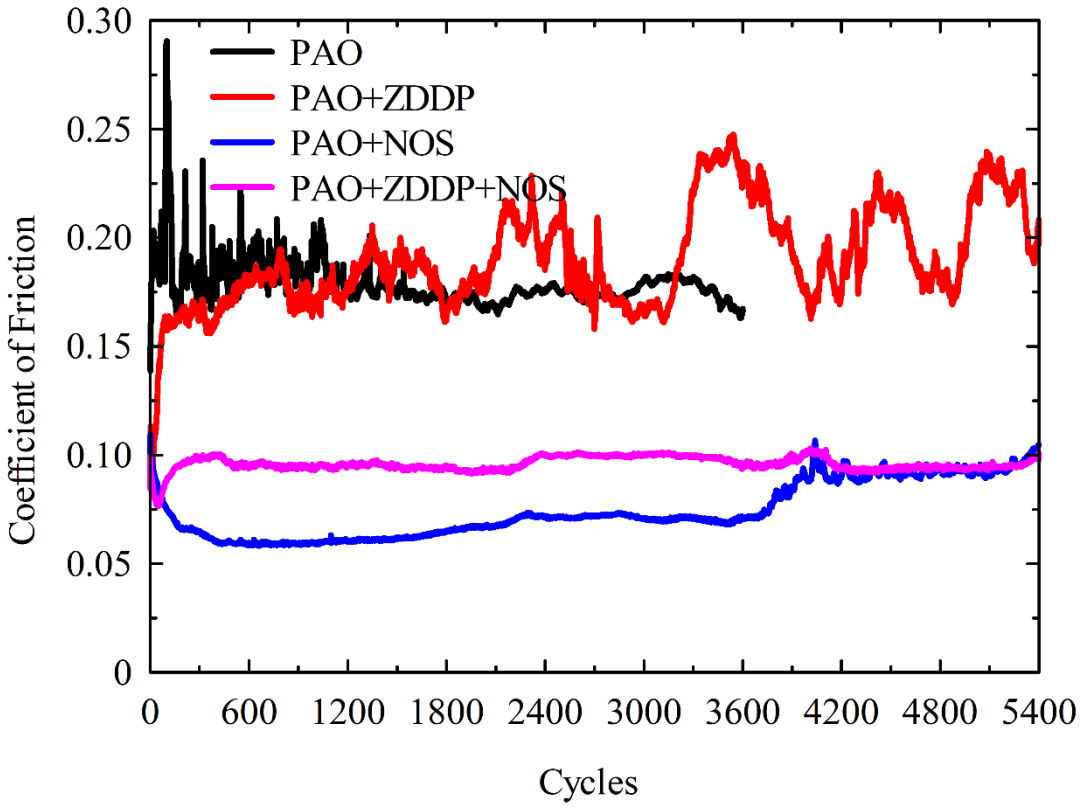


Figure 5–5. Friction coefficient with each lubricating oil at 5 N for 5400 cycles

In order to evaluate the durability of each lubricating oil, friction tests with a longer duration and heavier loads were implemented in this study. As shown in Figure 5–5, with PAO+NOS lubrication under a 5N load, the friction coefficient began to increase at about 3500 cycles until it stabilized at about 4000 cycles. With PAO+ZDDP+NOS lubrication, the friction coefficient was close to that with PAO+NOS lubrication; it increased at around 2000 and 4000 cycles. This may

be due to the coupling process of NOS adsorption film destruction, ZDDP tribofilm formation, and anti-wear effect. As shown in Figure 5–6, the friction coefficient with PAO+NOS lubrication at 8N load was similar to that at 5N load. The friction coefficient started to increase gradually after about 2000 cycles and exceeded that of PAO+ZDDP+NOS after about 3500 cycles and continues to rise. In contrast, the coefficient of friction remained essentially stable when lubricated with PAO+ZDDP+NOS. Although there were changes in the magnitude of the friction coefficient midway through the experiment, no consistent increase was observed. In addition, although it showed fairly good friction reduction performance when PAO+NOS was used alone, when the load or the experimental time increased, the friction coefficient would suddenly start to increase and exceed that with PAO+NOS+ZDDP.

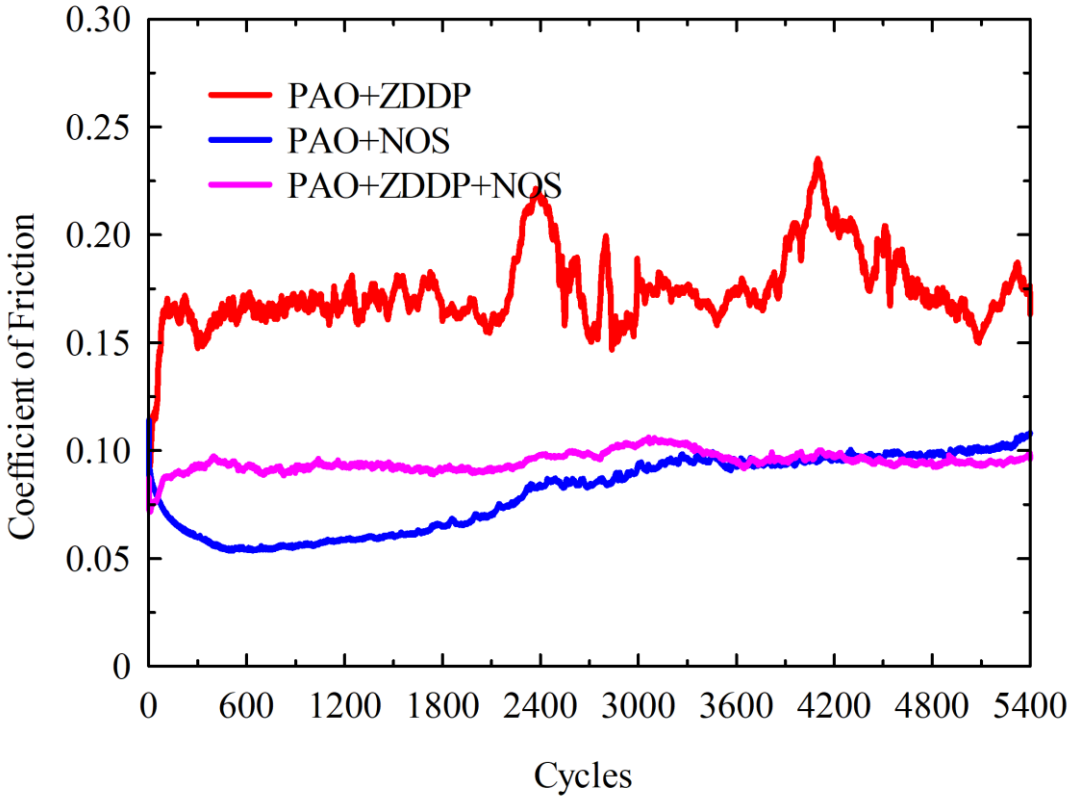


Figure 5–6. Friction coefficient with each lubricating oil at 5 N for 5400 cycles

### 5.3.2 Tribological behavior in the stabilization phase

The steady-state friction coefficient is shown in Figure 5–7. The black dashed line represents the steady state friction coefficient after 5400 cycles using PAO+ZDDP+NOS lubrication under 8N load as a reference. When the tests were 1800 cycles, the lowest coefficient friction was achieved with PAO+NOS lubrication. However, its friction coefficient increased significantly when the

tests were 5400 cycles. It indicates that the NOS adsorption film, while having good friction reduction properties is not durable enough under severe contact conditions. On the other hand, within 1800 cycles, although the friction coefficient was higher with PAO+ZDDP+NOS lubrication than with PAO+NOS lubrication, the increase in the absolute value of the friction coefficient over an extended time was smaller than that with other oils. Among them, the friction coefficient was almost the same at 5400 cycles, regardless of whether the load was 5N or 8N. It also indicates that the NOS+ZDDP mixture works better under more severe conditions and its better durability and stability.

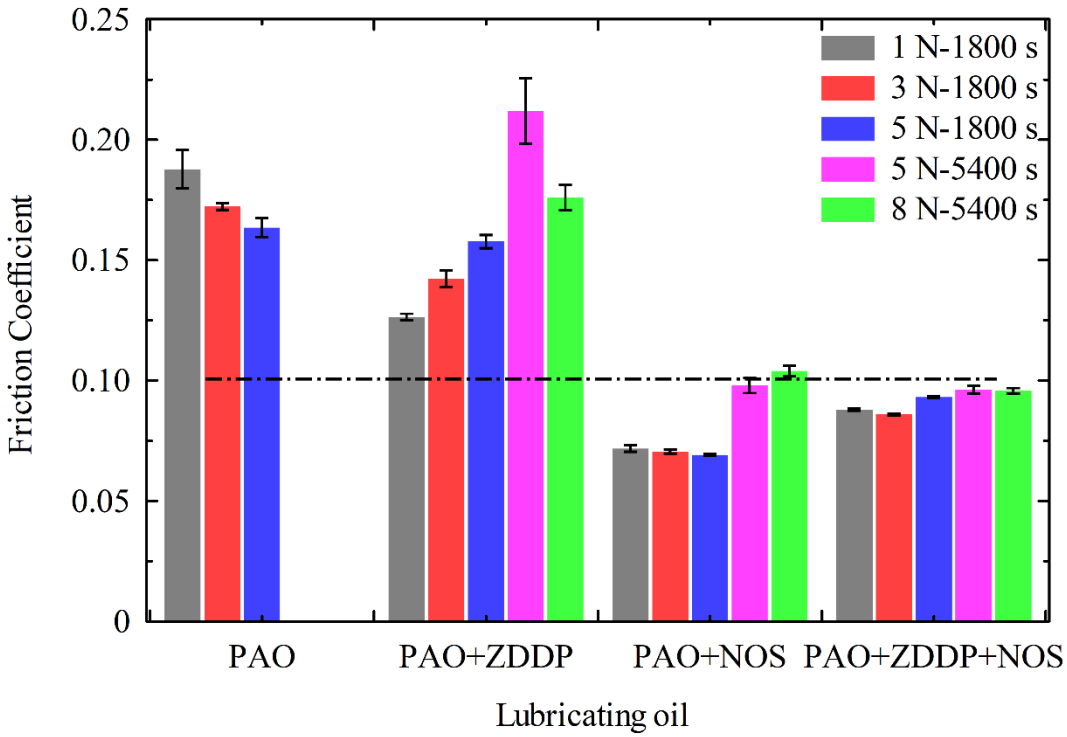


Figure 5–7. Steady-state friction coefficient

Figure 5–8 shows the relative wear diameters for each lubricating oil, with PAO at 8 N load and 5400 cycles as 1.0. After 1800 cycles, the contact area diameters of the balls lubricated with PAO+NOS and PAO+ZDDP+NOS were close at each load. After 5400 cycles at 5 N load, the contact area diameter of the balls lubricated with PAO+NOS increased considerably, while the contact area diameter of the balls lubricated with PAO+ZDDP+NOS remained the same as after 1800 sliding cycles. In addition, the wear diameter of PAO+ZDDP+NOS was the smallest at both 5N and 8N, indicating that the tribofilm formed by NOS+ZDDP was stronger than that formed by other lubricating oils in terms of durability and load capacity.

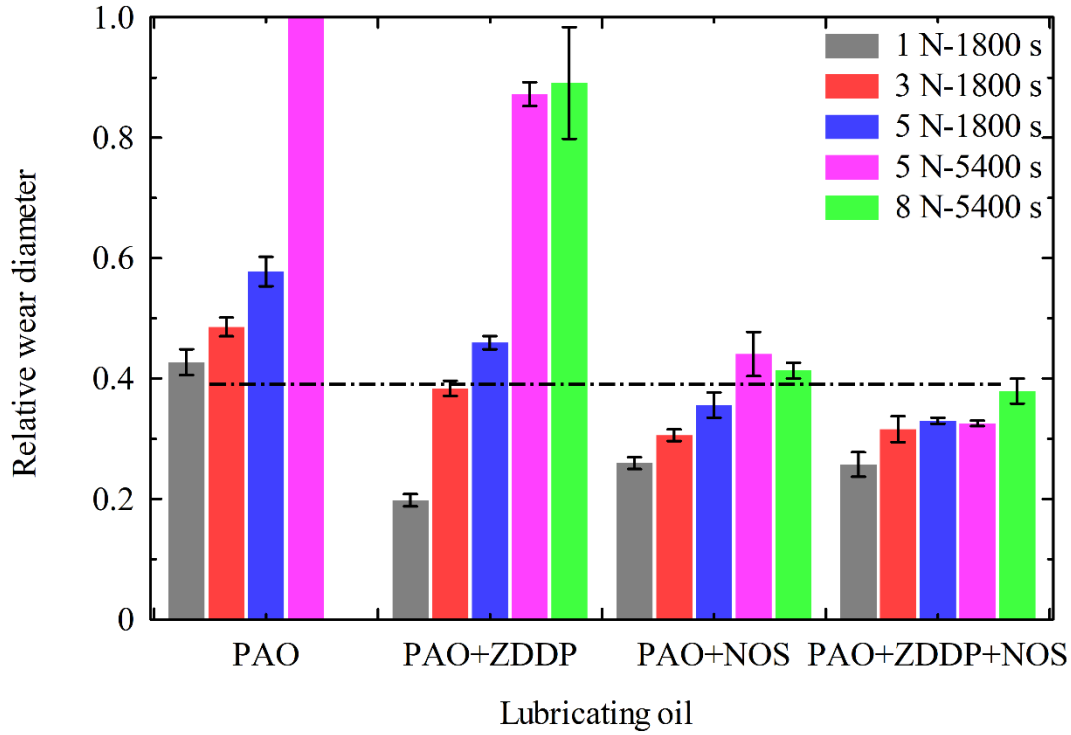


Figure 5–8. Relative wear diameters

### 5.3.3 Surface morphology observation

Figure 5–9 shows microscope images of the contact area on the balls after 1800 test cycles at 5 N load, which were lubricated with PAO, PAO+ZDDP, PAO+NOS, and PAO+ZDDP+NOS; referring to Figure 5–9a, b, c, and d. There were groove-like scars on all the balls. Since the kinematic viscosity of the base oil is only 4 $mm^2/s$ at 100°C, the oil film would have been very thin, so the balls would tend to wear. The additives noticeably improved the wear resistance. After 1800 cycles, the wear diameter was the largest with PAO (Figure 5–9a) and the smallest with PAO+ZDDP+NOS (Figure 5–9d).

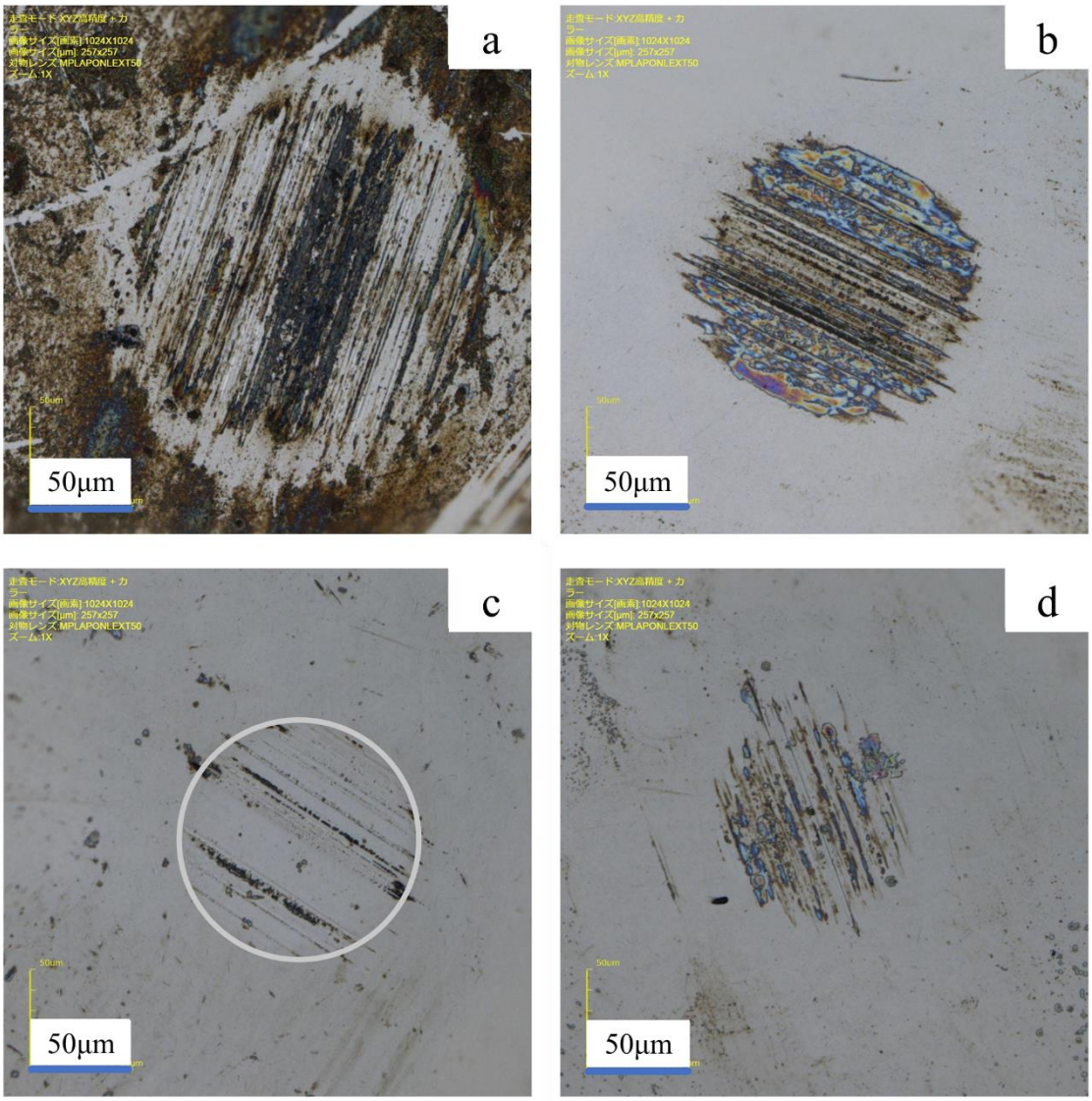


Figure. 5–9 Contact areas at 5N load after 1800 cycles.

The microscope image of the ball surface after 1800 test cycles at 5N load is shown in Figure 5–10. The microscopy images of the balls lubricated with PAO (Figure 5–10a) and PAO+ZDDP (Figure 5–10b) are similar: the contact area was covered with linear wear scars. Dark areas with black spots were observed in the contact area of the ball lubricated with PAO+NOS (Fig. 5–10c). When lubricated with PAO+ZDDP+NOS, as shown in Figure 5–10d, the formation of tribofilms was also observed. In order to obtain clearer surface characteristics, these balls were observed using SEM, and the results are shown in Figure 5–11. Figure 5–11a shows the wear scar filled with dark deposits, which may have been iron oxide, in the case of PAO lubrication. Black deposits are also evident at the edges of the contact area; they may have been the hydrocarbon byproducts from PAO. In contrast, with PAO+ZDDP lubrication, the deposits in the scars were

not evident, although wear scars are also visible in the SEM images. This indicates that although the morphology after wear was similar, sliding led to oxidation at the interface with PAO lubrication, whereas with PAO+ZDDP lubrication, the ZDDP tribofilm and the metal at the interface were damaged at the same time. In addition, fragments of the tribofilm were trapped in the scar, as shown by the red arrow in Figure 5–11b. In addition, black spots caused by adhesive wear [134] were also found in the friction film. On the other hand, with PAO+NOS lubrication, irregular fragments were observed in the contact area, as shown in Figure 5–11c. This could be a tribofilm formed by the oxygen-rich decomposition of NOS. Its formation may be related to the increase in friction coefficient. The tribofilm formed by PAO+ZDDP+NOS inherited the features of ZDDP tribofilm and NOS tribofilm, as shown in Figure 5–11d; however, this tribofilm seems to be thinner with fine wear debris trapped in the wear scars as shown by the red arrow.

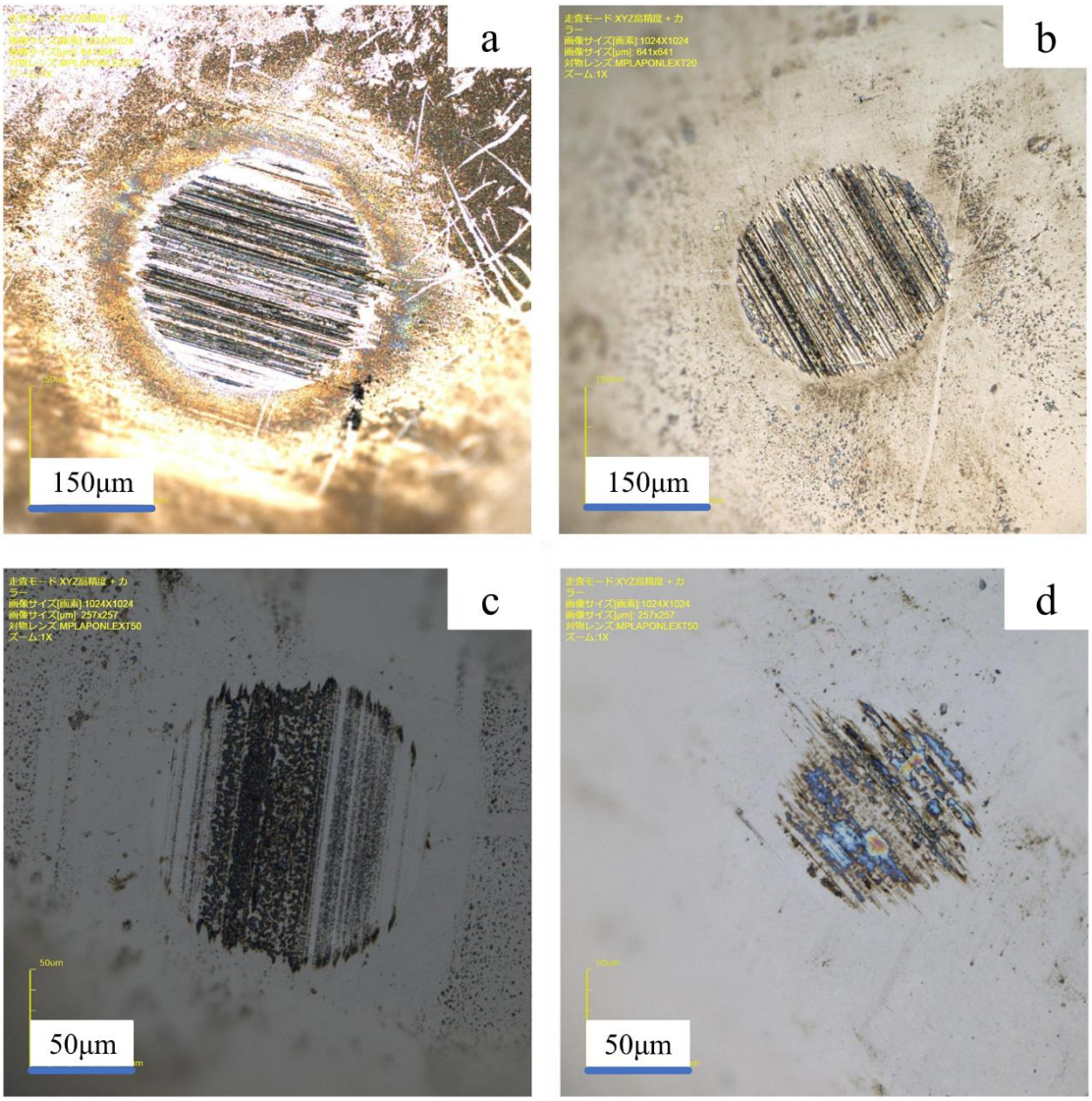


Figure. 5–10 Contact areas at 5N load after 5400 cycles.

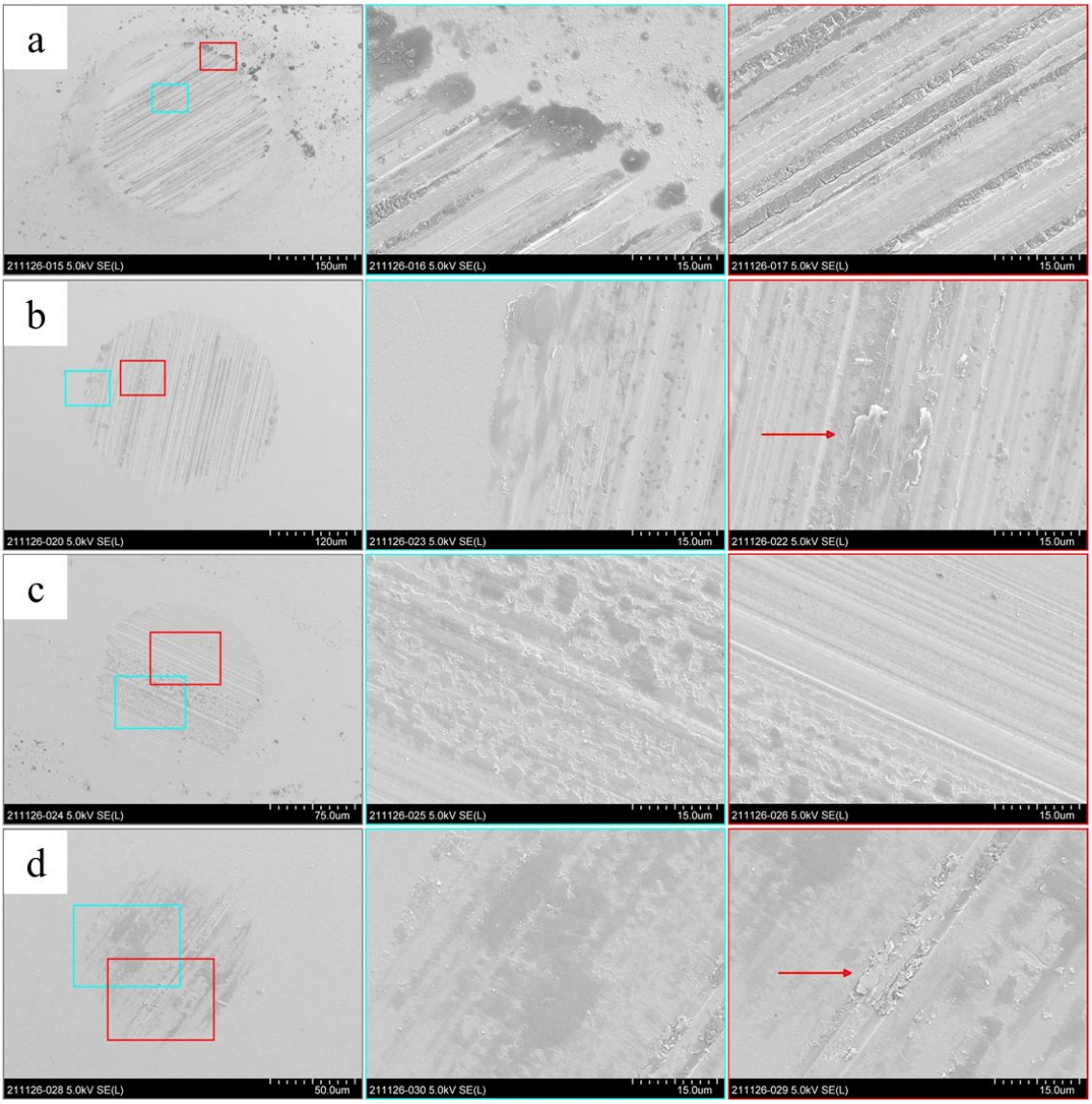


Figure 5–11. SEM images of the contact areas are shown in figure 5–10

### 5.3.4 Surface chemical analysis

The EDX results of the balls after 1800 testing cycles are shown in Figures 5–12 to 15, corresponding to the tribofilms formed with PAO, PAO+ZDDP, PAO+NOS, and PAO+ZDDP+NOS lubrication, respectively. Clear linear wear scars can be seen in the SEM images shown in Figure 5–12, which indicate that abrasive wear occurred under PAO lubrication. The elemental mapping shows oxygen presence, especially in the middle of the contact area. This could be due to the higher contact pressure in the middle of the contact area, and it caused more severe wear and oxidation. As shown in Figure 5–13, clear tribofilm is seen in the PAO+ZDDP lubricated contact area. Linear wear scars appear along the sliding direction of the contact area,

while no severe wear is seen on the outer side of the sliding direction. This indicates that under boundary lubrication, severe wear occurs in the region of high contact pressure, while outside this region, the ZDDP tribofilm effectively protects the contact surface. EDX detected zinc, phosphate, and surfer besides oxygen and carbon inside the tribofilm. A considerable distribution of C and S was detected inside and outside the contact zone. These could arise from detection errors or indicate the adsorption of ZDDP decomposition products, which could be alkyl chains, thiophosphates, or both. A dark gray area can be seen in the SEM image of Figure 5–14, which should be the contact area with PAO+NOS lubrication. Linear wear scars along the sliding direction, and speckle structures can be seen in the contact area. Among them, the linear wear scars are clearly characterized by high oxygen content. On the other hand, the aggregated speckle structure is rich in carbon, which may be formed by NOS. Figure 5–15 shows the results of the tribofilm formed with ZDDP+NOS mixture lubrication. Tribofilm fragments similar to those of ZDDP tribofilm are evident at both sides of the contact area, but the film was incomplete and piecemeal. The EDX mapping results support the assertion that the zinc- and phosphate-rich areas overlapped in the area where the ZDDP tribofilm is assumed to have been present. In addition, the carbon-rich spots overlapped the speckle structure formed by the NOS because the ZDDP tribofilm lacked carbon; similar carbon-rich spots are evident in Figure 5–14. Moreover, the tribofilm area lacked sulfur compared with the results shown in Figure 5–13.

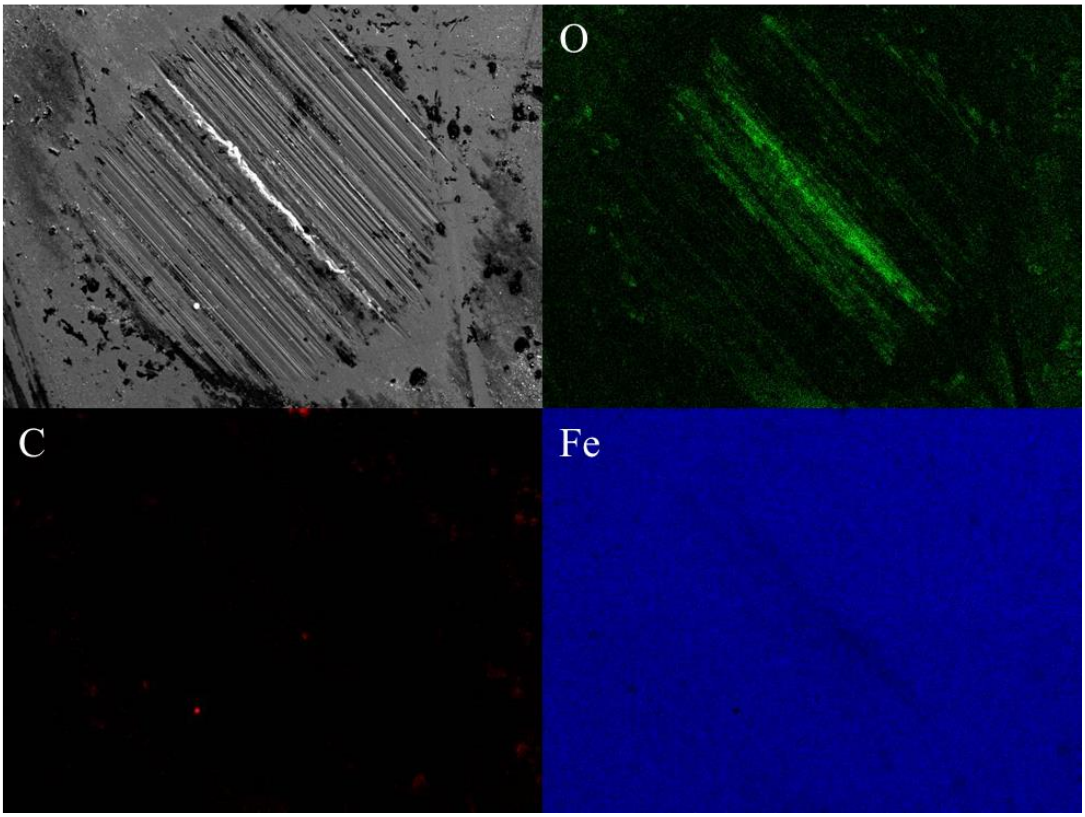


Figure 5–12. SEM image and EDX mapping of the contact area with PAO, 1800 cycles.

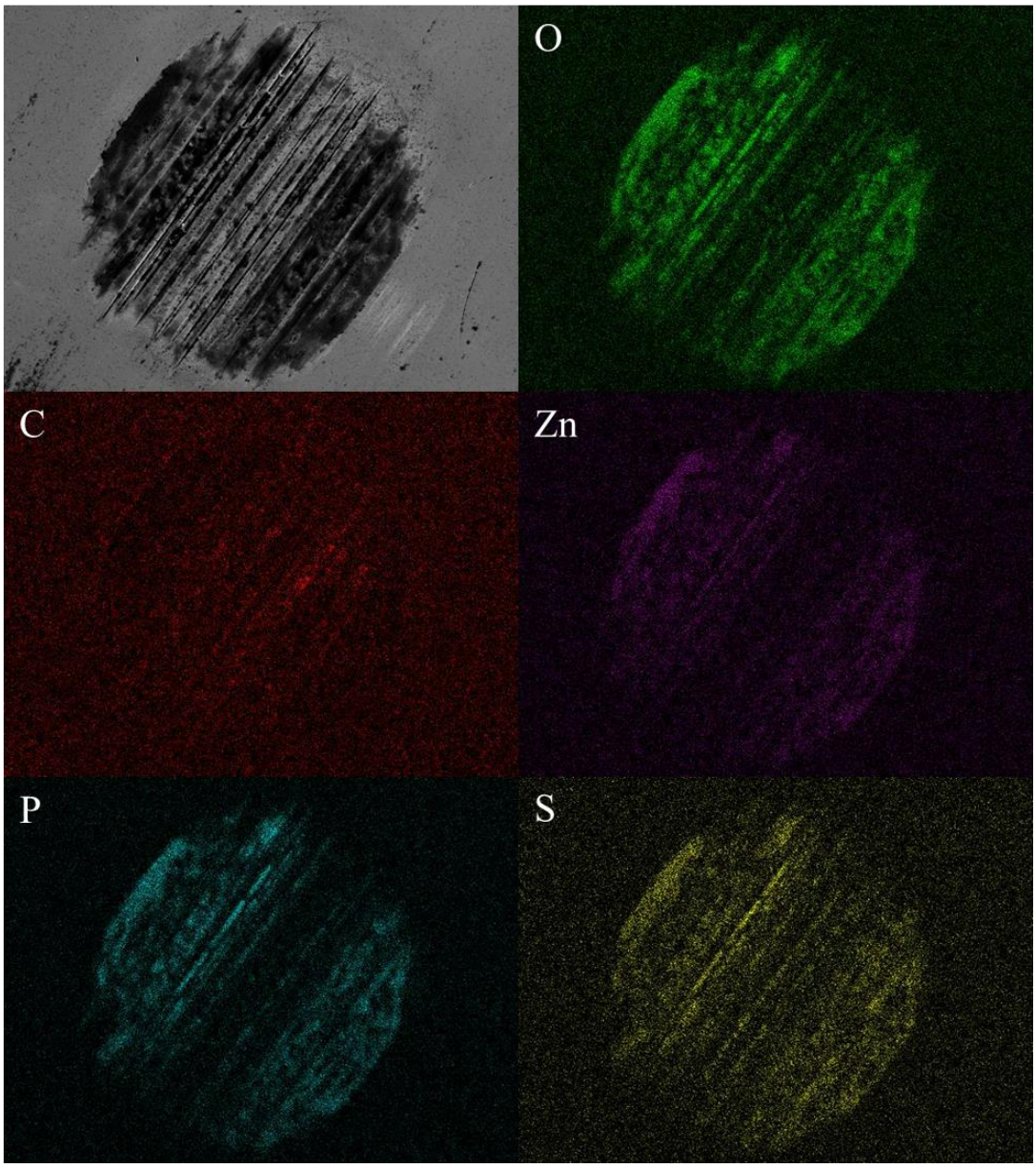


Figure 5–13. SEM image and EDX mapping of the contact area with PAO+ZDDP, 1800 cycles.

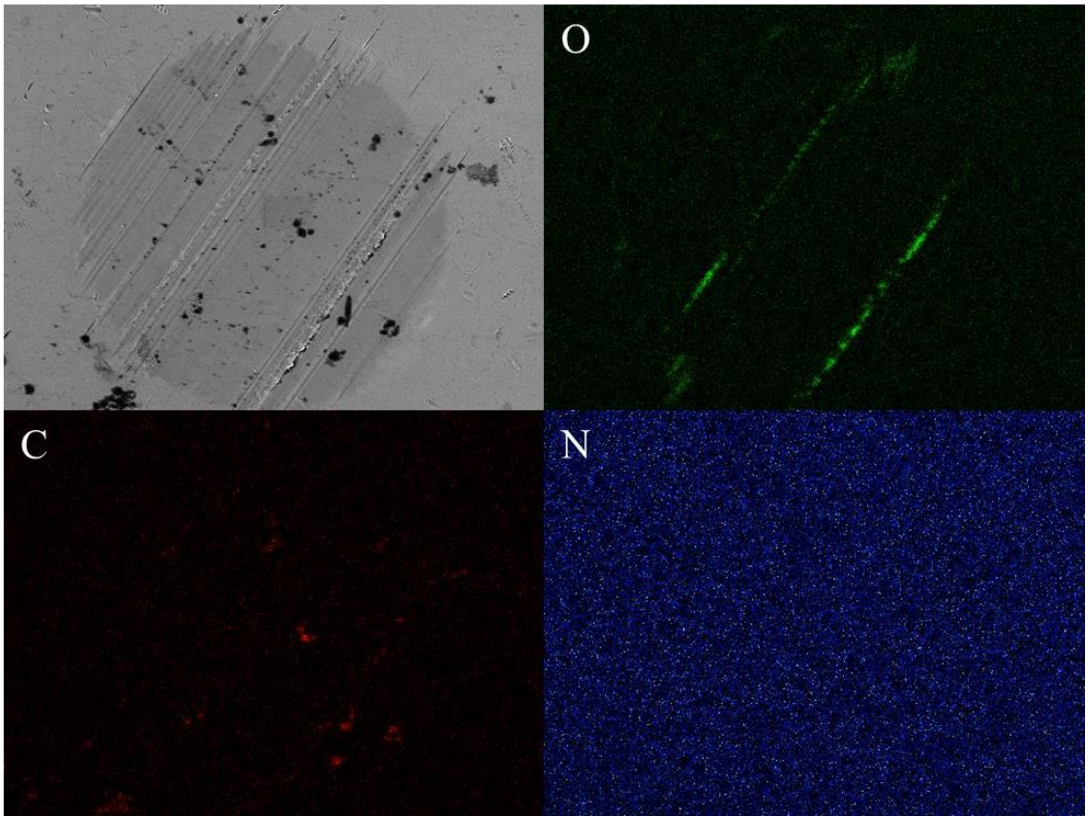

Figure 5–14. SEM image and EDX mapping of the contact area with PAO+NOS, 1800 cycles.

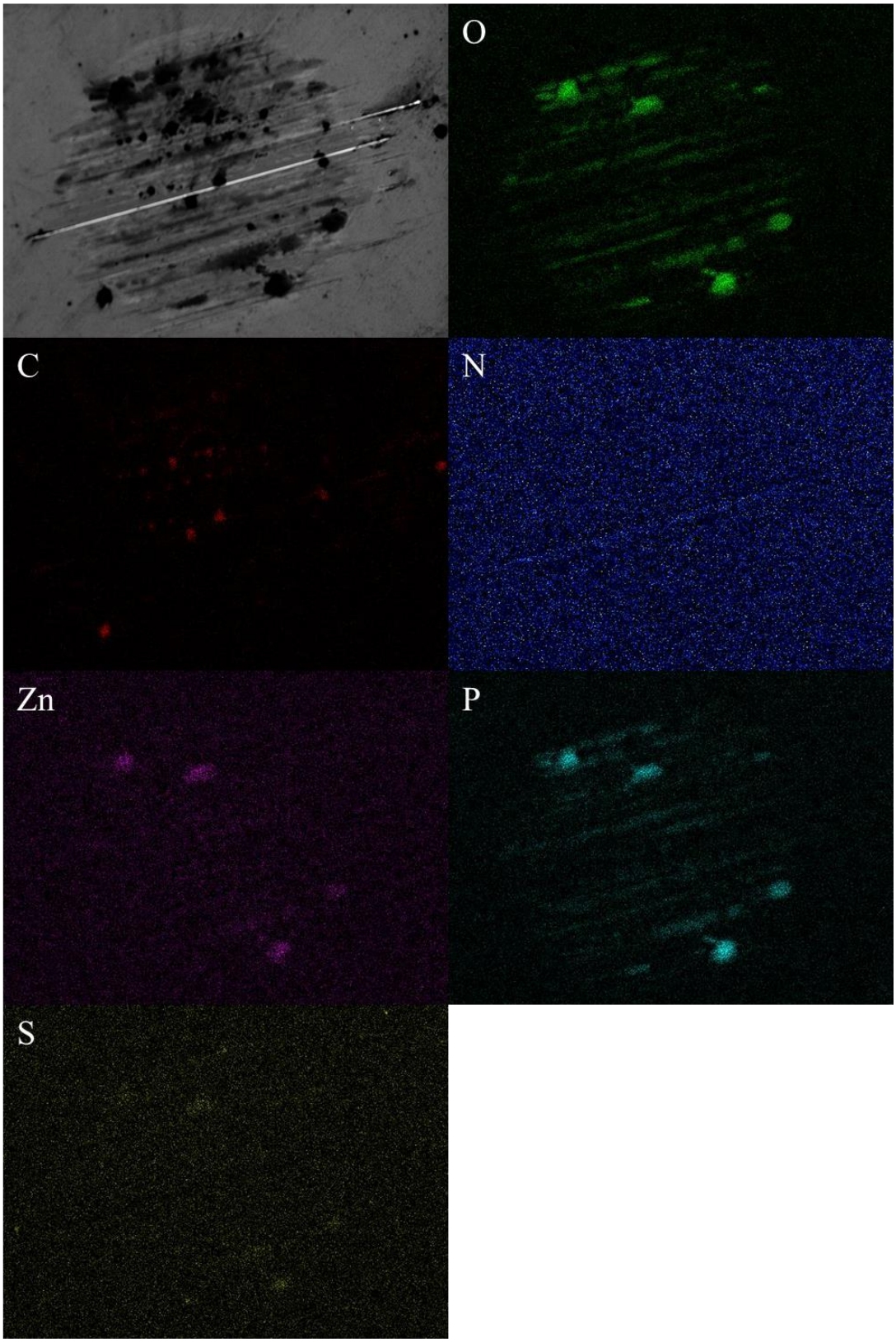


Figure 5–15. SEM image and EDX mapping of the contact area with PAO+ZDDP+NOS, 1800 cycles.

Figure 5–16, 5–17, and 5–18 show the EDX results after 5400 test cycles, corresponding to the tribofilms formed with PAO+ZDDP, PAO+NOS, and PAO+ZDDP+NOS lubrication, respectively. By comparing the results in Figures 5–13, 5–14, and 5–15, it is possible to understand the effect of test time on the tribofilm characteristic. As shown in Figure 5–16, after 5400 test cycles, the tribofilm formed by PAO+ZDDP underwent significant wear. The contact area was covered with linear abrasion marks along the sliding direction, which were rich in oxygen, phosphorus, and sulfur. Combined with the results in Figure 5–13, it shows that PAO+ZDDP is not effective in preventing wear under boundary lubrication. However, the fact that components from ZDDP were detected despite severe wear suggests that ZDDP did not maintain an upwardly raised tribofilm in boundary lubrication but rather grew in the abrasion marks while reacting with the metal at the interface. In Figure 5–17, a more pronounced tribofilm was formed with PAO+NOS lubrication compared to that shown in Figure 5–14 because both the speckled traces and the streaks along the sliding direction were not observed in Figure 5–14 but in Figure 5–17. This tribofilm formation may be the reason for the increase in the friction coefficient. In addition, the EDX results show that the speckled structure was rich in oxygen, from which it can be speculated that it may be an oxide formed by the reaction of NOS and interfacial metals. Unlike the usage of individual additives, the tribofilm after 5400 cycles, shown in Fig. 5–18, and the tribofilm after 1800 cycles, shown in Fig. 5–15, had almost the same characteristics when using PAO+ZDDP+NOS. This allowed it to maintain a stable low friction coefficient.

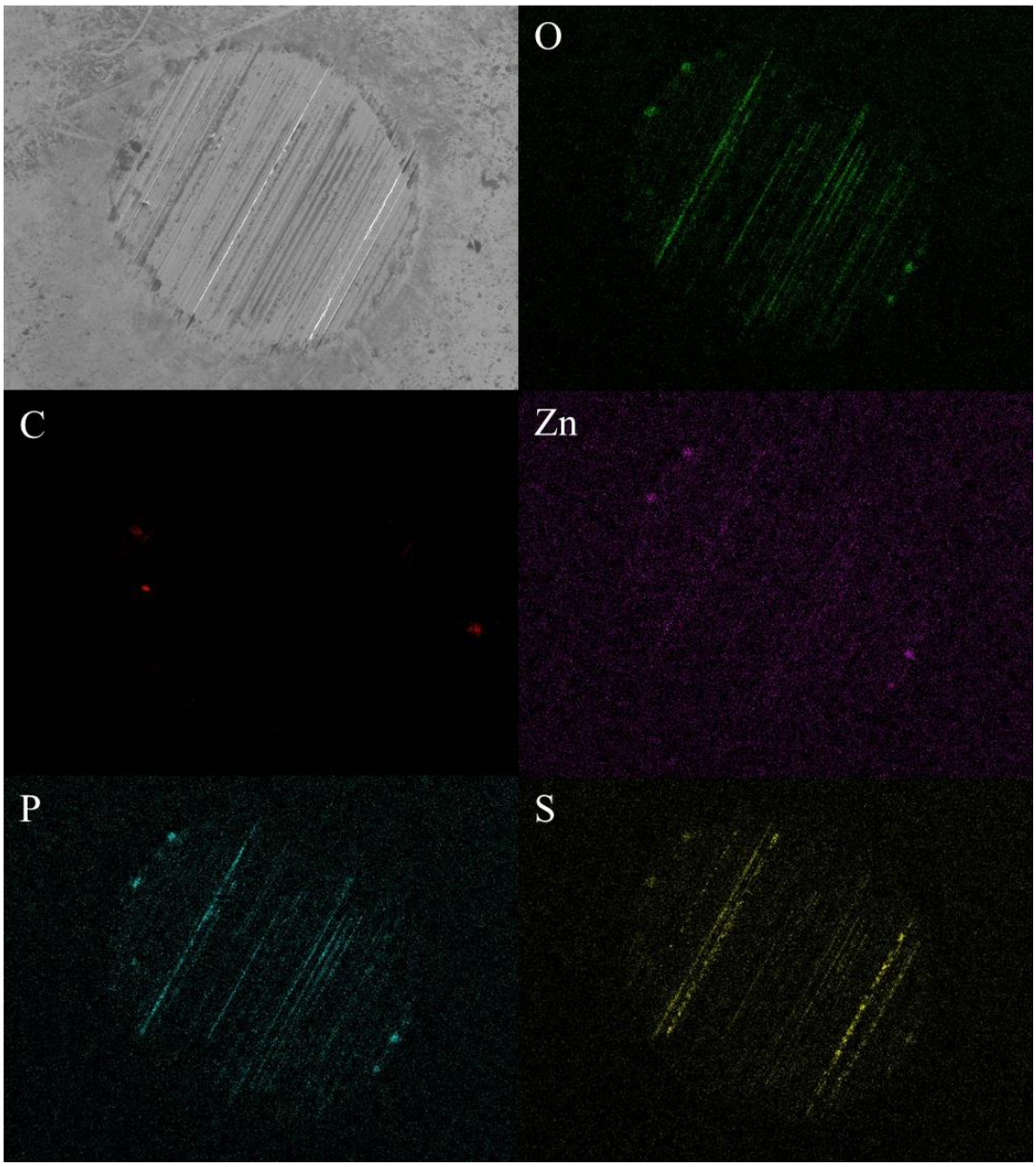


Figure 5–16. SEM image and EDX mapping of the contact area with PAO+ZDDP, 5400 cycles.

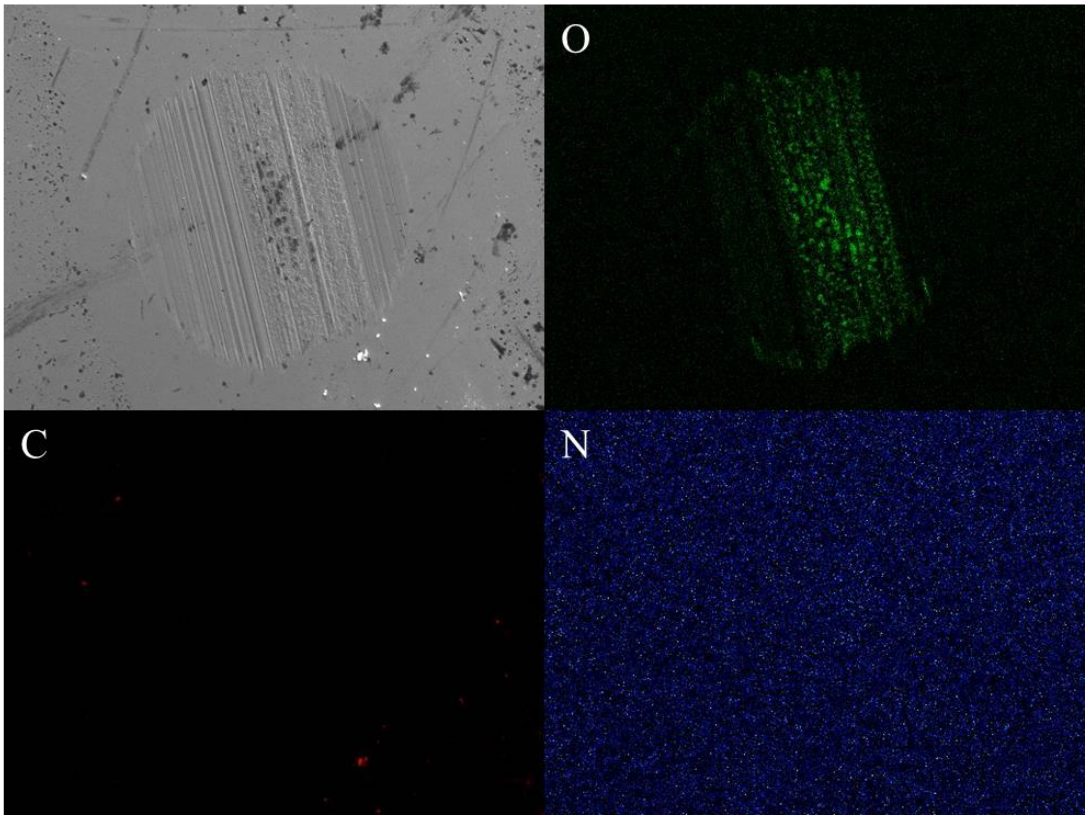

Figure 5–17. SEM image and EDX mapping of the contact area with PAO+NOS, 5400 cycles.

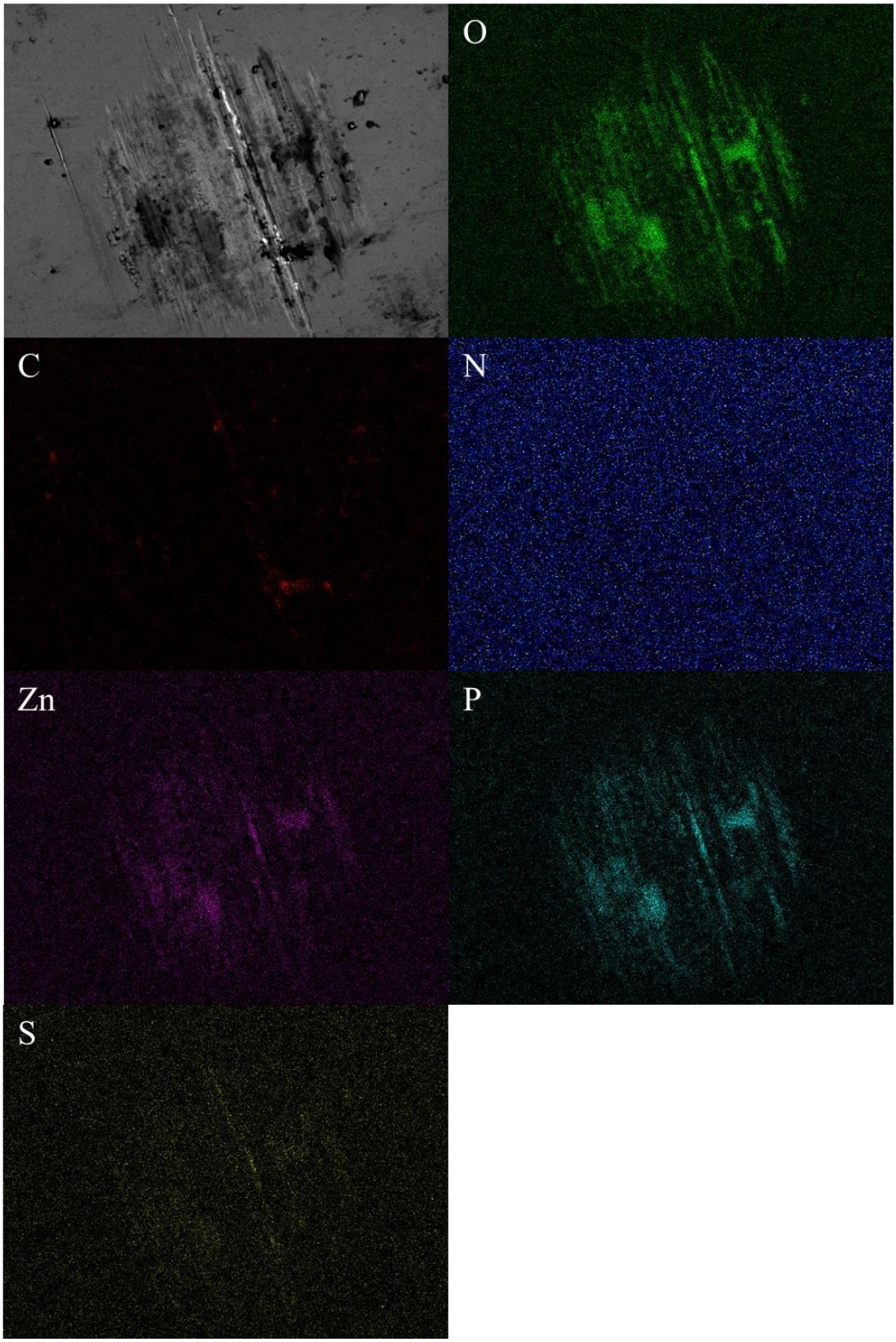


Figure 5–18. SEM image and EDX mapping of the contact area with PAO+ZDDP+NOS, 5400 cycles.

## 5.4 Conclusion

The lubrication characteristics of NOS and ZDDP at room temperature were discussed in the last chapter, thus explaining the lubrication mechanism of the NOS-ZDDP mixture. In this chapter, the performances of the lubricating oils were tested at 100°C, which was within the engine operating temperature. The contributions to friction-reducing and wear-resistance of each lubricating oil were compared. The results are summarized as follows.

1. The NOS additive alone provided considerable friction reduction performance, as it exhibited the lowest friction coefficient after the first 1800 sliding cycles. However, its friction coefficient increased significantly and eventually exceeded that of the NOS+ZDDP additive in the extended test. The EDX mapping results suggest that the formation of an oxygen-rich reactive layer is responsible for the increase in the friction coefficient.

2. After 5400 sliding cycles, the NOS-ZDDP mixture exhibited a lower friction coefficient than the other additives, and the size of the wear area was the smallest after both 1800 and 5400 sliding cycles.

# Chapter 6. Summary

## 6.1 Conclusion

The tribological effects of ZDDP, OFM, and ZDDP+OFM mixtures, when used as oil additives, were discussed in this paper. In this study, the authors divided the whole tribological phenomenon into two stages and verified and discussed them through different experiments respectively. In the first stage, the additives in the base oil solution adsorb to the metal surface through its polar group and exhibit a corresponding friction-reducing effect. In the second stage, a tribofilm is formed on the contact surface during the sliding, which determines the anti-wear and friction-reducing performance.

In Chapter 2, the density and the thickness of the adsorption film of OFM molecules were measured by the neutron reflectance method, and the same adsorption state was reproduced in the AFM, and the friction tests were performed. The results show that there is a direct relationship between the formation of the adsorption film and the reduction of the friction coefficient when OFM is used alone. As reported in previous studies, a significant friction reduction effect was seen when the adsorption film reached a certain density. In addition, many previous studies have reported the poor friction reduction effect of oleic acid at high temperatures, and previous studies have speculated that the reason for this is that the molecular structure of oleic acid prevents it from forming a dense adsorption film. However, the results of this study found that oleic acid desorbs from the metal surface at high temperatures. Without the lubrication of the adsorbed film, the friction coefficient naturally increases. On the other hand, when OFM and ZDDP were mixed, there was no direct relationship between the friction coefficient and the film density of OFM. In addition, when OFM with higher reactivity (oleic acid) and polarity (palmitic acid) was used, corrosion of metals was observed at high temperatures. From the AFM results, at 25°C, OLA+ZDDP exhibited better friction-reducing properties, while PLA+ZDDP and STA+ZDDP exhibited properties closer to those of ZDDP. At 100°C, the friction coefficient no longer exhibited dependence on contact pressure with OLA+ZDDP, while the friction coefficient maintained its dependence on contact pressure with PLA+ZDDP and STA+ZDDP. This suggests that even though all fatty acids form metal soaps by reaction with interfacial metals, their tribological effects are different, especially with STA+ZDDP and PLA+ZDDP mixtures. As their friction coefficients have the same dependence on contact pressure to the acid alone, indicating that their tribological properties are closer to those of the fatty acids alone.

In Chapter 3, tribofilms were formed by continuous rubbing of the iron surfaces using colloidal

probes. The tribological properties were also investigated by measuring the friction coefficient of the rubbed area. When ZDDP alone was used, the formation of tribofilm was observed in this study, as reported in previous studies. Moreover, the film formation of ZDDP was more active at 100°C compared to 25°C. When ZDDP and OFM were mixed, the formation of tribofilm was also observed with the lubrication of PLA+ZDDP. Although the results in Chapter 2 indicate that the adsorption density of palmitic acid increases in the presence of ZDDP, both the friction coefficient and the formation of tribofilm by rubbing indicate that ZDDP plays a decisive role in this mixture for its tribological properties. On the other hand, in the STA+ZDDP mixture, although tribofilm was not observed, the friction coefficient remained close to that of ZDDP, suggesting that the friction coefficient was still dominated by ZDDP, despite the possible role of stearic acid in slowing down the formation of tribofilm. On the other hand, the unsaturated oleic acid has different results from the saturated fatty acid. The mixture with ZDDP effectively reduces friction by forming metal soap. On the other hand, the results were reversed at 100°C. STA+ZDDP and PLA+ZDDP showed lower friction coefficients, while OLA+ZDDP showed friction coefficients closer to those of ZDDP. Notably, N-oleoyl sarcosine showed enhanced friction-reducing performance with ZDDP both at 25°C and 100°C.

Chapters 4 and 5 focus on the tribological effect of NOS+ZDDP and its mechanism. In order to evaluate the anti-wear performance and to perform a chemical analysis of the tribofilm, the author conducted friction experiments using a macroscopic ball-on-disk machine. The results of the friction tests showed that the mixture of ZDDP and NOS had good anti-wear and friction-reducing properties at 25°C. At 100°C, the friction coefficient of ZDDP+NOS was higher than that of NOS-alone lubrication due to the more active reaction of ZDDP. However, ZDDP+NOS showed better performance in the long time and high-load experiments. By observing the contact surface when the friction coefficient changed, the authors speculated on the mechanism of ZDDP+NOS lubrication: First, when NOS was used alone, NOS formed a dotted tribofilm on the contact surface as the experiment progressed, and the formation of the tribofilm led to an increase in the friction coefficient. However, when mixed with ZDDP, ZDDP retarded the formation of the tribofilm and maintained a relatively stable friction coefficient. On the other hand, NOS did not completely prevent the formation of ZDDP tribofilm, but the results of XPS and EDX analysis can be concluded that NOS reduced sulfide formation in the tribofilm. The sulfide is considered to have an extreme pressure effect, while the phosphate is considered to have an anti-wear effect. In the mixture of NOS+ZDDP, NOS effectively moderates the contact conditions, reduces sulfide formation, and maintains the anti-wear properties of ZDDP itself, thus demonstrating a synergistic effect in both friction reduction and anti-wear.

## 6.2 Prospect

Carbon emission reduction and environmental protection have become important issues in recent years. The development of hybrid and electric vehicles can reduce carbon emissions by saving energy. Also, as the processing accuracy of engine components improves, the usage of low-viscosity engine oils makes the engine temperature decrease irreversible. The reduction in oil temperature will directly lead to a reduction in the effectiveness of reactive additives such as ZDDP and MoDTC, and on the other hand, engine oils should ideally perform their friction reduction and wear prevention properties before the additives form a tribofilm. In addition, from an environmental point of view, it is preferable to use organic additives that do not contain metal ions. This study investigated the synergistic effect of ZDDP and NOS. NOS, which by its structure allows the formation of chelates with metals, resulted in enhanced adsorption properties. The results of this study show that NOS exhibited a synergistic effect with ZDDP, and X-ray analysis results show that NOS can prevent the formation of sulfide in tribofilms. However, this is insufficient to fully explain the friction reduction mechanism. In the studies so far, the lubrication mechanism has been resolved by analyzing the elemental distribution and chemical structure of the tribofilm. However, the necessary information is inevitably lost during the washing and drying process. Coupled with the limited ability of organic-based OFM to form tribofilms, today's methods cannot correspond to the performance analysis of metal soaps. *In-lubrication*, *Tribo-operando* analysis will be necessary for future studies. However, suitable analytical methods have not been established yet.

With the prevalence of electric vehicles, some readers may feel that the study of engine oil additives no longer fits the context of the times. Although this study was conducted with additives in engine oils, additive technology is not only present in engine oils. Cutting oils used in machining, release agents used in extrusion greases used in rotating bearings, are all inseparable from proven lubricant technology. However, as with oil additives, the lack of appropriate analytical techniques and approaches has led to a lack of understanding of the additives. The development in *In-lubrication* and *Tribo-operando* analysis is also an industry-wide technology need and an important unresolved issue to understand the additives in use and to design optimal additives for different purposes.

## Reference:

[1]. Climate Watch Historical GHG Emissions. 2022. Washington, DC: World Resources Institute. Available online at: https://www.climatewatchdata.org/ghg-emissions.
[2]. 運輸部門における二酸化炭素排出量.(国土交通省) R4 5th July, https://www.mlit.go.jp/sogoseisaku/environment/sosei_environment_tk_000007.html.
[3]. Based on IEA Statistics © OECD/IEA 2014. CO2 emissions from transport (% of total fuel combustion), www.iea.org/statistics. All rights reserved.
[4]. K. Holmberg, P. Andersson, and A. Erdemir, "Global energy consumption due to friction in passenger cars," Tribol. Int., vol. 47, pp. 221–234, 2012, doi: org/10.1016/j.triboint.2011.11.022.
[5]. H. Spikes, Friction Modifier Additives, Tribol. Lett., vol. 60, no. 5, pp. 1–26, 2015, doi: 10.1007/s11249-015-0589-z.
[6]. SAE J300, Engine Oil Viscosity Classification, APR2013.
[7]. SAE J300, Engine Oil Viscosity Classification, JAN2015.
[8]. K. Yamamori, Y. Uematsu, K. Manabe, I. Miyata, S. Kusuhara, and Y. Misaki, "Development of Ultra Low Viscosity 0W-8 Engine Oil," SAE Technical Paper, 2020, doi: org/10.4271/2020-01-1425.
[9]. M. Smeeth, H. Spikes, and S. Gunsel, "Boundary Film Formation by Viscosity Index Improvers," Tribol. Trans., vol. 39, pp. 726–734, 1996, doi: 10.1080/10402009608983590.
[10]. H. Spikes, "The history and mechanisms of ZDDP," Tribol. Lett., vol. 17, pp. 469–489, 2004, doi: 10.1023/B:TRIL.0000044495.26882.b5.
[11]. E.H. Loeser, R.C. Wiquist and S.B. Twiss, "Cam and Tappet Lubrication. III-Radioactive Study of Phosphorus in III-Radioactive Study of Phosphorus in the EP Film," ASLE Trans., vol. 1, pp. 329–335, 1958, doi: 10.1080/05698195808972348.
[12]. L. Taylor, A. Dratva and H.A. Spikes, "Friction and Wear Behavior of Zinc Dialkyldithiophosphate Additive," Tribol. Trans. 43, pp. 469–479, 2000, doi: 10.1080/10402000008982366.
[13]. H. Fujita and H.A. Spikes, "The formation of zinc dithiophosphate antiwear films," Proc. I. Mech. E Ser. J., vol. 218 pp. 265–278, 2004, doi: org/10.1243/1350650041762677.
[14]. H. Fujita, R.P. Glovnea and H.A. Spikes, "Study of Zinc Dialkydithiophosphate Antiwear Film Formation and Removal Processes," Part I: Experimental, Tribology Transactions, vol. 48, pp. 558–566, 2005, doi: 10.1080/05698190500385211.
[15]. I. Hutchings, "Tribology: Friction and Wear of Engineering Materials," Edward Arnold, London, 1992, ISBN: 978-0081009109.
[16]. E. H. Loeser, R.C. Wiquist and S.B. Twiss, "Cam and Tappet Lubrication. IV-Radioactive Study of Sulfur in the EP Film," ASLE Trans., vol. 2, pp. 199–207, 1959, doi:

10.1080/05698195908972371.
[17]. P. A. Bennett, “A Surface Effect Associated with the Use of Oils Containing Zinc Dialkyl Dithiophosphate,” ASLE Trans., vol. 2, pp. 78–90, 1959, doi: 10.1080/05698195908972360.
[18]. W. W. Hanneman and R. S. Porter, “The Thermal Decomposition of Dialkyl Phosphates and O,O-Dialkyl Dithiophosphates,” J. Org. Chem., vol. 29, pp. 2996–2998, 1964, doi: 10.1021/jo01033a048.
[19]. N. E. Gallopoulos. “Thermal Decomposition of Metal Dialkyldithiophosphate Oil Blends,” ASLE Trans., vol. 7, pp. 55–63, 1964, doi: 10.1080/05698196408972035.
[20]. J. S. Ashford, L. Bretherick, and P. Gould, “The thermal decomposition of zinc di-(4-methylpentyl-2) dithiophosphate,” J. Appl. Chem., vol.15, pp. 170–178, 1965, doi: org/10.1002/jctb.5010150403.
[21]. J. J. Dickert Jr. and C. N. Rowe, “Thermal decomposition of metal O,O-dialkyl phosphorodithioates,” J. Org. Chem. vol. 32, pp. 647–653, 1967, doi: org/10.1021/jo01278a031.
[22]. R. B. Jones and R. C. Coy, “The Chemistry of the Thermal Degradation of Zinc Dialkyldithiophosphate Additives,” ASLE Trans., vol. 24, pp. 91–97, 1981, doi: 10.1080/05698198108983001.
[23]. R. C. Coy and R. B. Jones, “The Thermal Degradation and EP Performance of Zinc Dialkyldithiophosphate Additives in White Oil,” ASLE Trans., vol. 24, pp. 77–90, 1981, doi: 10.1080/05698198108983000.
[24]. J. Zhang, M. Ueda, S. Campen, and H. Spikes, “Boundary Friction of ZDDP Tribofilms,” Tribol. Lett., vol. 69, no. 8, pp. 1–17, 2021, doi: org/10.1007/s11249-020-01389-4.
[25]. S. Gunsel, H. A. Spikes and M. Aderin, “In-Situ Measurement of ZDDP Films in Concentrated Contacts,” Tribol. Trans., vol. 36, pp. 276–282, 1993, doi: 10.1080/10402009308983159.
[26]. M. L. S. Fuller, M. Kasrai, G. M. Bancroft, K. Fyfe, and K. H. Tan, “Solution decomposition of zinc dialkyl dithiophosphate and its effect on antiwear and thermal film formation studied by X-ray absorption spectroscopy,” Tribol. Int., vol. 31, pp. 627–644, 1998, doi: org/10.1016/S0301-679X(98)00084-X.
[27]. M. Aktary, M. T. McDermott, and J. Torkelson, “Morphological evolution of films formed from thermooxidative decomposition of ZDDP,” Wear, vol.247, pp.172–179, 2001, doi: org/10.1016/S0043-1648(00)00525-1.
[28]. R. J. Bird and G. D. Galvin, “The application of photoelectron spectroscopy to the study of e. p. films on lubricated surfaces,” Wear, vol.7, pp. 143–167, doi:org/10.1016/0043-1648(76)90188-5.
[29]. F. M. Piras, A. Rossi, and N. D. Spencer, “Combined in situ (ATR FT-IR) and ex situ (XPS) Study of the ZnDTP-Iron Surface Interaction,” Tribol. Lett., vol. 15, pp. 181–191, 2003, doi:

org/10.1023/A:1024800900716.
[30]. J. M. Martin, J. L. Mansot, I. Berbezier, and H. Dexpert, “The nature and origin of wear particles from boundary lubrication with a zinc dialkyl dithiophosphate,” Wear, vol. 93, pp. 117–126, 1984, doi: org/10.1016/0043-1648(84)90064-4.
[31]. J. M. Martin, M. Belin, J. L. Mansot, H. Dexpert and P. Lagarde, “Friction-Induced Amorphization with ZDDP—An EXAFS Study,” ASLE Trans., vol. 29, pp. 523–531, 1986, doi: 10.1080/05698198608981716.
[32]. J. M. Martin, J. L. Mansot, I. Berbezier, M. Belin, and G. Balossier, “Microstructural aspects of lubricated mild wear with zinc dialkyldithiophosphate,” Wear, vol. 107, pp. 355–366, 1986, doi: org/10.1016/0043-1648(86)90165-1.
[33]. M. Belin, J. M. Martin and J. L. Mansot, “Role of Iron in the Amorphization Process in Friction-Induced Phosphate Glasses,” Tribol. Trans., vol. 32, pp. 410–413, 1989, doi: 10.1080/10402008908981907.
[34]. J. M. Martin, C. Grossiord, T. Le. Mogne, S. Bec, A. Tonck, “The two-layer structure of Zndtp tribofilms: Part I: AES, XPS and XANES analyses,” Tribol. Int., Vol.34, pp.523–530, 2001, doi: org/10.1016/S0301-679X(01)00029-9.
[35]. K. T. Miklozic, T. R. Forbus, and H. A. Spikes, “Film thickness and roughness of ZDDP antiwear films,” Tribol. Lett., vol. 26, pp. 161–171, 2007, doi: org/10.1007/s11249-006-9189-2.
[36]. H. Spikes, “Origins of the friction and wear properties of antiwear additives.” Lubri. Sci., vol. 18, pp. 223–230, 2006, doi:org/10.1002/ls.19.
[37]. N. N. Gosvami, J. A. Bares, F. Mangolini, A. R. Konicek, D. G. Yablon, and R. W. Carpick, “Mechanisms of antiwear tribofilm growth revealed in situ by single-asperity sliding contacts,” Science., vol. 348, pp. 102–106, 2015, doi:10.1126/science.1258788.
[38]. J. Zhang and H. Spikes, “On the Mechanism of ZDDP Antiwear Film Formation,” Tribol. Lett., vol. 63, no. 24, pp. 1–15, 2016, doi: 10.1007/s11249-016-0706-7.
[39]. L. Fang, S. Korres, W. A. Lamberti, M. N. Webster, R. W. Carpick, “What stress components drive mechanochemistry? A study of ZDDP tribofilm formation,” Faraday Discuss. Advance article, pp. 1–19, 2022, doi: 10.1039/d2fd00123c.
[40]. L. J. Taylor and H. A. Spikes, “Friction-enhancing properties of ZDDP antiwear additive: Part I—friction and morphology of ZDDP reaction films,” Tribol. Trans., vol. 46, pp. 303–309, 2003, doi:10.1080/10402000308982630.
[41]. L. Taylor, H. Spikes and H. Camenzind, “Film-Forming Properties of Zinc-Based and Ashless Antiwear Additives,” SAE Trans., vol. 109, pp. 2095–2105, 2000, http://www.jstor.org/stable/44746004.
[42]. Y. Yamamoto and S. Gondo, “Friction and wear characteristics of Molybdenum Dithiocarbamate and Molybdenum Dithiophosphate,” Tribol. Trans., vol. 32, pp. 251–257, 1989,

doi: 10.1080/10402008908981886.
[43]. C. Grossiord, K. Varlot, J. Martin, T. Le Mogne, and C. Esnouf, "$MoS_2$ single sheet lubrication by molybdenum," Tribol. Int., vol. 31, pp. 737–743, 1999, doi: 10.1016/S0301-679X(98)00094-2.
[44]. J. Graham, H. Spikes, and S. Korcek, "The friction reducing properties of molybdenum dialkyldithiocarbamate additives: part I–factors influencing friction reduction," Tribol. Trans., vol. 44, pp. 626–636, 2001, doi: 10.1080/10402000108982504.
[45]. D. N. Khaemba, A. Neville, and A. Morina, "New insights on the decomposition mechanism of Molybdenum DialkyldiThioCarbamate (MoDTC): A Raman spectroscopic study," RSC Adv., vol. 6, pp. 38637–38646, 2016, doi: 10.1039/c6ra00652c.
[46]. Y. Rai, A. Neville, and A. Morina, "Transient processes of $MoS_2$ tribofilm formation under boundary lubrication," Lubr. Sci., vol. 28, pp. 449–471, 2016, doi: 10.1002/ls.
[47]. Y. Shimizu and H. A. Spikes, "The Influence of Slide–Roll Ratio on ZDDP Tribofilm Formation." Tribol. Lett., vol. 64, no. 19, pp. 1–11, 2016, doi: org/10.1007/s11249-016-0738-z.
[48]. Y. Shimizu and H. A. Spikes, "The Tribofilm Formation of ZDDP Under Reciprocating Pure Sliding Conditions." Tribol. Lett., vol. 64, no. 46 2016, pp. 1–11, doi: org/10.1007/s11249-016-0776-6.
[49]. I. Langmuir, "The mechanism of the surface phenomena of flotation," Trans. Faraday Soc., vol. 15, pp. 62–74, 1920, doi: 10.1039/TF9201500062.
[50]. W. B. Hardy, I. Doubleday, "Boundary lubrication—the paraffin series," Proc. R. Soc. Lond. A. vol. 100, pp. 550–557, 1922, doi: 10.1098/rspa.1922.0017.
[51]. H. M. Wells and J. E. Southcombe, "The theory and practice of lubrication: the ''Germ'' process," J. Soc. Chem. Ind, vol. 39, pp. 51T–60T, 1920, doi: org/10.1002/jctb.5000390517.
[52]. W. Hardy and I. Bircumshaw, "Bakerian Lecture. Boundary lubrication. Plane surfaces and the limitations of Amontons' Law" Proc. R. Soc. Lond. A, Math. Phys. Eng. Sci., vol. 108, pp. 1–27, 1925, doi: 10.1098/rspa.1925.0056.
[53]. F. P. Bowden and D. Tabor, "Friction and Lubrication of Solids," Oxford University Press, London, 1950, ISBN: 978-0198507772.
[54]. C. M. Allen and E. Drauglis, "Boundary layer lubrication: monolayer or multilayer," Wear, vol. 14, pp. 363–384, 1969, doi: 10.1016/0043-1648(69)90017-9.
[55]. F. P. Bowden and L. Leben, "The friction of lubricated metals," Philos. Trans. R. Soc. A, vol. 239, pp.1–27, 1940, doi: 10.1098/rsta.1940.0007.
[56]. J. Ye, M. Kano, and Y. Yasuda, "Evaluation of local mechanical properties in depth in MoDTC/ZDDP and ZDDP tribochemical reacted films using nanoindentation," Tribol. Lett., vol. 13, pp. 41–47, 2002, doi: 10.1023/A:1016559807453.
[57]. S. Bec, A. Tonck, J. M. Georges, and G. W. Roper, "Synergistic effects of MoDTC and

ZDTP on frictional behaviour of tribofilms at the nanometer scale," Tribol. Lett., vol. 17, pp. 797–809, 2004, doi: 10.1007/s11249-004-8088-7.
[58]. M. I. De Barros Bouchet, J. M. Martin, T. Le-Mogne, and B. Vacher, "Boundary lubrication mechanisms of carbon coatings by MoDTC and ZDDP additives," Tribol. Int., vol. 38, pp. 257–264, 2005, doi: 10.1016/j.triboint.2004.08.009.
[59]. M. I. De Barros Bouchet, J. M. Martin, T. Le Mogne, P. Bilas, B. Vacher, and Y. Yamada, "Mechanisms of $MoS_2$ formation by MoDTC in presence of ZnDTP: Effect of oxidative degradation," Wear, vol. 258, pp. 1643–1650, 2005, doi: 10.1016/j.wear.2004.11.019.
[60]. Y. Yamamoto, S. Gondo, T. Kamakura, and N. Tanaka, "Frictional characteristics of molybdenum dithiophosphates," Wear, vol. 112, pp. 79–87, 1986, doi: org/10.1016/0043-1648(86)90202-4.
[61]. J. Graham, S. Korcek, and H. A. Spikes, "The friction-reducing properties of molybdenum dialkyldithiocarbamate additives. Part 1. Factors influencing friction reduction," Tribol. Trans., vol. 44, pp. 626–636, 2001, doi: org/10.1080/10402000108982504.
[62]. R. D. Evans, G. L. Doll, C. H. Hager, and J. Y. Howe, "Influence of steel type on the propensity for tribochemical wear in boundary lubrication with a wind turbine gear oil," Tribol. Lett., vol. 38, pp. 25–32, 2010, doi: org/10.1007/s11249-009-9565-9.
[63]. K. T. Miklozic, J. Graham, and H. Spikes, "Chemical and physical analysis of reaction films formed by molybdenum dialkyldithiocarbamate friction modifier additive using Raman and atomic force microscopy," Tribol. Lett., vol. 11, pp. 71–81, 2001, doi: org/10.1023/A:1016655316322.
[64]. R. Unnikrishnan, M. C. Jain, A. K. Harinarayan, and A. K. Mehta, "Additive–additive interaction: an XPS study of the effect of ZDDP on the AW/EP characteristics of molybdenum-based additives," Wear, vol. 252, pp. 240–249, 2002, doi: org/10.1016/S0043-1648(01)00865-1.
[65]. B. C. Windom, W. G. Sawyer, and D. W. Hahn, "A Raman spectroscopic study of $MoS_2$ and $MoO_3$: applications to tribological systems," Tribol. Lett., Vol. 42, pp. 301–310, 2011, doi: org/10.1007/s11249-011-9774-x.
[66]. K. Hoshino, H. Kawai, and K. Akiyama, "Fuel efficiency of SAE 5 W-20 friction modified gasoline engine oil," SAE Technical Paper 1998, doi: org/10.4271/982506.
[67]. M. Muraki, Y. Yanagi, and K. Sakaguchi, "Synergistic effect on frictional characteristics under rolling-sliding conditions due to a combination of molybdenum dialkyldithiocarbamate and zinc dialkyldithiophosphate," Tribol. Int., vol. 30, pp. 69–75, 1997, doi: org/10.1016/0301-679X(96)00025-4.
[68]. M. Kasrai, J. N. Cutler, K. Gore, G. Canning, G. M. Bancroft, and K. H. Tan, "The chemistry of antiwear films generated by the combination of ZDDP and MoDTC examined by X-ray absorption spectroscopy," Tribol. Trans., vol. 41, pp. 69–77, 1998, doi:

org/10.1080/10402009808983723.
[69]. J. M. Martin, C. Grossiord, K. Varlot, B. Vacher, and J. Igarashi, “Synergistic effects in binary systems of lubricant additives: a chemical hardness approach,” Tribol. Lett., vol. 8, pp. 193–201, 2000, doi: org/10.1023/A:1019147520893.
[70]. J. Graham, R. Jensen, and H. A. Spikes, “The friction-reducing properties of molybdenum dialkyldithiocarbamate additives. Part 2. Durability of friction reducing capability,” Tribol. Trans., vol. 44, pp. 637–646, 2001, doi: org/10.1080/10402000108982505.
[71]. A. Morina and A. Neville, “Understanding the composition and low friction tribofilm formation/removal in boundary lubrication,” Tribol. Int., vol. 40, pp. 1696–1704, 2007, doi: org/10.1016/j.triboint.2007.02.001.
[72]. A. Morina, A. Neville, M. Priest, and J.H. Green, “ZDDP and MoDTC interactions in boundary lubrication—The effect of temperature and ZDDP/MoDTC ratio,” Tribol. Int., vol. 39, pp. 1545–1557, 2006, doi: org/10.1016/j.triboint.2006.03.001.
[73]. M. Komaba, S. Kondo, A. Suzuki, K. Kurihara, and S. Mori, “The effect of temperature on lubrication property with MoDTC-containing lubricant–temperature dependence of friction coefficient and tribofilm structure–,” Tribol. Online, vol. 13, pp. 275–281, 2018, doi: 10.2474/trol.13.275.
[74]. U. B. Bray, C. C. Moore, and D. R. Merrill, “Improvements in diesel engine lubricating oils,” SAE Trans., vol. 34, pp. 35–42, 1939, https://www.jstor.org/stable/44467918.
[75]. C. F. Prutton, D. R. Frey, D. Turnbull, and G. Dlouhy, “Corrosion of metals by organic acids in hydrocarbon solvents,” Ind. Eng. Chem., vol. 37, pp. 90–100, 1945, doi: org/10.1021/ie50421a020.
[76]. B. J. Briscoe, D. C. B. Evans, and D. Tabor, “The influence of contact pressure and saponification on the sliding behavior of stearic acid monolayers,” J. Colloid Interface Sci. vol. 61, pp. 9–13, 1977, doi: org/10.1016/0021-9797(77)90411-8.
[77]. B. J. Briscoe and D. Tabor, “Rheology of thin organic films,” ASLE Trans. vol. 17, pp. 158–165, 1974, doi: org/10.1080/05698197408981452.
[78]. H. A. Spikes and A. Cameron, “A comparison of adsorption and boundary lubricant failure,” Proc. R. Soc. Lond. A., vol. 336, pp. 407–419, 1974, doi: org/10.1098/rspa.1974.0027.
[79]. K. Sato, H. Ouchi, H. Okubo, S. Watanabe, and S. Sasaki, “Investigation of the Lubrication Mechanism by In-Situ AFM Observation for the Formation Process of the Tribo-Films under Lubrication with Combined Solutions of ZDDP and Organic Friction Modifiers,” J. Japanese Soc. Tribol., vol. 67, pp. 354–365, 2022, doi: 10.18914/tribologist.21-00011.
[80]. F. Cyriac, T. X. Yi, S. K. Poornachary, and P. S. Chow, “Behavior and interaction of boundary lubricating additives on steel and DLC-coated steel surfaces,” Tribol. Int., vol. 164, no. 107199, pp. 1–15, 2021, doi: 10.1016/j.triboint.2021.107199.

[81]. F. Cyriac, T. X. Yi, S. K. Poornachary, and P. S. Chow, “Boundary lubrication performance of polymeric and organic friction modifiers in the presence of an anti-wear additive,” Tribol. Int., vol. 165, no. 107256, pp. 1014, 2022, doi: 10.1016/j.triboint.2021.107256.

[82]. M. Ratoi, V. B. Niste, H. Alghawel, Y. F. Suen, and K. Nelson, “The impact of organic friction modifiers on engine oil tribofilms,” RSC Adv., vol. 4, pp. 4278–4285, 2014, doi: 10.1039/c3ra46403b.

[83]. S. Soltanahmadi, E. A. Esfahani, I. Nedelcu, A. Morina, M. C. P. van Eijk, and A. Neville, “Surface reaction films from amine-based organic friction modifiers and their influence on surface fatigue and friction,” Tribol. Lett., vol. 67, no. 80, pp. 1–15, 2019, doi: 10.1007/s11249-019-1189-0.

[84]. T. Massoud, R. P. De Matos, T. Le Mogne, M. Belin, M. Cobian, B. Thiébaut, S. Loehlé, F. Dahlem, and C. Minfray “Effect of ZDDP on lubrication mechanisms of linear fatty amines under boundary lubrication conditions,” Tribol. Int., vol. 141, no. 105954, pp. 1–13, 2020, doi: 10.1016/j.triboint.2019.105954.

[85]. J. Dawczyk, J. Russo, and H. Spikes, “Ethoxylated amine friction modifiers and ZDDP,” Tribol. Lett., vol. 67, no. 106, pp. 1–15, 2019, doi: 10.1007/s11249-019-1221-4.

[86]. B. M. Fry, M. Y. Chui, G. Moody, and J. S. S. Wong, “Interactions between organic friction modifier additives,” Tribol. Int., vol. 151, no. 106438, pp. 1–8, 2020, doi: 10.1016/j.triboint.2020.106438.

[87]. J. Zhang and Y. Meng, “Boundary lubrication by adsorption film,” Friction, vol. 3, pp. 115–147, 2015, doi: 10.1007/s40544-015-0084-4.

[88]. S. Jiang, C. Yuan, and J. S.S. Wong, “Effectiveness of glycerol-monooleate in high-performance polymer tribo-systems,” Tribol. Int., vol. 155, no. 106753, pp. 1–9, 2021, doi: org/10.1016/j.triboint.2020.106753.

[89]. F. Cyriac, T. X. Yi, S. K. Poornachary, and P. S. Chow, “Effect of temperature on tribological performance of organic friction modifier and anti-wear additive: Insights from friction, surface (ToF-SIMS and EDX) and wear analysis,” Tribol. Int., vol. 157, no. 106896, pp. 1–21, 2021, doi: 10.1016/j.triboint.2021.106896.

[90]. S. Campen, “Fundamentals of Organic Friction Modifier,” PhD Thesis, Imperial College London, 2012, doi: 10.25560/39323.

[91]. M. Kano, Y. Yasuda, Y. Okamoto, Y. Mabuchi, T. Hamada, T. Ueno, J. Yec, S. Konishi, S. Takeshima, J. M. Martin, M. I. De Barros Bouchet, and T. L. Mogne, “Ultralow friction of DLC in presence of glycerol mono-oleate (GMO),” Tribol. Lett., vol. 18, pp. 245–251, 2005, doi: org/10.1007/s11249-004-2749-4.

[92]. H. Okubo, S. Watanabe, C. Tadokoro, and S. Sasaki, “Effects of concentration of zinc dialkyldithiophosphate on the tribological properties of tetrahedral amorphous carbon films in

presence of organic friction modifiers," Tribol. Int., vol. 94, pp. 446-457, 2016, doi: 10.1016/j.triboint.2015.10.008.
[93]. H. Okubo, C. Tadokoro, and S. Sasaki, "Tribological properties of a tetrahedral amorphous carbon (ta-C) film under boundary lubrication in the presence of organic friction modifiers and zinc dialkyldithiophosphate (ZDDP)," Wear, vol. 332–333, pp. 1293–1302, 2015, doi: 10.1016/j.wear.2015.01.023.
[94]. H. Abdullah Tasdemir, M. Wakayama, T. Tokoroyama, H. Kousaka, N. Umehara, Y. Mabuchi, and T. Higuchi "Ultra-low friction of tetrahedral amorphous diamond-like carbon (ta-C DLC) under boundary lubrication in poly alpha-olefin (PAO) with additives," Tribol. Int., vol. 65, pp. 286–294, 2013, doi: 10.1016/j.triboint.2013.03.014.
[95]. H. Abdullah Tasdemir, M. Wakayama, T. Tokoroyama, H. Kousaka, N. Umehara, Y. Mabuchi, and T. Higuchi "Wear behaviour of tetrahedral amorphous diamond-like carbon (ta-C DLC) in additive containing lubricants," Wear, vol. 307, pp. 1–9, 2013, doi: 10.1016/j.wear.2013.08.011.
[96]. G. A. Salensky, M. G. Cobb, and D. S. Everhart, "Corrosion-Inhibitor Orientation on Steel," Ind. Eng. Chem. Prod. Res. Dev., vol. 25, pp. 133–140, 1986, doi: 10.1021/i300022a002.
[97]. R. M. Pines and J. D. Spivack, "A laboratory study of N-oleoyl sarcosine as a rust inhibitor in some petroleum products," Corrosion, vol. 13, pp. 92–96, 1956, doi: 10.5006/0010-9312-13.10.92.
[98]. G. Tatsumi, M. Ratoi, Y. Shitara, K. Sakamoto, and B. G. Mellor, "Effect of organic friction modifiers on lubrication of PEEK-steel contact," Tribol. Int., vol. 151, no. 106513, pp. 1–11, 2020, doi: 10.1016/j.triboint.2020.106513.
[99]. K. Oura, V. G. Lifshits, A.A. Saranin, A. V. Zotov, and M. Katayama, "Surface Science, An Introduction," Springer, 2003, ISBN: 978-3540005452.
[100]. F. P. Bowden, J. N. Gregory, and D. Tabor, "Lubrication of metal surfaces by fatty acids," Nature, vol. 156, pp. 97–101, 1945, doi: 10.1038/156097a0.
[101]. D. A. Fischer, Z. S. Hu, and S. M. Hsu, "Molecular orientation and bonding of monolayer stearic acid on a copper surface prepared in air," Tribol. Lett., vol. 3, pp. 41–45, 1997, doi: 10.1023/A:1019148131061.
[102]. D. Tabor and R. H. S. Winterton, "The direct measurement of normal and retarded van der Waals forces," Proc. R. Soc. Lond. A, Math. Phys. Eng. Sci., vol. 312, pp. 435–450, 1969, doi: 10.1098/rspa.1969.0169.
[103]. J. Israelachvili, Y. Min, M. Akbulut, A. Alig, G. Carver, W. Greene, K. Kristiansen, E. Meyer, N. Pesika, K. Rosenberg, and H. Zeng, "Recent advances in the surface forces apparatus (SFA) technique," Rep. Prog. Phys. vol. 73, no. 036601, pp. 1–16, 2010, doi: 10.1088/0034-4885/73/3/036601.

[104]. B. M. Fry, G. Moody, H. Spikes, and J. S. S. Wong, “Adsorption of organic friction modifier additives,” Langmuir, vol. 36, pp. 1147-1155, 2020, doi: 10.1021/acs.langmuir.9b03668.
[105]. S. Campen, J.H. Green, G.D. Lamb, and H.A. Spikes, “In situ study of model organic friction modifiers using liquid cell AFM; saturated and mono-unsaturated carboxylic acids,” Tribol. Lett., vol. 57, no. 18, pp. 1–20, 2015, doi:10.1007/s11249-015-0465-x.
[106]. T. Hirayama, T. Torii, Y. Konishi, M. Maeda, T. Matsuoka, K. Inoue, M. Hino, D. Yamazaki, and M. Takeda, “Thickness and density of adsorbed additive layer on metal surface in lubricant by neutron reflectometry,” Tribol. Intl., vol. 54, pp. 100–105, 2012, doi: 10.1016/j.triboint.2012.04.012.
[107]. N. Yamashita, T. Hirayama, N. L. Yamada, H. Watanabe, K. Onodera, and T. Sato, “Highly Swollen Adsorption Layer Formed by Polymeric Friction Modifier Providing Low Friction at Higher Temperature,” Tribol. Lett., vol. 69, no. 65, pp. 1–11, 2021, doi: 10.1007/s11249-021-01443-9.
[108]. N. L. Yamada, N. Torikai, K. Mitamura, H. Sagehashi, S. Sato, H. Seto, T. Sugita, S. Goko, M. Furusaka, T. Oda, M. Hino, T. Fujiwara, H. Takahashi, and A. Takahara, “Design and performance of horizontal-type neutron reflectometer SOFIA at J-PARC/MLF,” Eur. Phys. J. Plus, vol. 126, no. 108, pp. 1–13, 2011, doi: 10.1140/epjp/i2011-11108-7.
[109]. M. Hino, T. Oda, M. Kitaguchi, N. L. Yamada, S. Tasaki, and Y. Kawabata, “The ion beam sputtering facility at KURRI: Coatings for advanced neutron optical devices,” Nucl. Instrum. Methods. Phys. Res. A. Accel. Spectrometers, Detect. Assoc. Equip., vol. 797, pp. 265–270, 2015, doi: 10.1016/j.nima.2015.06.046.
[110]. A. Nelson, “Co-refinement of multiple-contrast neutron/X-ray reflectivity data using MOTOFIT,” J. Appl. Crystallogr., vol. 39, no. 2, pp. 273–276, 2006, doi: 10.1107/S0021889806005073.
20[111]. S. Campen, J. Green, G. Lamb, D. Atkinson, and H. Spikes, “On the increase in boundary friction with sliding speed,” Tribol. Lett., vol. 48, pp. 237–248, 2012, doi: 10.1007/s11249-012-0019-4.
[111]. S.M. Campen, J. Green, G. Lamb, D. Atkinson, and H. Spikes, “On the increase in boundary friction with sliding speed,” Tribol. Lett., vol. 48, pp. 237–248, 2012, doi: 10.1007/s11249-012-0019-4.
[112]. T. Hirayama, M. Maeda, Y. Sasaki, T. Matsuoka, H. Komiya, M. Hino, “Growth of adsorbed additive layer for further friction reduction,” Lubri. Sci., vol. 31, pp.171–178, 2019, doi:org/10.1002/ls.1420.
[113]. K. T. Miklozic, T. R. Forbus, and H. A. Spikes, “Performance of friction modifiers on ZDDP-generated surfaces,” Tribol. Trans., vol. 50, pp. 328–335, 2007, doi: 10.1080/10402000701413505.

[114]. A. Morina, A. Neville, M. Priest, and J. H. Green, “ZDDP and MoDTC interactions and their effect on tribological performance - Tribofilm characteristics and its evolution,” Tribol. Lett., vol. 24, pp. 243–256, 2006, doi: 10.1007/s11249-006-9123-7.
[115]. H. Okubo, C. Tadokoro, and S. Sasaki, “In situ Raman-SLIM monitoring for the formation processes of MoDTC and ZDDP tribofilms at Steel/Steel contacts under boundary lubrication,” Tribol. Online, vol. 15, pp. 105–116, 2020, doi: 10.2474/TROL.15.105.
[116]. K. Onodera, Y. Sato, K. Sato, S. Watanabe, and S. Sasaki, “Study on friction performance under co-existence of MoDTC and adsorption FM,” J. Japanese Soc. Tribol., vol. 66, pp. 77–85, 2021, doi: 10.18914/tribologist.20-00011.
[117]. K. Onodera, K. Sato, S. Watanabe, and S. Sasaki, “Study on friction and adsorption performance under co-existence of ZnDTP and FM,” J. Japanese Soc. Tribol., vol. 66, pp. 363–371, 2021, doi: 10.18914/tribologist.20-00014.
[118]. H. Fujita and H. A. Spikes, “Study of zinc dialkyldithiophosphate antiwear film formation and removal processes, part II: Kinetic model,” Tribol. Trans., vol. 48, pp. 567–575, 2005, doi: 10.1080/05698190500385187.
[119]. M. Ratoi, V. Anghel, C. Bovington, and H. A. Spikes, “Mechanisms of oiliness additives,” Tribol. Int., vol. 33, pp. 241–247, 2000, doi: 10.1016/S0301-679X(00)00037-2.
[120]. D. W. Kim and K. W. Kim, “Tribological characteristics of Cr/CrN/a-C: H: W/a-C: H coating under boundary lubrication conditions with glycerol mono-oleate (GMO) and molybdenum dithiocarbamate (MoDTC),” Wear, vol. 342–343, pp. 107–116, 2015, doi: 10.1016/j.wear.2015.08.011.
[121]. J. L. Bradley-Shaw, P. J. Camp, P. J. Dowding, and K. Lewtas, “Self-assembly and friction of glycerol monooleate and its hydrolysis products in bulk and confined non-aqueous solvents,” Phys. Chem. Chem. Phys., vol. 20, pp. 17648–17657, 2018, doi: 10.1039/c8cp01785a.
[122]. K. Holmberg and A. Erdemir, “Influence of tribology on global energy consumption, costs and emissions.” Friction, vol. 5, pp. 263–284, 2017, doi: org/10.1007/s40544-017-0183-5.
[123]. R. K. Banerjee, C. R. Jagga, and A. Sethuramiah, “Friction and surface morphological studies in plastic deformation under boundary lubrication condition,” Tribol. Trans., vol. 44, pp. 233–241, 2001, doi: 10.1080/10402000108982453.
[124]. T. Ichihashi, M. Kudo, and S. Mori, “Relation between the friction characteristics of wet clutches and the concentration of additives obtained by in-situ observation of oil film,” J. Japanese Soc. Tribol., vol. 58, pp. 581–588, 2013, doi: 10.18914/tribologist.58.08_581.
[125]. I. Nedelcu, E. Piras, A. Rossi, and H. R. Pasaribu, “XPS analysis on the influence of water on the evolution of zinc dialkyldithiophosphate-derived reaction layer in lubricated rolling contacts,” Surf. Interface Anal., vol. 44, pp. 1219–1224, 2012, doi: 10.1002/sia.4853.
[126]. A. Rossi, F. M. Piras, D. Kim, A. J. Gellman, and N. D. Spencer, “Surface reactivity of

tributyl thiophosphate: Effects of temperature and mechanical stress," Tribol. Lett., vol. 23, pp. 197–208, 2006, doi: 10.1007/s11249-006-9051-6.
[127]. R. Heuberger, A. Rossi, and N. D. Spencer, "XPS study of the influence of temperature on ZnDTP tribofilm composition," Tribol. Lett., vol. 25, pp. 185–196, 2007, doi: 10.1007/s11249-006-9166-9.
[128]. M. Crobu, A. Rossi, F. Mangolini, and N. D. Spencer, "Chain-length-identification strategy in zinc polyphosphate glasses by means of XPS and ToF-SIMS," Anal. Bioanal. Chem., vol. 403, pp. 1415–1432, 2012, doi: 10.1007/s00216-012-5836-7.
[129]. D. Schuetzle, R. O. Carter III, J. Shyu, R. A. Dickie, J. Holubka, and N. S. McIntyre "Chemical interaction of organic materials with metal substrates. Part I: ESCA studies of organic phosphate films on steel.," Appl. Spectrosc., vol. 40, pp. 641–649, 1986, doi: 10.1366/0003702864508548.
[130]. Y. Matsui, S. Aoki, and M. Masuko, "Influence of coexisting functionalized polyalkylmethacrylates on the formation of ZnDTP-derived tribofilm," Tribol. Int., vol. 100, pp. 152–161, 2016, doi: 10.1016/j.triboint.2015.12.018.
[131]. P. G. Harrison, M. J. Begley, T. Kikabhai, and F. Killer, "Zinc (II) bis (O, O′-dialkyl dithiophosphates): Interaction with small nitrogen bases. The crystal and molecular structure of hexakis (μ-O, O′-diethyl dithiophosphato)-μ4-thio-tetrazinc, Zn4[S2P(OEt)2]6S," J. Chem. Soc. Dalt. Trans., vol.5, pp. 925–928, 1986, doi: 10.1039/DT9860000925.
[132]. E. S. Yamaguchi, A. Onopchenko, M. M. Francisco, and C. Y. Chan, "The relative oxidation inhibition performance of some neutral and basic zinc dithiophosphate salts," Tribol. Trans., vol. 42, pp. 895–901, 1999, doi: 10.1080/10402009908982298.
[133]. 村木正芳、図解トライボロジー、日刊工業新聞社、2006
[134]. K. Vyavhare, R. B. Timmons, A. Erdemir, B. L. Edwards, P. B. Aswath, "Tribochemistry of fluorinated ZnO nanoparticles and ZDDP lubricated interface and implications for enhanced anti-wear performance at boundary lubricated contacts," Wear, vol 474–475, no. 203717, 2021, pp. 1–16, https://doi.org/10.1016/j.wear.2021.203717.

## Acknowledgements

I would like to thank the following people and many others, without whom I would not have been able to complete this research and receive my PhD.

First, I would like to express my sincere gratitude to my committee, Professors Tomoko Hirayama, Professor Atsushi Matsubara, and Professor Masaru Komori, for their dedicated support, invaluable patience, and thorough feedback. This journey would not have been possible without my defense committee, who generously provided their knowledge and expertise.

I would like to express my deepest gratitude to my supervisor, Professor Tomoko Hirayama. She accepted me with great enthusiasm, despite the fact that I had been very anxious about the new research topic and my doctoral education. Although I was always under-prepared in my research and presentation materials and often asked her to correct my poor papers and slides, she enthusiastically guided me from beginning to end and helped me to improve myself, for which I would like to express my deepest gratitude. I am deeply grateful to Professor Naoki Yamashita in the same laboratory, who carefully read each and every document I sent him, from the application form for the Japan Society for the Promotion of Science Research Fellowship in D1 to the defense presentation materials in D3, and gave me various suggestions. His keen perspective taught me many things, from research policy to how to present my research. In admiration of him, I often felt I had to work harder, and I was motivated by the desire to be closer to him, which inspired me to complete my PhD research. I also had a lot of fun with him at the drinking parties because of his warm and caring personality. I would like to express my sincere gratitude.

I am very grateful to my co-researchs from ENEOS, Dr. Kazuo Tagawa, Dr. Kazuhiro Yagishita, Mr. Tadashi Oshio, and Mr. Hideo Tsuneoka, for the research funding and for their help in providing test samples, supporting experiments, and frequent discussions. I would like to express my sincere gratitude to all of you for your tremendous support. Thanks to your efforts, I was able to carry out my PhD research. Once again, I would like to express my deepest gratitude to all of you.

I would like to express my sincere gratitude to Prof. Dongjiang Han of the Chinese Academy of Sciences. Although it was only a short year, he taught me a lot about how to conduct research and how to think. He also helped me to establish research methods and conduct experiments. He is not only a teacher, but also an important friend in my life, and I am grateful for the happy time I spent with him.

Words cannot express my gratitude to Professor Norifumi. L. Yamada from the High Energy Accelerator Research Organization. Thanks for the patient support of neutron reflectivity measurements.

Special thanks to Mr. Naoya Hatano, who provided considerable guidance and assistance in the design and fabrication of the experimental setup. I would like to thank him for his guidance and advice based on his abundant knowledge. I would also like to thank Professor Naohide Tomita, my supervisor during my master's degree, who taught me a lot.

Thanks should also go to Mr. Wataru Yagi in the lab for his advice and help throughout my PhD life. I learned not only presentation skills from him, but also a lot of thinking about my research, summarizing and generalizing my knowledge of tribology. I also got a lot of energy from his always lively and cheerful personality. I would like to express my gratitude to him and wish him the best of luck in obtaining his PhD in the near future. I am also grateful to the graduates, Mr. Takumi Saito, Mr. Shunsuke Nakamura and Mr. Seiji Murata. They were the first generation of students in the laboratory, and although they were younger than me, they carried out researches on tribology earlier than I did. I was able to learn a lot of experimental techniques and ways of thinking from them. All three of them are very observant and thoughtful, and have a high rate of learning and growth. This often stimulates me and motivates me to move forward. Thanks to their help in various ways, my research has been able to advance to some extent.

Many thanks to the undergraduate and master's students in the lab, whose names I cannot list here. With keen insight and thoughtfulness, they provided accurate comments in their seminar presentations of my research progress. Although they are younger than me, they were so reliable that I often felt spoiled by them. They were all very bright and constructive, and I learned a lot from their proactive approach to research. I regret very much that I was not able to teach them much as seniors. Although our time together was short, we got along very well. I would like to take this opportunity to express my gratitude and appreciation for the enriching research life they brought to me.

I would like to express my sincere gratitude to Ms. Nami Fukao, the secretary of our laboratory, for her indispensable support to my research. In particular, her prompt response in managing funds and purchasing equipment has enabled my research to progress so smoothly. Her help is greatly appreciated. I would like to express my gratitude to her.

I also sincerely appreciate the financial support from the Grant-in-Aid for the Japan Society for

the Promotion of Science Research Fellow (Grant Number JP1152364).

I would like to express my sincere gratitude to my friends and family who supported me. I would like to mention a few names in particular here, I would like to thank Mr. Yuecong Wu and Ms. You Guan, and Mr. Yaoyuan Zhang, my dear friends for their emotional support. I would be remiss in not mentioning the Gotoh family, Morio, Etsuko, Rie and Aya for their help and care in my life. I would also like to thank my parents, Mr. Shen Liang and Ms. Guo Mei, for allowing me to complete this ten-year study abroad experience and for supporting me spiritually, financially, and in many other ways, even though I had nothing to do with the word excellence most of the time. I would like to thank my wife, my soul mate, Weiyi Wang, for her support and companionship, and for her passionate love without hesitation. Thank you to my pet Maru the Pomeranian.

At the end of this article, I would like to thank myself who has not given up. May there be peace in the world.

Weiqi Shen
Kyoto, February, 2023

# Publications

## Journal articles

- W. Shen, T. Hirayama, N. Yamashita, M. Adachi, T. Oshio, H. Tsuneoka, K. Tagawa, K. Yagishita, N. L. Yamada, “Relationship between interfacial adsorption of additive molecules and reduction of friction coefficient in the organic friction modifiers-ZDDP combinations”, Tribology International. Volume 167, 107365
- W. Shen, D. Han, T. Hirayama, N. Yamashita, T. Oshio, H. Tsuneoka, K. Tagawa, K. Yagishita, “N-Oleoyl Sarcosine as an Engine Oil Friction Modifier, Part 1: Tribological Performance of NOS+ZDDP Mixture at 100°C”, Tribology Online, Volume 17, Issue 3, pp. 216-226
- W. Shen, D. Han, T. Hirayama, N. Yamashita, T. Oshio, H. Tsuneoka, K. Tagawa, K. Yagishita, “N-Oleoyl Sarcosine as an Engine Oil Friction Modifier, Part 2: Elucidation of Friction-Reducing Mechanism at Room Temperature Focusing on Contribution of NOS in NOS+ZDDP Mixture”, Tribology Online, Volume 17, Issue 3, pp. 227-238

## Conference presentations

- ガソリン用エンジン油の省燃費性能向上に関する検討（第 2 報）、トライボロジー会議秋、2020 別府（オンライン）
- ガソリン用エンジン油の省燃費性能向上に関する検討（第 3 報）、トライボロジー会議秋、2021 松江
- ガソリン用エンジン油の省燃費性能向上に関する検討（第 4 報）、トライボロジー会議春、2022 東京
- ZDDP と複数摩擦調整剤併用系のトライボロジー特性、トライボロジー会議秋、2022 福井
- 省燃費性向上におけるエンジンオイル添加剤の機能に関する検討、自動車技術会学生ポスターセッション、 2021 オンライン
- エンジンオイル添加剤併用系における分子吸着と摩擦特性の評価、関西潤滑懇談会 7 月例会、2021 オンライン
- ZDDP とオレイルサルコシンの併用による摩擦低減メカニズムに関する検討、関西潤滑懇談会 9 月例会、 2022 オンライン
- エンジン油添加剤の併用による摩擦低減に関する検討、極限環境対応極微細表面構造付与先進流体軸受(U2)研究会、2021 彦根
- Combined Use of ZDDP and Organic Friction Modifier Leads to Lower Coefficient of Friction; A Study Using Atomic Force Microscope, WTC, 2022, France, Lyon